Next Generation Anodes for Lithium-Ion Batteries

First Quarter Progress Report 2020

Jack Vaughey
Argonne National Laboratory
9700 South Cass Avenue
Lemont, IL 60439
Phone: (630) 252-8885
E-mail: vaughey@anl.gov

Brian Cunningham, DOE-EERE-VTO Program Manager
Hybrid Electric Systems, Battery R&D
Phone: (202) 586-8055
E-mail: brian.cunningham@ee.doe.gov

Table of Contents

Silicon Deep Dive Overview

Project Introduction

Silicon has received significant attention as an alternative to the graphitic carbon electrode presently used in lithium-ion batteries due to its high capacity, stability, and availability. Compared to graphitic carbon, elemental silicon's capacity is nearly an order of magnitude higher (~3600 mAh/g silicon vs 372 mAh/g Graphite), however, problems including large crystallographic expansion (~320%) upon full lithiation, slow lithium diffusion, and high reactivity at high states of charge have hindered full scale commercialization. In a cell, these electrochemical and diffusion issues are manifested as particle cracking, particle isolation (binder failure), electrolyte reactivity, and electrode delamination issues. Because of the technological advances possible if a silicon anode can be designed and proven, researchers in multiple disciplines have pushed to understand these physical issues and advance the field and create a viable silicon-based electrode.

Next Generation Anodes for Lithium-Ion Batteries, also referred to as the Silicon Deep Dive Program, is a consortium of five National Laboratories assembled to tackle the barriers associated with development of an advanced lithium-ion electrode based upon silicon as the active material. This research program has several goals including (1) evaluating promising silicon materials that can be either developed internally, in association with private companies, or from academic collaborators in quantities sufficient for electrode preparation by the consortiums facilities, (2) developing a silicon-based electrode that meets BatPac specifications, and (3) executing full cell development strategies that leverage DOE-EERE-VTO investments in electrode materials and characterization. The primary objective of this program is to understand and eliminate the barriers to implementation of a silicon-based anode in a lithium-ion cell. The five National Laboratories (ANL, NREL, LBNL, ORNL, and PNNL) involved are focused on a single program with continuous interaction, clear protocols for analysis, and targets for developing both an understanding and a cell chemistry associated with advancing silicon-based electrodes for lithium-ion cells. This undertaking is a full electrode/full cell chemistry project with efforts directed at understanding and developing the chemistry needed for advancing silicon-based anodes operating in full cells. Materials development efforts include active material development and evaluation, binder synthesis, surface functionalization, safety, strategies to mitigate lithium loss, and electrolyte additives. Efforts include cross-lab diagnostic research including a wide range of electrochemical, chemical and structural characterization of the system across length- and time-scales. Specialized characterization techniques developed with DOE-EERE-VTO funding, include neutrons, MAS-NMR, optical, and X-ray techniques being employed to understand operation and failure mechanisms in these silicon-based anodes. The project is managed as a single team effort spanning the Labs, with consensus decisions driving research directions and toward development of a functioning stable silicon-based electrode.

The Silicon Deep Dive project seeks to identify the limiting factors of silicon-based electrodes that need to be overcome to produce a viable functioning LIB electrode and full cell. The issues include understanding and controlling silicon surface chemistry, lithium loss due to side reactions, active material interactions, and the role of electrolyte stability. The goal of the project is to utilize our understanding of silicon and silicide reactivity, electrode formulation, and binder and electrolyte formulations, to design a functioning silicon-based electrode for a lithium-ion cell that meets DOE-EERE goals. Combined with the SEISta's efforts focused on interfacial reactivity, key variables can be isolated and studied to improve the performance of a silicon-based cell. This interaction is maintained and accomplished through joint meetings, face to face discussions, and extensive collaborations between the teams.

FY19/FY20 Deep Dive Goals:

FY19Q4	Construct and evaluate cells based on optimizing lithium inventory, binder, electrolyte formulation, and testing protocol to achieve a 300 Wh/kg cell design based on BatPaC modeling.
FY20Q1	Evaluate two new binder - slurry – silicon laminate combinations that lead to improved stability and a 15% improvement in performance compared to baseline for a high silicon-loading (>60%) electrode.
FY20Q2	Assess and evaluate multiple surface driven coatings that utilize a multivalent surface substitution. Develop an understanding of the formation mechanism on the cycling stability of the underlying silicon electrode; propose a mechanism of formation.
FY20Q3	Assess the stability of electrode level silicon baseline materials on cycling and determine the range of species that solubilize and leach into the electrolyte.
FY20Q4	Combine the advancements made over various aspects of the silicon electrode by the Silicon Deep Dive team evaluate them at the full system level and optimize a best full cell with a commercial cathode that using BatPac can be determined to deliver > 350 Wh/kg for 120 cycles; Evaluate the energy fade on standing for 2 mos and demonstrate an improvement over baseline of 20%.
FY20Q4	Have published a document that will enable other research and development groups to analyze stability of the SEI on a silicon-based anode, thus enabling developers or researchers to continually improve silicon cell stability (joint milestone with the SEISta). Approach

Approach

Oak Ridge National Laboratory (ORNL), National Renewable Energy Laboratory (NREL), Pacific Northwest National Laboratory (PNNL), Lawrence Berkeley National Laboratory (LBNL), and Argonne National Laboratory (ANL) have teamed together to form an integrated program. Technical targets have been developed and regular communications have been established. Throughout the program, there is a planned focus on understanding, insights into, and advancement of, silicon-based materials, electrodes, and cells. All anode advancements will be verified based on life and performance of full cells. Toward that end, baseline silicon-based materials, electrodes, and cells have been adopted, along with full cell testing protocols.

In examining improvements, changes to the baseline cell technology will be minimized. As an example, silicon active material coating improvements will be verified on baseline silicon materials in electrodes fabricated by the battery research facilities. All other components in the prototype cells (i.e. positive electrode, separator, and electrolyte) will be from the baseline technology. While there are many testing protocols that can be utilized to benchmark the baseline technology, this program has adopted a testing protocol from the literature that has worked well for lithium-ion cells with silicon containing anodes. Shown pictorially in Figure 1 the test starts with three slow (C/20) formation cycles, an HPPC cycle, and then the C/3 aging cycles. The test ends with another HPPC cycle and three more slow (C/20) cycles. All constant current cycling is symmetric between charge and discharge rates. The tests are run at 30°C. If there is little or no aging in the first 100 cycles, the protocol can be repeated. This protocol effectively examines capacity, impedance, and aging effects in about a month's worth of testing. As the program matures, materials developments will be incorporated into baseline silicon-based materials, electrodes, and cells. Scale-up of materials, incorporation of materials advancements into electrodes and prototype cells, and characterization and testing of cells, as well as evaluation of safety and abuse tolerance are part of a wide range of integrated studies supported by battery research facilities at the National Labs working closely with the program. These research facilities include the Battery Abuse Testing Laboratory (BATLab), the Cell Analysis, Modeling, and Prototyping (CAMP) facility,

the Materials Engineering Research Facility (MERF), and the Post-Test Facility (PTF). At the present time the baseline silicon is from Paraclete Energy (Chelsea, MI).

The fundamental understanding of silicon-based electrode active materials is based on extensive electrochemical and analytical diagnostic studies on components, electrodes, and cells conducted within the program. This effort contains in-situ and ex-situ studies on full and specialty cells, including reference electrode

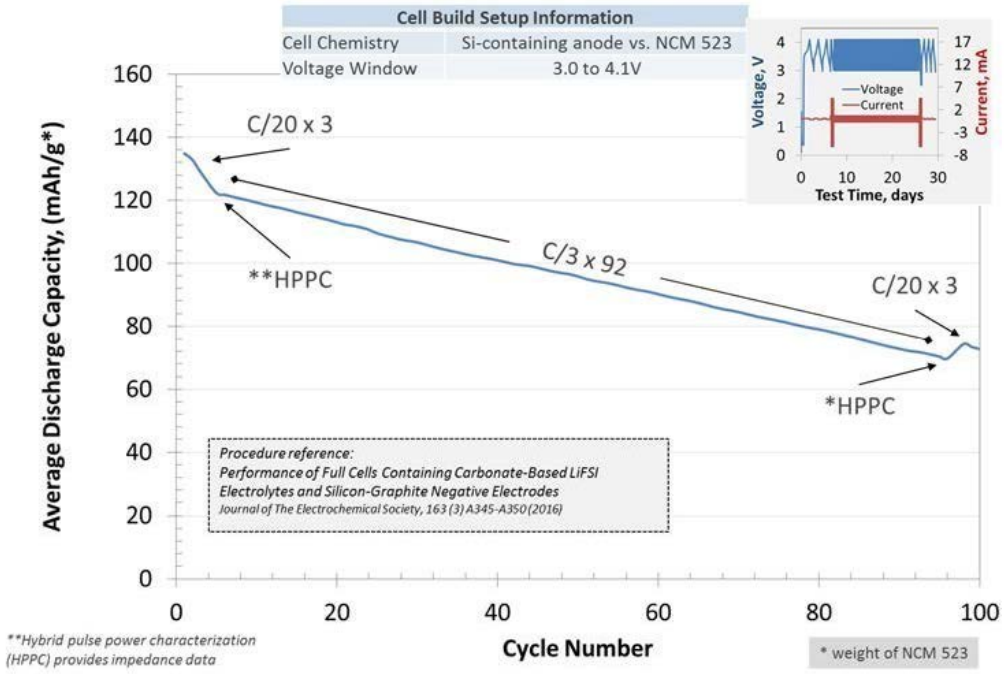

Figure 1. Full cell testing protocol.

cells. Overall, the diagnostic studies are intended to help establish structure-composition-property relationships, including lithium-reactivity at the silicon surface and bulk transport and kinetic phenomena. Additionally, these studies form the basis for accurately assessing component and electrode failure modes.

Supported by diagnostic studies, materials development on silicon-based materials, electrodes, and cells is being conducted to enhance interfacial stability, accommodate volume changes, and improve overall performance and life. Key to this effort is the development and testing of coatings and additives designed to modify and stabilize the dynamic silicon-electrolyte interface. Further, functional polymer binders designed to accommodate volume changes, increase conductivity, and improve adherence are being developed and analyzed. Finally, the program is exploring active material development, including hydride or organically functionalized silicon, silicide materials, high surface area passivated silicon created by high energy ball-milling, and thin films.

Communication of programmatic progress to the battery community is critical. This will generally be accomplished through publications, conference and AMR presentations, reports, and reviews. Further, the program is open to industrial collaboration that does not limit program innovation or the free flow of information. Finally, this program is highly integrated with our sister program on SEI-Stabilization (SEISta), centered at NREL. In general, SEISta is focused on the development and characterization of model systems, well-defined active area thin film electrodes, silicon wafers, and interfacial phenomena (e.g. SEI formation, changes, and growth).

Milestone Update FY2019Q4

Construct and evaluate cells based on optimizing lithium inventory, binder, electrolyte formulation, and testing protocol to achieve a 300 Wh/kg cell design based on BatPaC modeling.

For FY19, several materials focused initiatives were undertaken that focused on identified areas of need that should improve silicon-based electrode performance by improving silicon electrode structure, formulation, and stability. Among these multi-lab programmatic efforts,

- new or modified surface treatments on active silicon were explored extensively using many different approaches, including organic functionalization (ZZhang, Neale), inorganic coatings (Tong, Lu), *in-situ* coatings (Key, Dogan, Han, Vaughey), and carbon (Abraham, CAMP). Interface modification can lead to less surface reactivity leading to a thinner SEI, less reactivity with electrolyte, and less loss of lithium to parasitic side reactions.
- electrode level studies developing an understanding of how the interface between the silicon and the components of a working electrode are constructed. Studies focused on the binder/slurry properties and alternatives (LuZhang), slurry optimization (Armstrong, Veith, Trask, Dunlop), particle/binder stability (Neale, Coyle), alternative binders (JGZhang), and electrode construction (Trask, Dunlop). Electrode level studies are crucial to ensure that, on extended cycling, the electrode structure and cell environment are stable leading to longer cell life, slower capacity fade due to particle isolation, and more reliable manufacturing.
- Mechanistic studies to understand performance degradation are important for improving calendar and cycle life studies. Teams have been studying lithium consuming side reactions (Abraham), active particle degradation (Bloom), solubilization of the SEI (Johnson, LuZhang, Liu), and modeling of the total electrode processes (Dees). Together these studies shed light on the various cycle to cycle reactions that slowly remove active lithium from the electrochemical cell, seen as calendar and cycle life degradation.

The FY19Q4 milestone involved identifying leading results from the whole cross-lab team and incorporating them into a series of larger format cell builds to recognize performance enhancements compared to the DeepDive baseline based on Paraclete Energy silicon. In association with CAMP and BatPAC researchers, the baseline cell chemistry (with an NMC532 cathode) was modeled with an optimum n:p ratio, conductive carbon, binder, and electrolyte content, and porosity. BatPAC predicted 253 Wh/kg; however, with a 50% improvement in ASI the energy density could reach 285 Wh/kg. The FY19 milestone was constructed to utilize advances in the program to improve performance and identify a pathway to at least 300 Wh/kg. In these cases, the cell optimization choices addressed were interfacial impedance (coatings, electrode construction), electrode stability (binders), and enhancing cell power by increasing lithium diffusion to the surface (surface modification).

In discussions with team members, various materials research programs were identified for cell build inclusion (see Figure 1). Pathways to be studied included (1) Mg/Ca Zintl electrolyte additives to increase Coulombic efficiency and increase cycle life, (2) PEO-oligomer surface modified silicon to increase cell power, and (3) utilization of lower pH PAA binder solutions to improve electrode quality. Preliminary screening and scale up efforts were initiated and updated regularly with CAMP and program leads. For the cell builds, two cathodes were examined – HE5050 Li_2MnO_3-Li(NMC)O_2 (Toda) and NMC532. The NMC532 was a standard from the EERE/VTO HEHV program and has a typical capacity of 180 mAh/g (to 4.1V) while the HE5050, from the EERE/VTO Voltage Fade program, delivers >220 mAh/g in a similar voltage window after a 4.5V activation step. Preliminary CAMP and Post Test studies indicated that at higher silicon electrode contents, the n:p ratio and other cell build variables could be thrown off by lithium losses (SEI, corrosion), poor utilization of the silicon, or electronic isolation of cathode particles due to the need for thicker positive electrodes to balance the cell. As available, electrodes used in the study were capacity matched with electrodes from the electrode library.

Cathode	Anode	Electrolyte
NMC	Paraclete Si	Gen2 + 10wt.% FEC
HE5050	Paraclete Si	Gen2 + 10wt.% FEC
NMC	Paraclete Si	Zintl-Phase Electrolyte
HE5050	Paraclete Si	Zintl-Phase Electrolyte
NMC	Surface Modified Silicon	Gen2 + 10wt.% FEC
HE5050	Surface Modified Silicon	Gen2 + 10wt.% FEC
NMC	Paraclete Si/ modified slurry	Gen2 + 10wt.% FEC
HE5050	Paraclete Si/ modified slurry	Gen2 + 10wt.% FEC

Figure 1. Cell Build matrix from CAMP for FY19Q4 Milestones

Electrode Stability: Studies from FY19 by CAMP, Armstrong, and Lu Zhang have identified a 'catch-22' in the creation of silicon-rich binders for the DeepDive program. The electrode slurries used were made near pH10 (aq.) by the reaction of LiOH with PAA(OH) to form LiPAA. Although higher pH solutions are known to dissolve surface passivation silica, the slurries demonstrated an optimum viscosity for the coating process

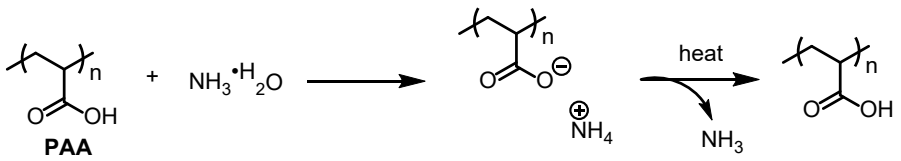

Figure 2. Reaction scheme for increasing slurry viscosity at lower pH based on ammonium coordination chemistry to PAA.

and the electrodes produced had the best electrochemical performance. Electrodes made with lower pH solutions had more visible clumping and a less uniform appearance. Zeta potential analysis on these slurries by ORNL indicated that to improve loadings and homogeneity, a higher silicon particle dispersion was achievable if created closer to pH7 (aq). In a collaborative study between the process groups, the LuZhang Group undertook an extended study of methods to increase viscosity of a more neutral pH solution of the binder, while maintaining electrode quality, in support of program milestones. A methodology based on using ammonium salts that could be added to the slurry mixture to temporarily increase viscosity and pH was identified. Upon casting, gentle heating released the ammonia to reform the more desirable neutral pH PAA binder solution. Extended testing of NH_3 • PAA binder system developed showed promise for year-end demonstration. When compared to baseline, PAA-NH_3 cells have higher initial and average capacity and better capacity retention than those of standard PAA-Li cells, however, the initial coulombic efficiency of PAA-NH_3 cells was lower than that of PAA-Li cells. It is speculated that this may be due to the reduction of acidic protons of PAA during the discharge process since pristine PAA cells also have lower initial coulombic efficiency than PAA-Li cells. In Figure 3, the cycling of these various compositions studied is shown, with significant variability in performance attesting to the critical role of the binder chemistry. However, for a DeepDive baseline study the lack of a defined optimum

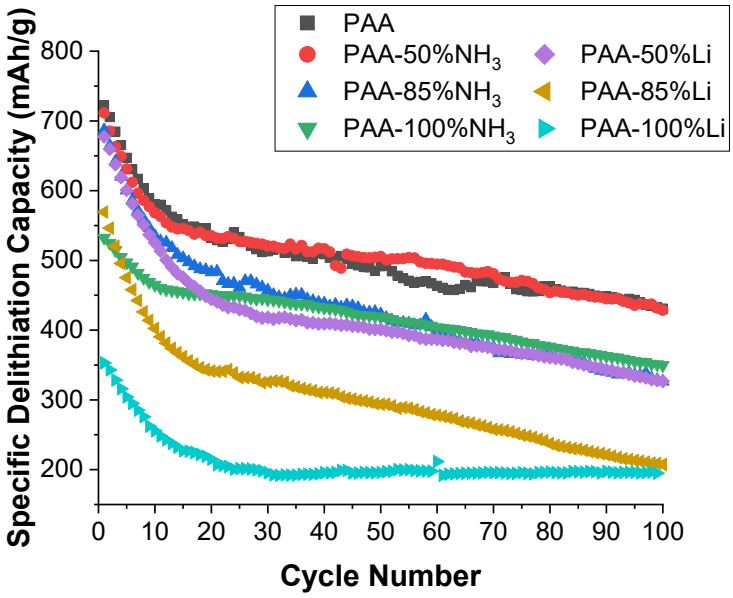

Figure 3. Cycling of a series of Si/Gr cells with various PAA-type binders developed.

stoichiometry at the time of cell build was identified by the team as not ready to be incorporated in the end of year program cell build and standard LiPAA was chosen for the evaluation.

Functionalized Silicon: As an alternative to the baseline Paraclete silicon, the team chose a collaborative silicon derived from surface modification of a hydride-terminated silicon material. The surface hydride ligand creates multiple opportunities to build in surface compositional control. The general synthetic process developed is shown in Figure 4 for a series of epoxy-ligands used by the ZZhang group.

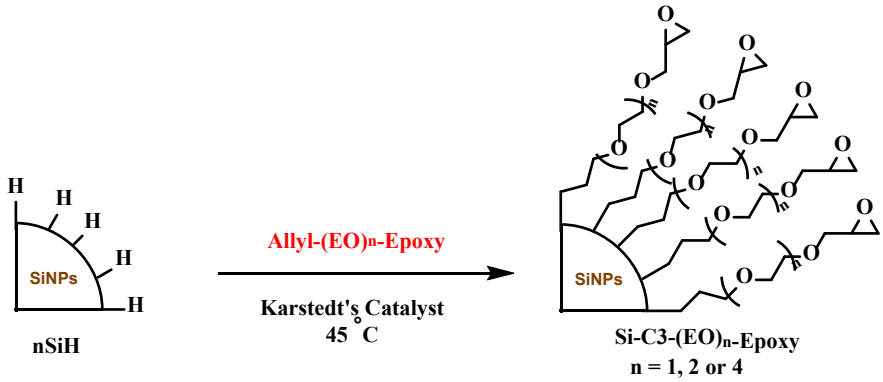

Figure 4. Generalized synthetic approach to create various functional silicon surfaces.

The initial samples of hydride terminated silicon were provided by the Neale Group at NREL, synthesized by a gas phase condensation reaction initiated from silane gas, SiH_4. As part of the SEISta effort, the Neale group has worked to control particle size, stability, and improve quantities of these materials to make them available to program participants. Based on preliminary evaluation from the Zhang Group, an EC-terminated sidechain was chosen for its similarities to the known electrolyte chemistry, SEI computability, and screening reactions.

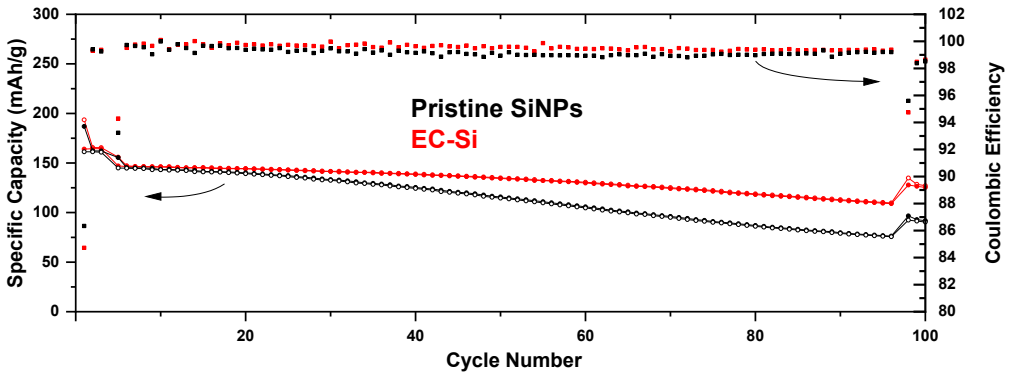

Figure 5. Cycling data for an ethylene carbonate (EC) substituted side chain

Cycling data is shown in Figure 5. Compared to silicon nanoparticles terminated by hydride anions (cycled against a NMC622 cathode), the EC sidechain material has a lower fade rate and appears more stable over early cycling (> 20cycles). Required scale-up of the desired material was undertaken by S. Jiang (ZZhang Group) and a modified process based on using hydrofluoric acid to partially dissolve the surface passivation silica layer was developed. Process studies and screening reactions have been discussed in recent F2F meetings (Jiang, F2F, Jan 2019). Using there process, H-Si materials could be scaled (50g) to meet CAMP cell build requirements. However, safety group requested process limitations limited production to 1-1.5g batches due to the HF waste stream and volumes. The effort was not chosen to go forward as part of the baseline study due to scale-up difficulties within the time frame allotted for the process and quality control concerns of combining ~50 small batches. The FY19Q4 cell build proceeded with baseline Paraclete silicon.

Studies using the Zintl additives have been discussed as a new DeepDive/SEISta thrust topic since Spring 2019. Mechanistically these additives have been identified as easy to add in-situ coating formers that significantly curtail surface reactions in a silicon electrode by formation of a $Li_{14}MgSi_4$-type phase at the surface that is redox-inactive but a good lithium-ion conductor. This barrier allows for good electrochemical contact while limiting the side reactions, self-discharge, and thicker SEI that may form due to excessive silicide reactivity. Figure 6 highlights the general flexibility of the additives and the breadth of materials that exist in this phase space. Screening work by ANL and NREL researchers identified optimum additives type, amounts, and voltage windows. The Key group purified and scaled the electrolytes and additives to the volumes required by CAMP. Cathodes for the study (NMC532, HE5050) were both provided by CAMP in thicknesses required based on preliminary results.

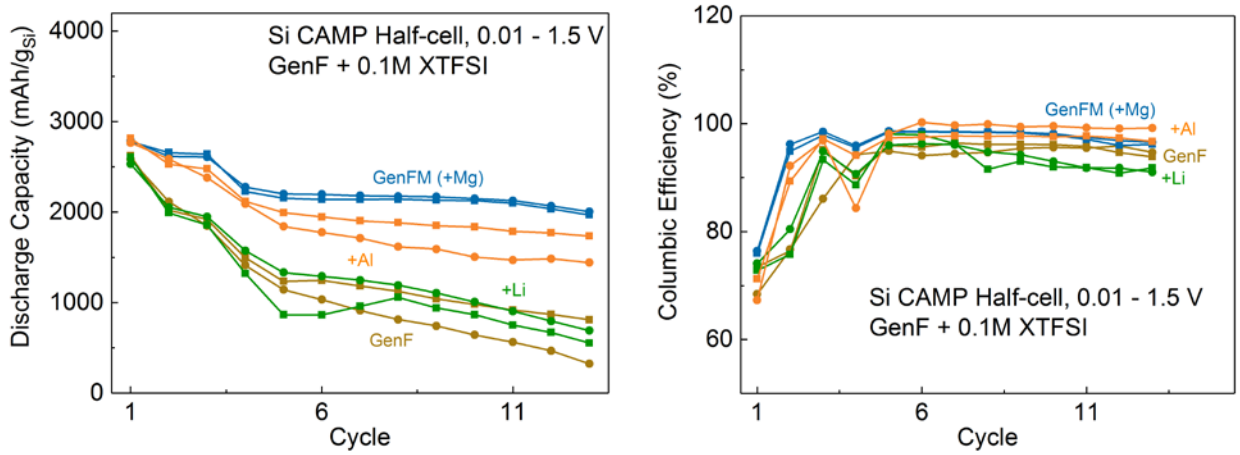

Figure 6. Effect of various cations on the cycling (Coulombic efficiency, capacity fade) properties of silicon-electrodes with in-situ formation of $Li_{14}XSi_4$ (X=Mg, Ca, Al, Zn) surface phases

Cell Builds: CAMP initiated cell testing was done using 80% silicon Paraclete baseline electrodes, two different cathodes (NMC532, HE5050), and two different Zintl additives ($Ca(TFSI)_2$, $Mg(TFSI)_2$) with baseline Gen2+10%FEC electrolytes. Electrolytes, provided by the Key Group, were purified and tested in coin cells before usage. For this study a single layer xx3450 pouch cell matrix was constructed, (4 cell repetition) and evaluated using the standard silicon DeepDive CAMP protocols. For testing the NMC532 was cycled in a 3.0 – 4.1 V window, while the HE5050 went through a standard 4.5V activation step, before following the same cycling routine.

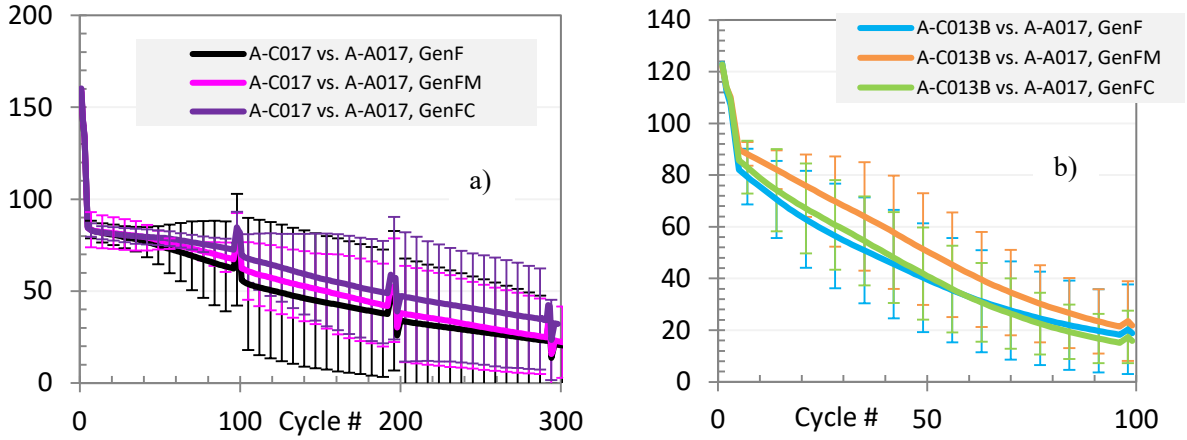

Figure 7. Cycling (300 cycles) silicon anode vs an a) HE5050 cathode and a b) NMC532 cathode (b) for systems with the three electrolyte additives. Top performer was the FEC/$Ca(TFSI)_2$ additive, followed by FEC/$Mg(TFSI)_2$, and FEC baseline.

Results: Extended cycling studies in pouch cells confirmed the positive effects on cycling life and performance of the Zintl additives. Performance in the higher capacity HE5050 cells (Figure 7a) was superior for cell life, cycles, and capacity retention compared to baseline. The improvements in long-term Coulombic efficiency are highlighted in Figure 8 (for the HE5050 cells). For the NMC532 based cells (see Figure 7b), cycling issues associated with capacity fade were noted and attributed to poor electrode matching and insufficient cathode capacity. Diagnostic studies on the both sets of cells by the Post Test facility indicated several issues associated

with electrode delamination for only the pouch cells. Data was provided to the BatPAC team for analysis. SEM photographs of the cycled pouch cells are shown in Figure 9.

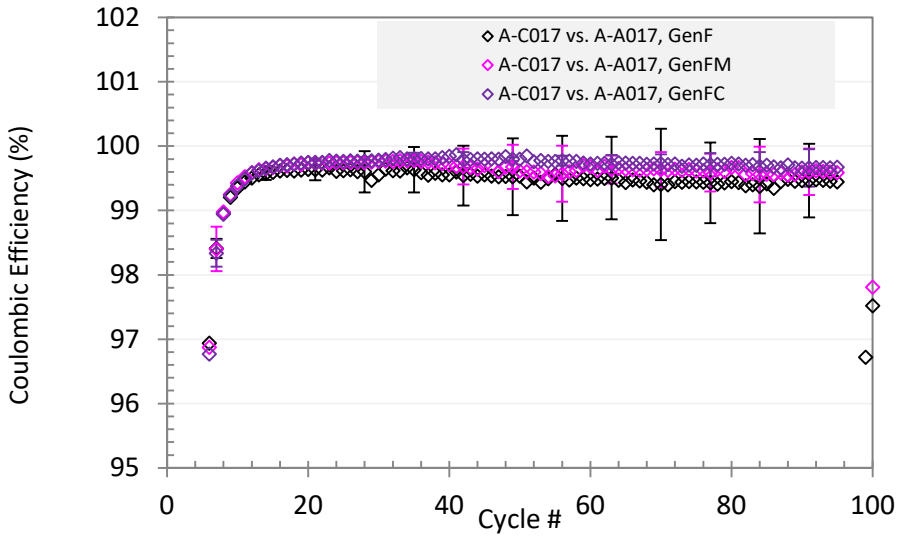

Figure 8. Coulombic efficiency of the HE5050/Si cells with various Zintl additives. FEC/$Ca(TFSI)_2$ based additives are the most stable and have the highest efficiency, followed by the FEC/$Mg(TFSI)_2$ additive, and the FEC only baseline.

Figure 9. Opened NMC532 cells highlighting delamination problems that are associated with premature cell failure during the baseline evaluation FY19Q4 testing.

Possible causes under consideration include current collector oxidation, pressure (evaluated - CAMP F2F Jan 2019), and tab weld stability. Further analysis of the NMC532 cells is underway at Post Test.

Further analysis of the electrochemical data has been performed by BatPAC researchers (Ahmed Group/ANL) to address cell optimization of cell parameters and design would have on performance. Based on the cycling data collected at CAMP, the Zintl additives had a positive impact on the overall performance of the cell. In both cases using HE5050, the actual data gave values of approximately 230 Wh/kg at the cell level. Under conditions used in the baseline model calculations, the performance data can be optimized within BatPAC. Under these conditions, the cells were found to deliver 265 Wh/kg, a 6% increase over the baseline. Analysis indicated the main issue effecting performance was high initial cell impedance. Post-test analysis and modeling indicate that it like arose from tab welds, current collector adhesion, or initial surface passivation issues. The measured values were near 100 Ω-cm, approximately 10X the value associated with commercial graphite electrodes, ~ 8 Ω-cm.

Within the model, it can be found that reducing the cell impedance to 25 Ω-cm (~3X graphitic electrodes) would raise the energy density to > 300 Wh/kg and has been identified as a future effort within DeepDive. The new cell electrolyte chemistries employed were successful in increasing the energy density of the baseline cells however issues associated with delamination, cell balancing, and electrode-binder interactions have been identified as the limiting factors in cell performance. The data from cell builds identified the need for a high capacity cathode (i.e. HE5050) to offset the higher capacities of a standard silicon-based powder electrode, while issues associated with binder failure and delamination on the anode are under investigation. The high resistance on cycling of these cells, although more typical for silicon-based systems, was higher than anticipated based on initial BatPAC models. Strategies to improve electrode conductivity and performance have been incorporated into FY20 research plans in association with ORNL, ANL, and NREL researchers after breakout sessions on the topic were held at the last F2F meeting.

Milestone Update FY2020Q1

Evaluate two new binder - slurry – silicon laminate combinations that lead to improved stability and a 15% improvement in performance compared to baseline for a high silicon-loading (>60%) electrode.

Electrode preparation and creation is a critical component of materials evaluation and guaranteeing that the materials under evaluation are consistent across the program. Provided by CAMP/ANL, the electrodes used in the program are a continuing effort based on available silicon (presently Paraclete Energy), binder processing, carbon additives, percent active, storage, and processing history. Advances in the experimental program can be fed into the electrode construction facilities for evaluation versus the baseline materials and, if better, be added to the baseline. Recent collaborative work between ORNL and ANL electrode development teams has been focusing on developing knowledge of the electrode slurry mixtures, binder pH, additives, and coating quality.

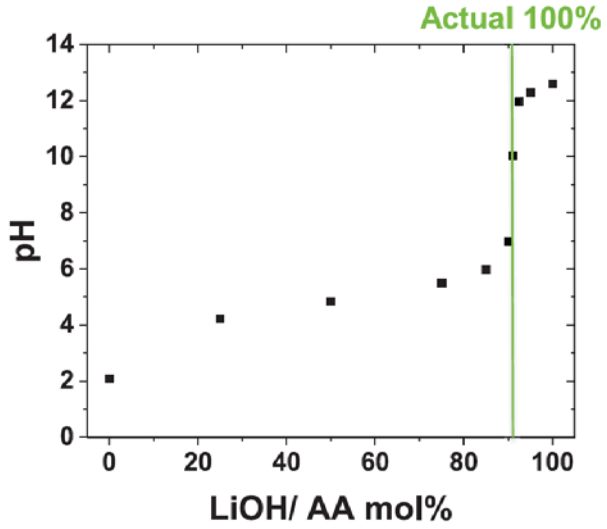

Figure 1. Titration curve for a LiOH – HPAA binder mixture highlighting the range of pH the slurry experiences. Initial CAMP slurry binders are processed near pH 10.

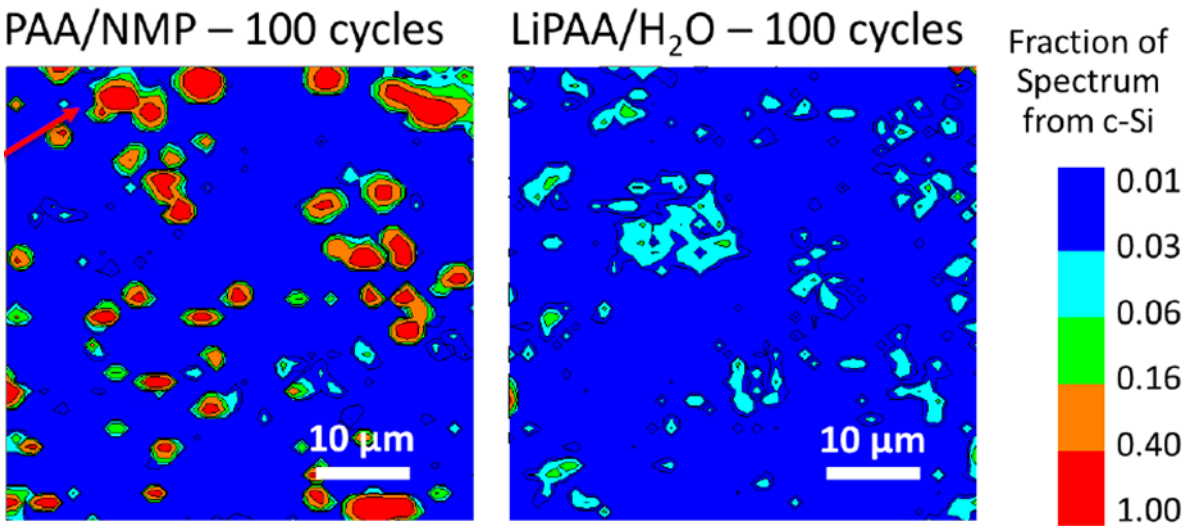

Figure 2. Raman study a PAA-based electrode vs LiPAA-based electrode. For the PAA based electrode, the amount of electronically (or ionically) isolated crystalline silicon is much higher than the same cycle electrode made with a LiPAA binder system.

In support of this FY20Q1 milestone, we report on our (1) understanding of the PAA binder chemistry involved, (2) silicon dispersion in the slurry, and (3) the role of carbon additives and stack pressure. As the PAA effort includes study information derived from LuZhang Groups FY19Q4 year-end milestone, the program is described in brief with emphasis on the aspects that are related to the slurry team interactions with ORNL and CAMP.

PAA Stability: The baseline CAMP silicon rich (80%) electrodes use an LiOH titrated PAA-based binder, coated onto copper foil. The titration is designed to replace the terminal protons with lithium cations, as seen in titration curve in Figure 1. This treatment utilizes an LiOH solution that effectively removes all the protons from the poly-acrylic acid (PAA) binder. Screening studies indicated that the LiPAA based binder was more uniform and was less likely to have isolated silicon particles after cycling (Figure 2), although CAMP analysis indicates the PAA-based electrodes had slightly better capacity utilization. Previous reported work in the program had shown that excess base (> pH11) resulted in inferior electrode quality possibly due to silica dissolution at high pH affecting surface chemistry and porosity. Although a possible quality control issue, based on electrode quality and initial performance testing, the higher pH10 slurry solutions were used since the slurry viscosity yielded higher quality electrodes. To gain a better understanding of the need for proton replacement, collaborative Zeta Potential slurry studies with ORNL were undertaken. Results indicated that a better dispersion of the baseline Paraclete silicon was found near more neutral pH slurry solutions (see Figure 3), especially with addition of an additional small molecular weight PAA dispersant.

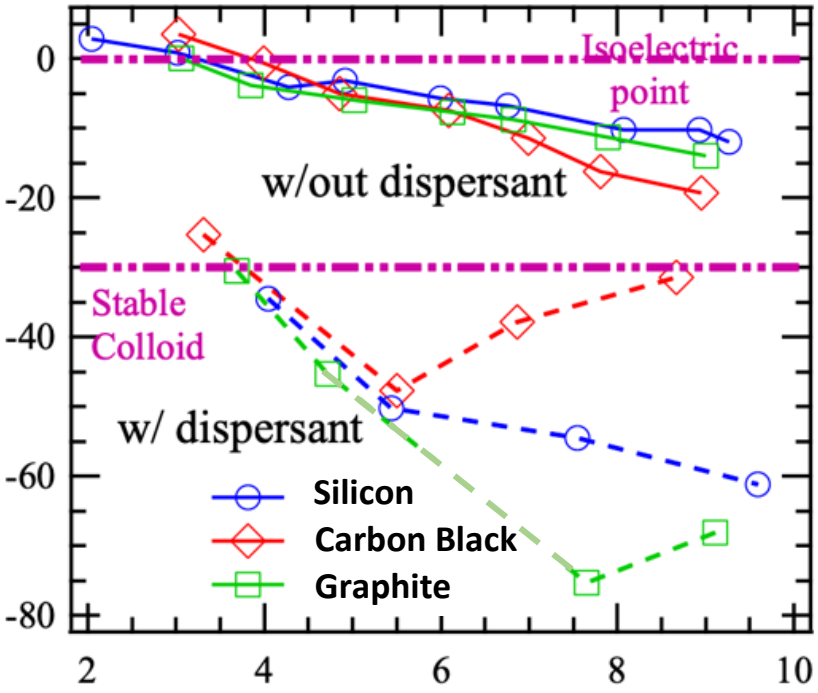

Figure 3. Stable silicon suspensions as a function of pH and electrode component. Most stable colloidal suspensions occur below -30 mV

Studies by CAMP with ORNL showed that electrodes created from neutral pH slurries without the use of a small molecular weight PAA dispersants, did not perform as well, consistent with Figure 2. Addition of the dispersant moved the silicon surface Zeta Potential response below -30mV, indicative of a stable colloidal dispersion. An analysis of the CAMP electrodes process was undertaken (Figure 4) to identify variables related to mixing order,

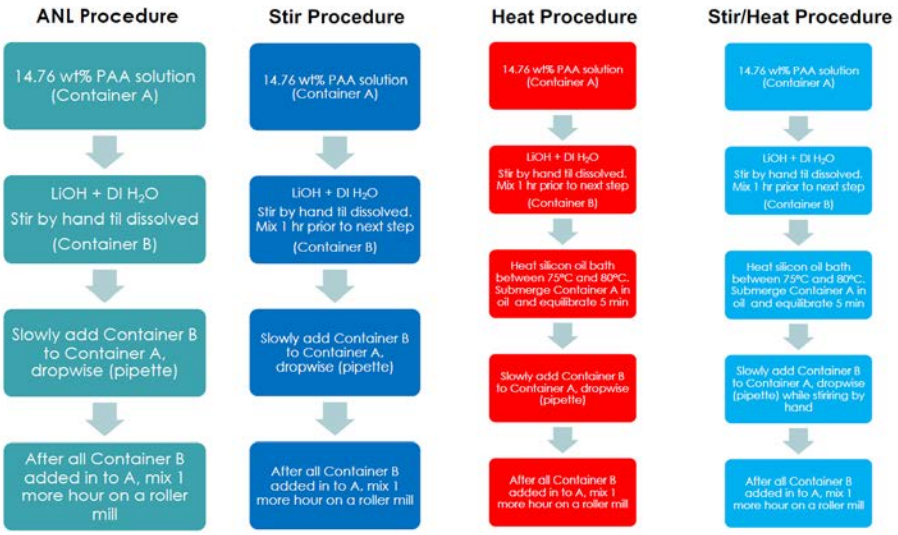

Figure 4. Analysis of CAMP/ANL slurry process to identify Processing Variables

heating steps, and timed steps that could play a role in electrode quality.

For this evaluation, the rheological properties of PAA and LiPAA aqueous binder solutions were measured as a function of mixing conditions. The shear rate/hysteresis behavior of the resulting solutions was studied to mimic CAMP casting protocols to evaluate the role of binder on the laminate stability and performance.

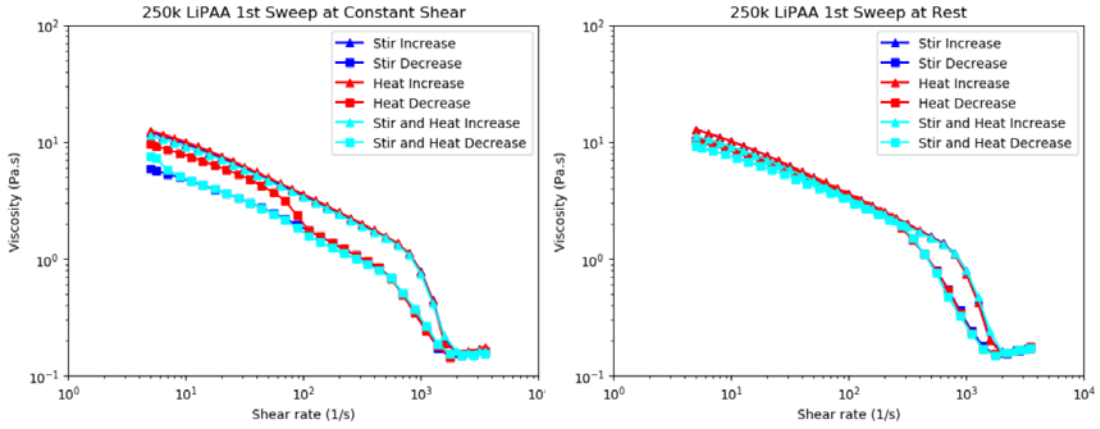

Figure 5. Viscosity of 250K MW LiPAA as a function of shear rate with varying mixing methods and a constant shear hold at 3500 s-1 and B) Viscosity of 250K MW LiPAA as a function of shear rate with varying mixing methods with a shear rest.

In the pursuit to reproduce CAMP procedures as well as define the stability/usage window of binder stock systems used to fabricate silicon-based electrodes, various aqueous solutions of PAA and LiPAA binders were prepared a function of mixing conditions, and the viscosity was evaluated over a range of shear rates in the electrode casting regime. Visual observation identified differences in PAA and LiPAA solution viscosities based on the method of fabrication. Initially, three methods were evaluated; 1) stirring, 2) stirring with the addition of

heat, and 3) heating. A viscosity shear rate sweep beginning at 5 and increasing to 3500 s^{-1}, an additional 5-minute hold at 3500 s^{-1} or 5-minute rest, and subsequent decreasing sweep back to 5 s^{-1} was conducted for each

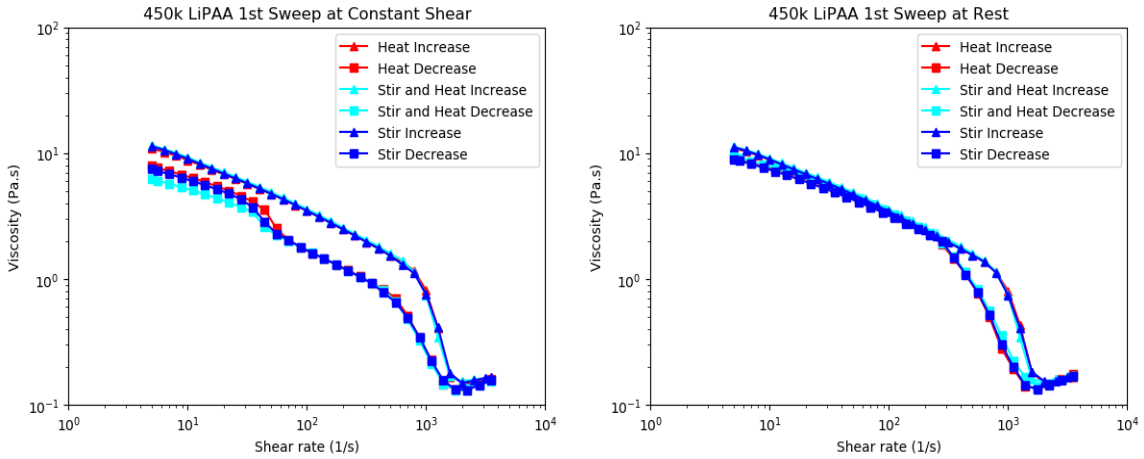

Figure 6. Viscosity of 450K MW LiPAA as a function of shear rate with varying mixing methods and a constant shear hold at 3500 s-1 and B) Viscosity of 450K MW LiPAA as a function of shear rate with varying mixing methods with a shear rest.

solution. The resulting flow behavior of the 250k or 450K molecular weight LiPAA solution, irrespective of mixing method, exhibited hysteresis behavior indicating structural changes are occurring in the polymer solution as a function of processing conditions. Figures 5 and 6, show the results. The hysteresis also appears to be dependent upon shear history. This hysteresis will further impact the recovery of the electrode slurry after casting, which in turn will impact the outcome of potential casting defects in the final electrode structure. Initial cell builds based on these observations (FY19Q4) were similar to baseline (see Figure 7), however interactions with the carbon black and other processing variables are being evaluated as uncontrolled variables.

Electrode ID	Binder Solution	Dispersant	Coating Loading Based off of Cell Build Punches	Porosity	First Cycle C/10 Discharge	1st Cycle Efficiency	Reversible C/10 Charge	Irrev Cap Loss
LN3174-113-2	450k PAA	NONE	1.13 [mg/cm²]	~54.9 [%]	1892 [mAh/g]	66 [%]	1235 [mAh/g]	35 [%]
LN3174-114-2	450k PAA	1.8k PAA	1.07 [mg/cm²]	~58.9 [%]	1909 [mAh/g]	67 [%]	1204 [mAh/g]	38 [%]
LN3174-115-4	450k Li-PAA	1.8k PAA	1.13 [mg/cm²]	~58.3 [%]	2164 [mAh/g]	68 [%]	810 [mAh/g]	63 [%]
LN3174-116-4	450k Li-PAA	NONE	1.13 [mg/cm²]	~54.9 [%]	2226 [mAh/g]	66 [%]	863 [mAh/g]	70 [%]

Figure 7. Preliminary cell testing analysis on the role of slurry dispersants with high silicon electrodes.

As an alternative to the LiOH neutralization scheme used presently, the LuZhang Group undertook an extended study of methods to increase viscosity of a more neutral pH solution of the binder, while maintaining electrode quality. A methodology based on using ammonium salts that could be added to the slurry mixture to temporarily increase viscosity and pH was identified. Upon casting, gentle heating released the ammonia to reform the more desirable neutral pH PAA binder solution. Figure 8 highlights the reaction pathway used. When compared to baseline, PAA-NH_3 cells have higher initial and average capacity and better capacity retention than those of standard PAA-Li cells, however, the initial coulombic efficiency of PAA-NH_3 cells was lower than that of PAA-

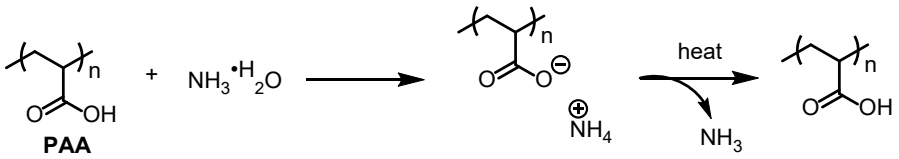

Figure 8. Reversible neutralization process for PAA based on NH_4OH rather than LiOH bases.

Li cells. This may be due to the reduction of acidic protons of PAA during the discharge process since pristine PAA cells also have lower initial coulombic efficiency than PAA-Li cells. Studies are moving to focus on working with CAMP and ORNL to assess the protons activity on the slurry mixture on cycling.

In addition to assessing the role of slurry pH, neutralization methodology, PAA polymer molecular weight, slurry viscosity, and various mixing parameters, the role of the high surface area conductive carbon additives was also evaluated. These carbons can be a source of protons, act as a template for catalytic reactions, or migrate to alter electronic isolation of the active silicon (see Figure 2). For these high silicon electrodes studied, the C45 carbon was mainly replaced by two alternative battery carbons, namely SFG-6 flake graphite or Kureha Hard Carbon. Electrodes that uses these carbons were acceptable but showed evidence of clumping and non-homogeneities that may affect performance. Figure 9 highlights the full cell electrochemical performance of these electrodes. In general, the hard carbons had the highest Coulombic efficiency and lowest fade rate and capacity. The

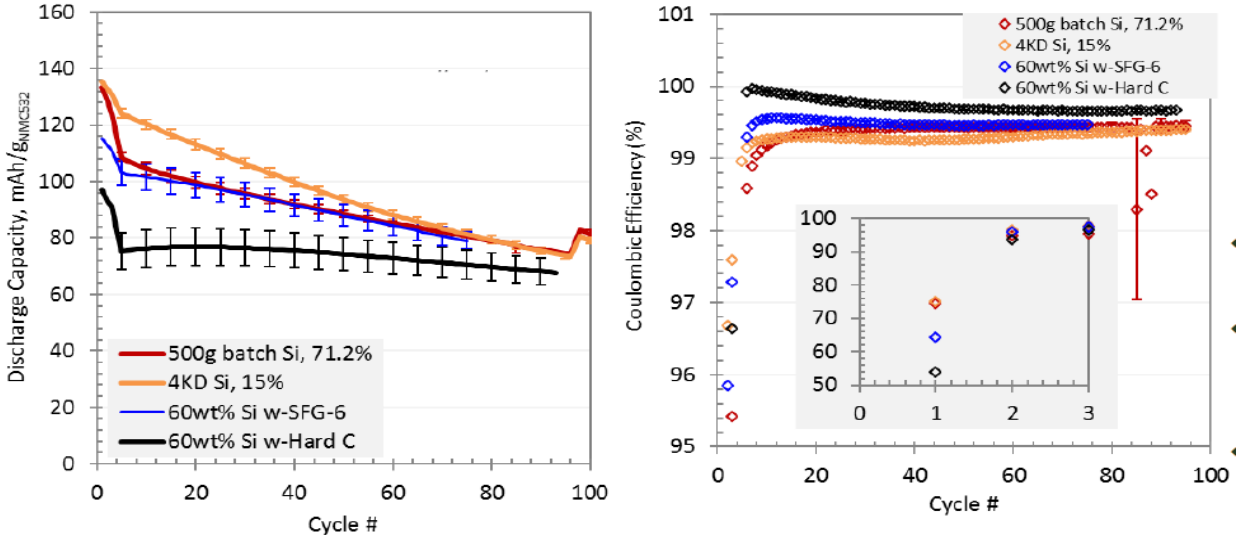

Figure 9. Full Cell performance of the various carbon additives evaluated for their role in electrode performance.

graphitic carbon SFG-6 had much higher capacity, but a lower CE. For either conductive additive, no significant advantage versus the CAMP standard TIMCAL C45 was noted.

As noted in the FY19Q4 milestone discussion, the various types of high silicon electrodes studied have mechanical problems associated with the particle volume expansion, electrode homogeneity, current collector oxidation, and surface degradation and binder stability. For several of these electrodes, the Post-Test facility determined delamination issues associated with the binder-silicon-current collector was a significant cause of the higher than expected impedance. In an evaluation of this phenomena, the 80% silicon electrodes were studied

by the CAMP team as a function of pressure, to maintain the connection between the active material and the current collector. Various pressures were evaluated with some improvement in performance, a result in support of loss of contact being a cause of the higher impedance. In comparison to the baseline system (Gen2+FEC), the most improved performance was at 76 psi (~5 atm), where significant capacity remained with the lowest capacity fade rate. The performance was in line (see Figure 10) with the two Zintl additives measured at standard pressure and opens up the possibility of combining the two approaches.

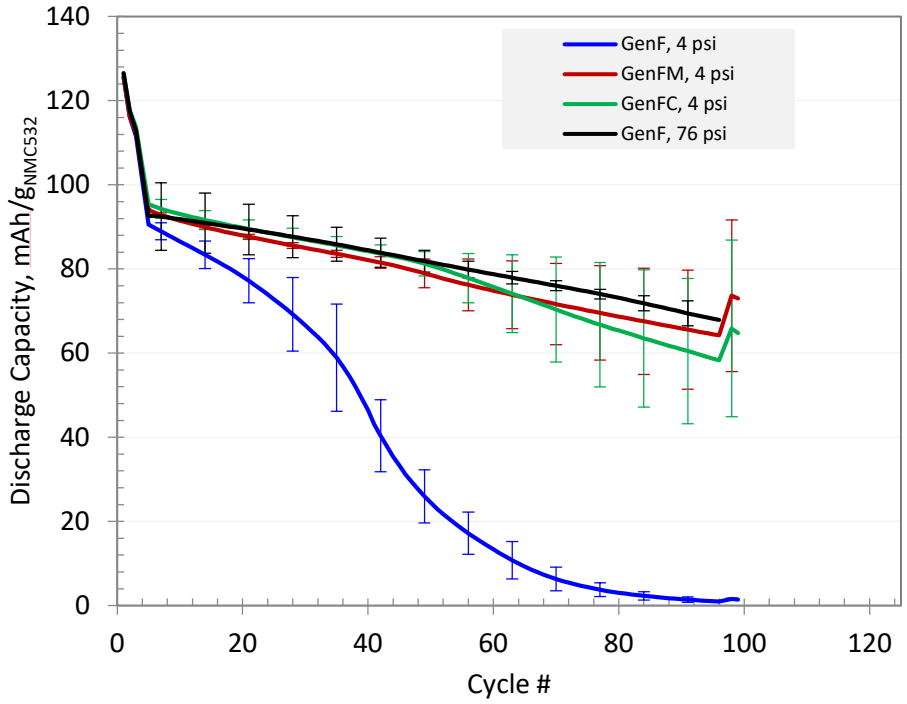

Figure 10. 80% silicon electrodes cycled with Zintl electrolyte additives and versus cell stack pressure.

Several slurry and lamination variables have been evaluated for their effect on the electrode and its electrochemical properties. Variables such as the type of carbon, the graphitic carbons and carbon black had similar performance, while higher capacity hard carbons (Kureha) showed stable performance, but with a hit in full cell capacity. Lithiating PAA was an important variable as it was a performance variable for slurry stability, silicon utilization (on cycling), and electrode quality. Cells constructed using LiPAA binders tended to show lower 1st cycle irreversibility, possibly due a small lithium concentration boost at the silicon-binder interface. Achieving a similar viscosity with an proton salt precursor rather than a lithium salt was achieved, however, no significant performance boost was noted. Changing the slurry properties by adding a dispersant (lower MW PAA polymers) was identified as a route to better slurry properties in terms of silicon dispersion and surface stability (lower pH), however issues associated with mixing order and properties were evident. Studies correlating processing history and slurry aging have been undertaken. Overall, several variables have been identified and evaluated in full cells. Many of these variables (proton concentration, stack pressure, silicon dispersion, PAA oligomer additives) were found to have a positive effect on the baseline anode material performance; variables including carbon type and non-Li pH adjustment, were found to not have a significant effect on performance. These studies have informed our efforts and research directions as issues associated with electrode stability, properties, and construction appear to be limiting overall energy density observations and have become a focus topic in the DeepDive effort.

Silicon Electrode Diagnostic Studies

Electrochemical Performance of High-Content Silicon Electrodes in Full Cells (ANL)

M.-T.F. Rodrigues, S. E. Trask, D.P. Abraham

Background

The use of blended silicon-graphite (Si-Gr) negative electrodes increases the energy density of lithium-ion cells over those containing only graphite (Gr) electrodes. However, volume changes in the silicon particles that occur during cycling causes deterioration of the solid-electrolyte interphase (SEI) layer on the particles resulting in further electrolyte reduction that immobilizes Li^+ ions and creates capacity fade. Various approaches are being actively pursued to improve the performance of silicon-based negative electrodes, which include

- optimally sized silicon to prevent particle fracture and minimize reactions with the electrolyte,
- appropriate binders that allow electronic conduction while maintaining electrode integrity during cycling,
- electrolyte additives that enhance the stability of the silicon particle-electrolyte interface, which is continually disrupted during silicon expansion and contraction exposing fresh surfaces for solid electrolyte interphase (SEI) formation that trap additional lithium.

Another approach is to zero the graphite content and increase the silicon content of the electrodes. This approach is being considered because silicon and graphite respond differently to the binder, electrolyte additives, and surface chemistry. For instance, it could be difficult to find a binder that is optimal for both silicon and graphite, as the silicon surfaces are hydrophilic, whereas graphite surfaces are hydrophobic. Additionally, it could be difficult to find an electrolyte that is optimal for both silicon and graphite; for example, 10 wt% FEC may be optimal for silicon, but 2 wt% FEC is optimal for graphite.

Here we present the electrochemical performance of full cells prepared using "4KD" silicon particles from Paraclete Energy; these silicon particles have a native oxide layer and no additional coatings. The composition and constitution of the electrodes used in the full cells are as follows:

- 80% 4KD Silicon, 10% carbon black, 10% LiPAA binder (CAMP A017) – Negative Electrode
- 90% NMC532 ($LiNi_{0.5}Mn_{0.3}Co_{0.2}O_2$), 5% carbon black, 5% PVdF (CAMP C013B) – Positive Electrode

Measurements were conducted in cells equipped with a reference electrode (RE). Each cell contained 20.3 cm^2 electrode disks spaced by two layers of a 25 µm thick microporous separator (Celgard 2325) and Gen2 + 10 wt% FEC electrolytes. Lithium metal was plated *in situ* onto the tip of a thin copper wire (25 µm dia.) to form a microprobe RE; this lithium RE was sandwiched between the separators and provided information on the positive and negative electrode potentials. The cells were tested on a Maccor cycler, using standard protocols.

Results

Using these electrodes, cell voltage and electrode potential profiles during cycling are shown in Figure 1. As the cell is cycled between 3-4.1 V, the true positive and negative electrode potentials at the end of charge and discharge gradually increase over the 100 cycles, and the cycling window narrows. For example, when the cell is charged from 3.0 to 4.1 V at cycle 2, the positive potential changes from 3.71V to 4.22 V; at cycle 99, the potential changes from 3.84 V to 4.3 V. The higher upper potential (4.3 V vs. 4.2 V at cycle 2) indicates increasing delithiation of the oxide during cycling and the narrower cycling window (0.46 V vs. 0.51 V at cycle 2) indicates ongoing capacity loss. This capacity loss results from a net loss of cycling Li ions, most likely from incorporation/immobilization in the solid electrolyte interphase (SEI) of the silicon negative electrode. Perhaps, more important are the potential variations at the negative electrode, which change from 0.71 to 0.12 V during cycle 2 and from 0.84 to 0.2V during cycle 99. The changes and the narrowing potential window indicate that

the silicon particles are being utilized less (less volume changes) as aging progresses, which would be expected to gradually decrease the rate of capacity fade.

The discharge capacities vs. cycle number for the NMC532/Si cell are shown in Figure 2. The specific capacities are listed per gram of the NMC532 oxide in the positive electrode (and also per gram of silicon in the negative electrode in parenthesis). The charge and discharge capacities during the 1st C/20 cycle are 180 (1700) and 118.3 (1117) mAh/g, yielding a coulombic efficiency (CE) of ~66 %. The CE reflects the loss of Li^+ ions to the SEI during the first charge cycle as the silicon expands during particle lithiation. The capacities continue to decrease during the early cycles indicating continued SEI formation. The charge and discharge capacities during the 3rd C/20 cycle are 109 (1027) and 103 (968) mAh/g, yielding a CE of ~94%, which indicates that Li^+ ions continue to be lost to the SEI. However, the 3rd cycle CE is greater than the 1st cycle CE indicating progressively decreasing Li^+ loss to the SEI with cycling.

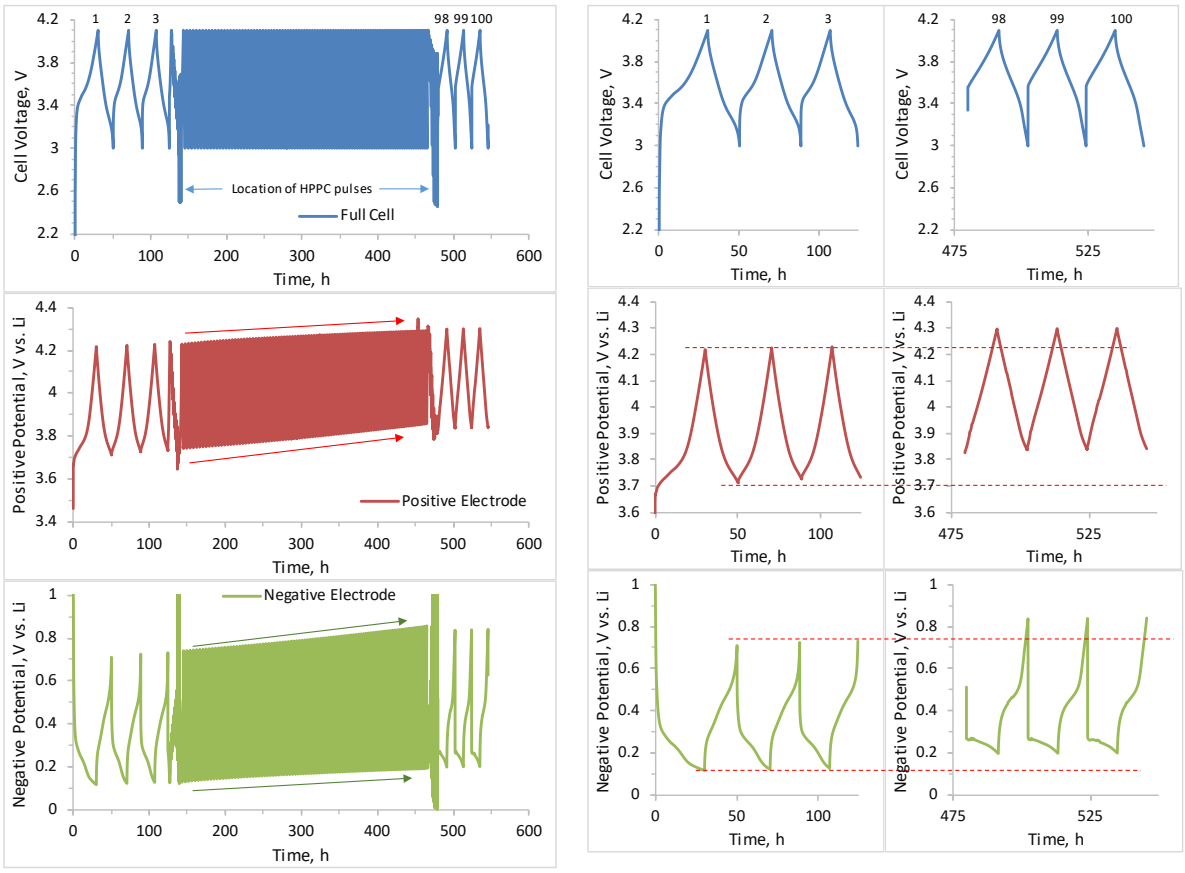

Figure 1 (Left Panel). Changes in the full cell voltage, and positive/negative electrode potentials during cycle-life aging (3-4.1 V, 30 °C) test of a NMC532/Si cell. Cycles 1-3 (formation) and cycles 98-100 (diagnostic) are at a ~C/20 rate, whereas cycles 4-97 (aging) are at a ~C/3 rate; all C-rates are based on the initial cell capacity. The Right Panels show details of the formation (1-3) and diagnostic (98-100) cycles.

When the cycling rate is increased to C/3, the CE increases and stabilizes around 99.4% for most of the cycles. The discharge capacity during cycle 4 (1st C/3 cycle) is 81.4 (769) mAh/g; the lower value (relative to the C/20 capacity) is indicative of cell impedance, which will be discussed later. During the 100th cycle (final C/20 cycle), the charge and discharge capacities are 64.3 (607.2) and 63.4 (599) mAh/g, yielding a CE of ~98.6 %. In general, the CE's are always slightly lower during the slower cycles, presumably because of the slightly higher capacity and the longer time available for SEI formation/consolidation. These capacity changes are shown in terms of

capacity retention versus cycle 2 (Figure 2, right panel). The retention is ~59% during the final cycle of the protocol, which is comparable to the values displayed by a full cell with the Si-15Gr electrode (data not shown). This similarity is because after some of the initial cycles, only silicon (no graphite) is cycled in the latter cell.

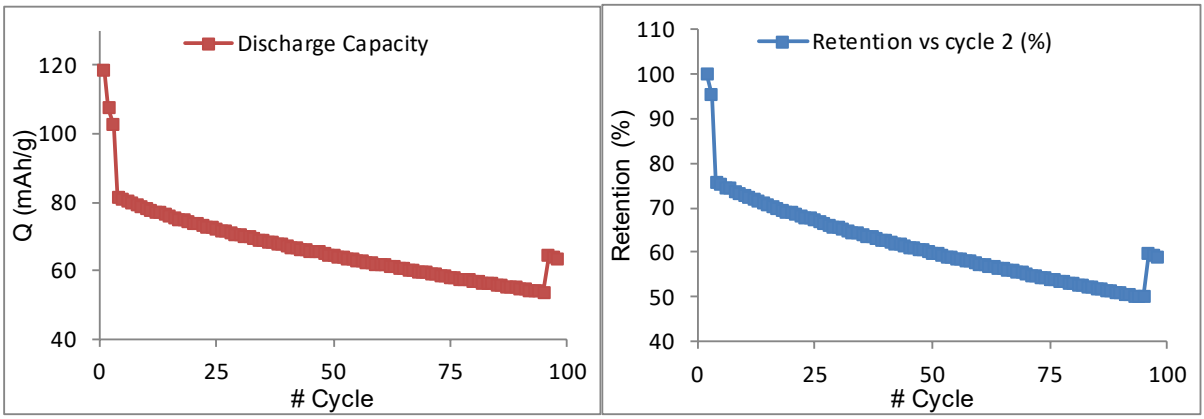

Figure 2. Discharge capacities (mAh/g-oxide, left panel) and capacity retention vs. cycle 2 (right panel) during the cycle-life aging (3-4.1 V, 30 °C) test of a NMC532/Si cell. Cycles 1-3 (formation) and cycles 98-100 (diagnostic) are at a ~C/20 rate, whereas cycles 4-97 (aging) are at a ~C/3 rate; all C-rates are based on the initial cell capacity.

An alternative view of the data are shown in Figure 3. Here cycle 2 and cycle 100 potential-capacity profiles, both obtained at C/20 rate, are shown as hysteresis plots. Observe the cycle 2 full cell data. The charge and discharge capacities are 120.1 and 107.5 mAh/g-oxide, respectively; the discharge curve only reaches 12.6 mAh/g because of this difference. Another noteworthy feature is the hysteresis between the charge and discharge curves; this feature is a consequence of the hysteresis in the negative (Si) electrode data. As the cell loses capacity, the successive cycles gradually move to the right. The red curve shows the cycle 100 full cell data; the data show a slightly greater hysteresis and significantly lower cell discharge capacity. The changes in the electrode data are also instructive. For cycle 100, the positive electrode cycles at higher potentials and shows a small hysteresis, which is not evident in the cycle 2 data (also see Figure 4). The cycle 100 negative electrode lithiation and delithiation potentials are also different from those of cycle 2; the profile shape differences suggest changes in the lithiated silicon that apparently result from the breaking and reformation of Li-Si bonds during the electrochemical cycling.

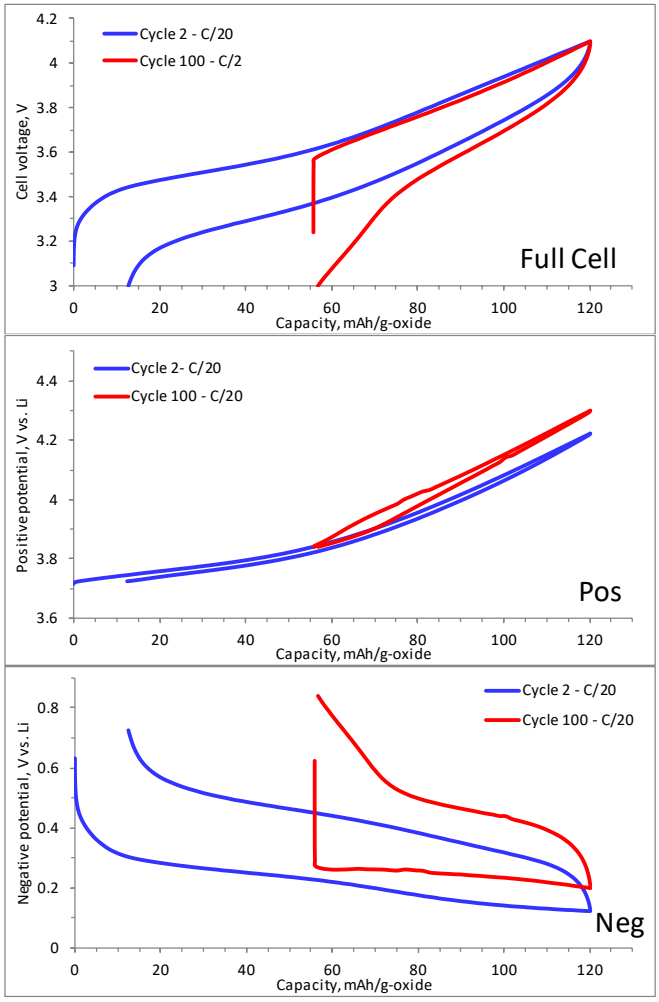

Figure 3. Potential-capacity profiles from cycle 2 (blue) and cycle 100 (red) of a NMC532/Si cell. The cycle-life aging (3-4.1 V, 30 °C) test alters the potential profiles and changes the hysteresis characteristics of the electrodes. The cycle 100 data is shifted to account for the discharge capacity loss displayed by the cell.

Cell impedance data were obtained, after the formation (initial) and C/3 aging cycles (final), using the hybrid pulse power characterization (HPPC) protocol. Impedance calculated from the HPPC tests provide a measure of the cell's ability to deliver and accept high current pulses. A typical HPPC test comprises repetitions of a pulse profile that contains constant-current discharge and charge pulses, followed by 10% depth of discharge (DOD) constant-current C/1 discharge segment, each followed by a 1 h rest period to allow the cell to return to equilibrium. Our protocol contained a 10s 3C discharge and a corresponding 10s 2.25C charge pulse separated by 40 s open circuit. The upper voltage cut-off limit was set to 4.3 V and the lower-voltage cut-off limit was set at 3.0 V. Discharge-pulse area specific impedance (ASI) data from the NMC532/Si cell are shown in Figure 5.

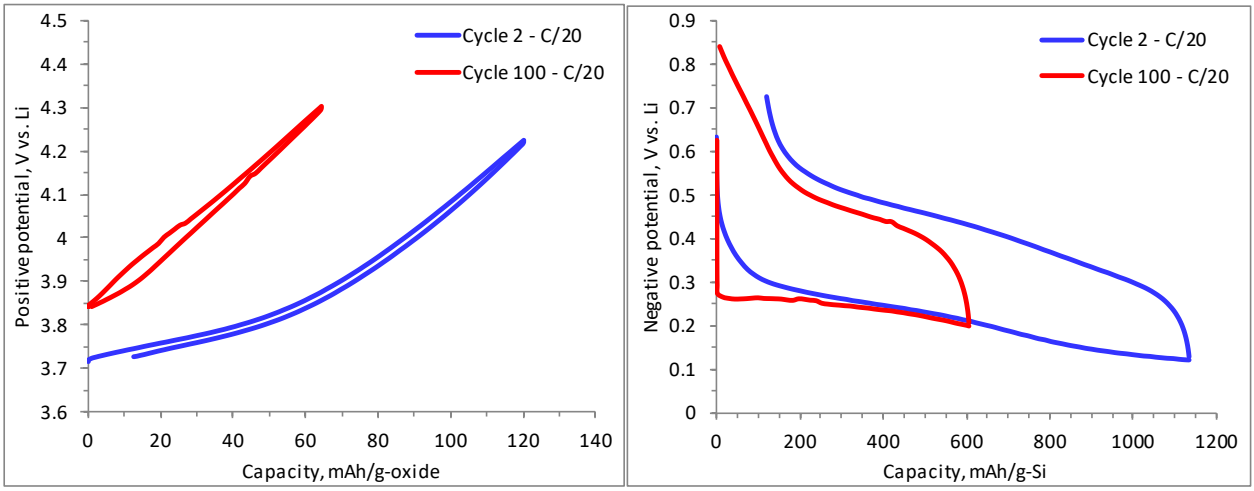

Figure 4. Potential-capacity profiles from cycle 2 (blue) and cycle 100 (red) of a NMC532/Si cell. These data are the same as those in Figure 3, but without the capacity-fade offsets. Also note that the capacity data are shown per gram of the active material in the electrode (per gram oxide for the positive and per gram silicon for the negative electrode).

Features that are evident in Figure 5 are as follows. Initially, after the formation cycle, the cell is able to sustain 7 pulses before hitting the voltage limits; in contrast, after aging, the cell is able to complete only 3 10s pulses. This difference is because of the (i) electrode potential shifts that are a consequence of capacity fade and (ii) increase in cell impedance during aging. Both electrodes contribute to the cell impedance, with the negative electrode being the larger contributor at lower cell voltages. Additional insights can be gained by replotting the ASI data as a function of electrode potentials, as shown in Figure 6. These data take into account the electrode potential shifts that occur during aging. For both electrodes the ASI at any given potential increases on aging; the increase is greater for the silicon electrode. Note that the data shown for a discharge pulse, during which the oxide is lithiated and the silicon is being delithiated. That is, the ASI reflects the difficulty of lithiating the oxide and delithiating the silicon; these processes become increasingly difficult with cycling, apparently because of changes in the electrode (including the active materials).

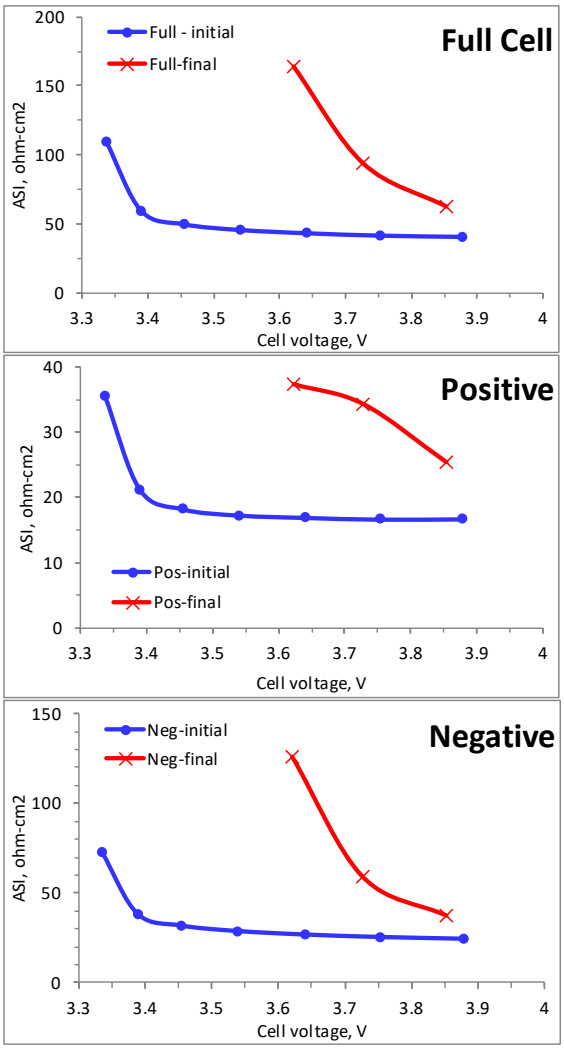

Figure 5. Discharge pulse (10 s, 3C, 30°C) ASI as a function of NMC532/Si cell voltage. Data shown are from the full cell, positive electrode and negative electrode, after the formation (initial) and aging (final) cycles. The markers indicate location of the pulse; the lines are guides for the eye. Note that the Y-axes scales are different for each plot.

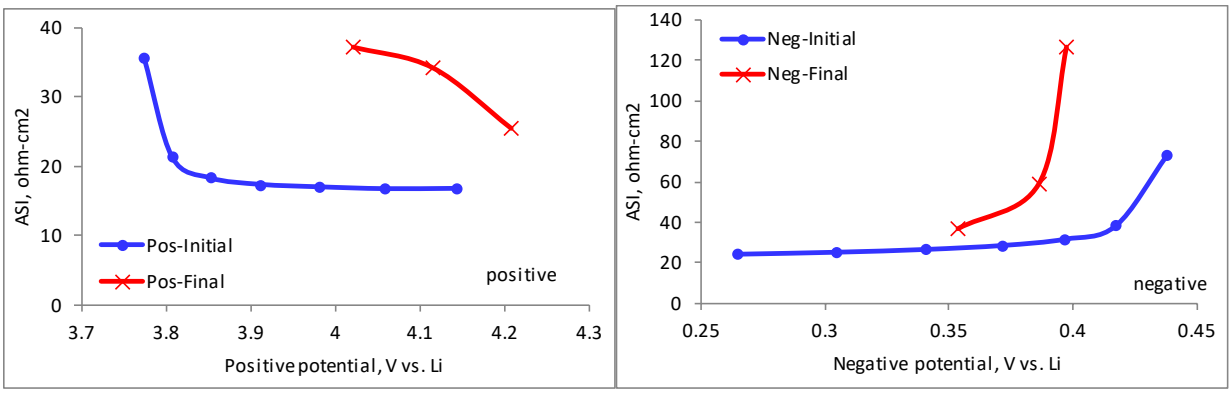

Figure 6. Discharge pulse (10 s, 3C, 30°C) ASI as a function of positive electrode (left) and negative electrode (right) potentials. Data shown are after the formation (initial) and aging (final) cycles. The markers indicate location of the pulse; the lines are guides for the eye. Note that the Y-axes scales are different for each plot.

Conclusions

We collected cycling data from an NMC532/80Si cell containing the Gen2 + 10 wt% FEC electrolytes. The highlights from our data are as follows:

- The positive and negative electrode potentials increase during the cycle-life aging. The positive potential increase could accelerate electrolyte oxidation and other deleterious reactions. Less silicon is cycled because of the negative cycling window changes; this would decrease the electrode volume expansion and hence reduce the rate of capacity fade as the aging progresses.
- Cell capacity retention after 100 cycles is ~59%; this value is similar to the retention of a full cell with a Si-15Gr electrode.
- An increase in voltage hysteresis is seen for both electrodes. The change is more significant for the silicon electrode, which may indicate changes to the silicon from the Li-Si bond breaking and reformation processes.
- The initial impedance of the silicon electrode is more than twice that of a typical graphite electrode.
- The increase in cell impedance is seen for both electrodes and is greater for the silicon electrode. The discharge pulse data indicates that it becomes increasingly difficult to lithiate the oxide and delithiate the silicon as the cycle-life aging progresses.

Silicon - Containing Anodes with Extended Cycle and Calendar Life (PNNL)

Ji-Guang Zhang, Xiaolin Li

Background

Nanoscale silicon or a highly porous structured silicon have been widely used as a solution to avoid pulverization of silicon particles that can occur for silicon particles > 150nm during cycling process. However, the large surface area of nanoscale silicon or micron sized porous silicon may lead to a continuous reaction between lithiated silicon and electrolyte. As a result, this reaction would lead to continuous growth of SEI layer and a gradual increase of cell impedance. Another possible degradation mechanism is the cross talk between silicon anode and cathode. Possibilities include (1) mitigation of dissolved Mn from the NMC cathode poisoning the silicon anode, (2) the transported Mn cations disrupting the ability of the SEI layer to efficiently transport Li to the interface by blocking available cation sites, and (3) the commonly used FEC additive may polymerize and form a film at the cathode electrolyte interface (CEI) leading to impedance increase. Therefore, minimizing the surface area of silicon and identifying a stable electrolyte are critical for long term stability of silicon-based Li-ion batteries.

In this project, we will develop new approaches to extend the cycle life and calendar life of silicon-based Li-ion batteries by designing a stable porous silicon structure. A more stable electrolyte will be developed to improve the mechanical strength and ionic conductivity of SEI layer. Micron sized silicon particles with nanoscale porosity and protected by an effective carbon coating will be developed to further minimize the interaction between silicon and electrolytes. The degradation mechanism of silicon anodes during shelf storage will also be systematically investigated to enable high energy Li-ion battery with silicon-based anodes and increase market penetration of EVs and PHEVs as required by DOE/EERE.

Results

In this quarter, we continued our studies on localized high concentration electrolytes (LHCE) and their applications towards silicon anodes. We tested BTFE (designated - La; bis(2,2,2-trifluoroethyl) ether) and TTE (designated - Lb; 1,1,2,2-tetrafluoroethyl-2,2,3,3-tetrafluoropropyl ether) based LHCE in full cells of NMC532||Si/Gr. The anode is composed of 88 wt% Si/Gr composite (BTR New Energy Materials, Shenzhen, Guangdong, PRC), 10 wt% polyimide (P84, HP POLYMER GmbH) and 2 wt% carbon black (C65, Imerys). The silicon loading level is 2.7 mg/cm^2. The cathode is provided by CAMP/ANL with a composition of 90 wt% $Li[Ni_{0.5}Mn_{0.3}Co_{0.2}]O_2$ (NMC532, Toda), 5 wt% carbon black (C45, Imerys), and 5 wt% polyvinylidene fluoride (Solef 5130, Solvay). The loading level and electrode density of the cathode is 11.4 mg/cm^2 and 2.7 g/cm^2, respectively. The loading level of each anode and cathode is set to establish an n:p ratio of 1.2 in the full-cell. Before performing a full-cell test, the silicon anode was pre-lithiated by cycling 3 times at a C-rate of 0.1C (=90 mA/g) in the 2032 coin-type half-cell with Li metal as a counter electrode. The operational voltage window is from 0.02 V to 1.5 V. After the silicon electrodes reached the fully delithiated state, they were collected by disassembling the cell. Then they were paired with a cathode for full-cell test in the 2032 coin-type cell. The full-cell is initially cycled for 3 cycles at the C-rate of 0.05C (=6.5 mA/g, where the weight is based on only cathode material), then further cycled at the C-rate of 0.33C (42.9 mA/g). The voltage window is between 3.0 V to 4.1 V. Figure 1 compares the cycling performance of Si/Gr||NMC532 full cells using baseline electrolyte (Gen2 + 10 wt% FEC) and La and Lb electrolytes, noted above. After formation cycling, the capacity retention of the cell using the baseline electrolyte is 80% after 200 cycles. In contrast, the capacity retention of the cell using La and Lb electrolytes are 94% and 88% after 200 cycles, respectively. A repeat run of a sample with electrolyte Lb (designated Lb-Re) in Figure 1. Figure 2 compares the coulombic efficiency (CE) of NMC532||Si/Gr full cells using baseline electrolyte and La or Lb electrolytes. At the 200th cycle, CE of cells using baseline electrolyte, La, Lb, and Lb-Re were 99.77%, 99.99%, and 99.95%, respectively. This trend is consistent with the trend of the capacity retention shown in Figure 1.

Micron size porous silicon (p-Si) with nanoscale porosity has been reported to be a good candidate to enable long term stability of a silicon-based anode. However, as produced porous silicon itself has a low electronic conductivity which is not suitable for LIB application. This has been addressed by Yi et al., (Adv. Energy Mater.2013, 3, 295–300) who improved the conductivity by developing a high cost CVD process to carbon coat p-Si. Realizing carbon coating was a useful adaption of the p-Si, we have developed a low cost, wet chemical process to coat carbon on p-Si with excellent electrochemical properties. The carbon coating was accomplished through a wet chemical method that utilizes a filling pores with pitch followed by a high temperature carbonization process. In this approach, the porous silicon was prepared by heating an "SiO" sample at elevated temperature to favor SiO_2 grain growth. This was followed by HF etching to remove SiO_2 formed in this process. Pitch, a well-studied graphite precursor, was coated on the porous silicon using an impregnation method at room temperature. The pitch precursor fill the pores but also coats the surface of p-Si therefore preserving porosity that can help accommodate the large volume change of silicon during cycling. The porous Si/C material was mixed with graphite in the ratio of 20:80 and cast into electrodes with conductive carbon and PI binder with the ratio of 88:1:11. The anode was pre-lithiated, harvested, and tested against NMC622 cathode in single layer ~60 mAh pouch (SLP) cells. Using our La LHCE electrolyte, the SLP was cycled between 2 to 4.35V at ~ 0.5C rate and capacity checked every 50 cycles at low rate. As shown in Figures 3 and 4, the two SLP cells showed excellent performance and repeatability. The capacity retention is ~95% over 200 cycles. The SLP capacity is ~53 mAh with ~90% first cycle coulombic efficiency (CE). The CE quickly increased and stabilized around ~99.8%. Further optimization of the porous Si/C material and LHCE is still undergoing.

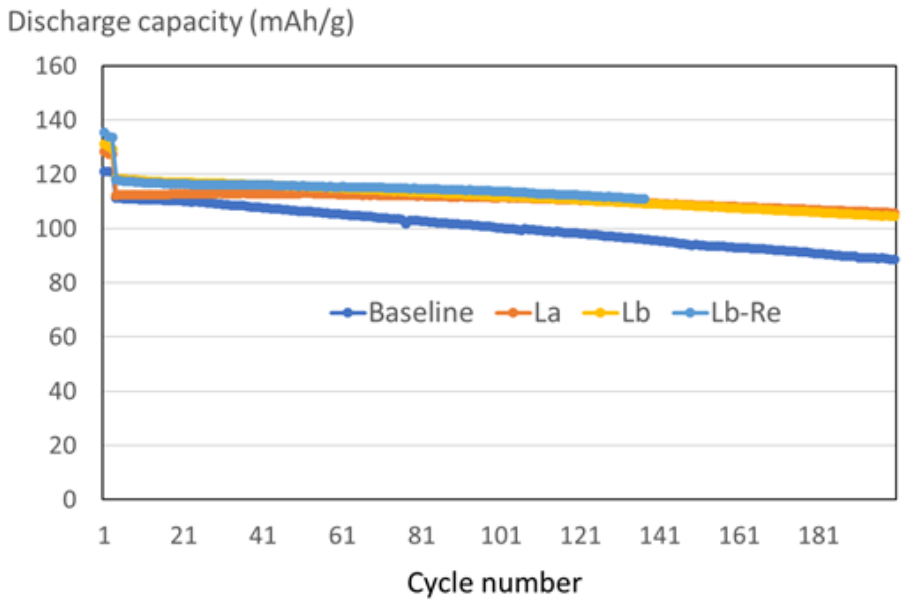

Figure 1. Capacity retention of NMC532||Si/Gr cells using baseline, La, and Lb electrolytes cycled between an operating voltage window of 3 to 4.1 V.

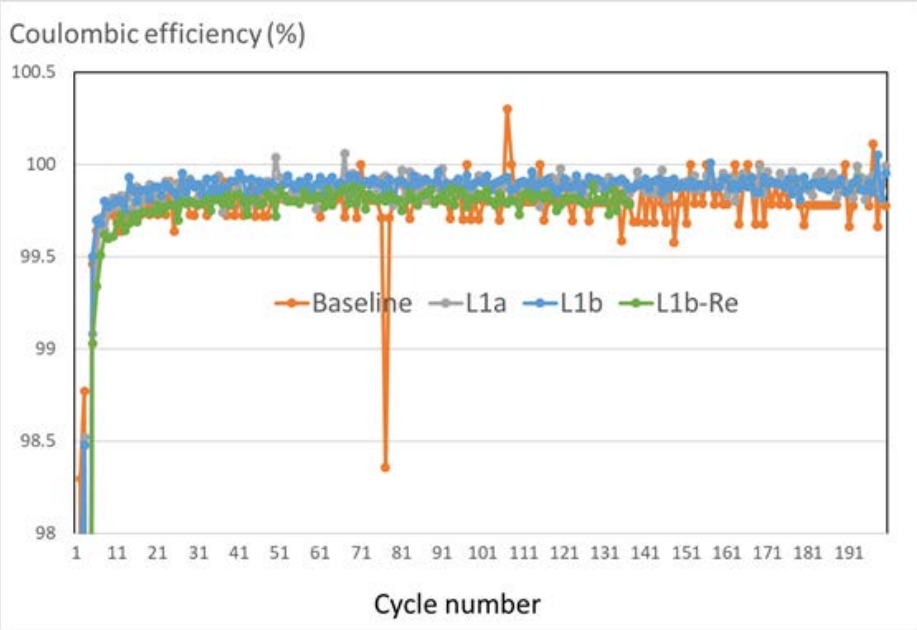

Figure 2. Coulombic efficiency of NMC532||Si/Gr cells using baseline, La, and Lb electrolytes cycled between an operating voltage window of 3 to 4.1 V.

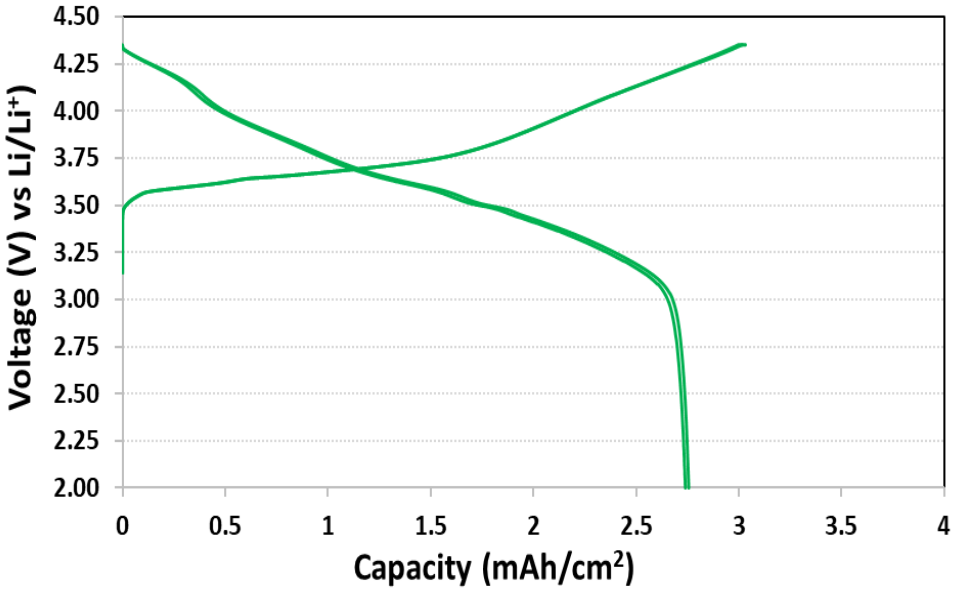

Figure 3. Electrochemical performance of the single layer pouch cell of p-Si/C||NMC622 using LHCE electrolyte La. 1st cycle charge/discharge curve.

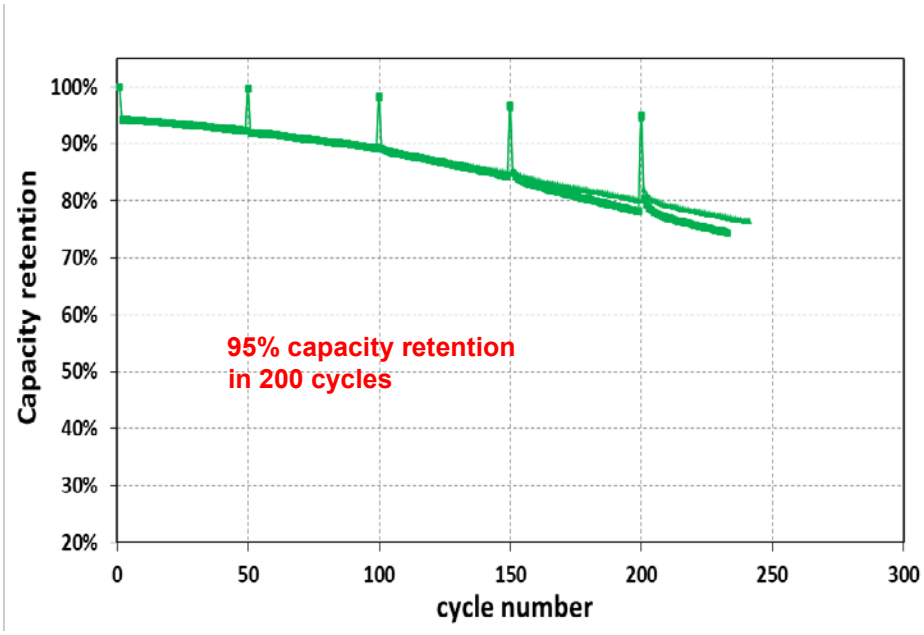

Figure 4. Electrochemical performance of the single layer pouch cell of p-Si/C||NMC622 using LHCE electrolyte La. Capacity retention.

Conclusions

LHCE electrolyte created with both BTFE and TTE diluents have been demonstrated to greatly improve the cycling stability of pre-lithiated silicon anodes. Full cell of p-Si/C||NMC622 with La electrolyte shows 94% capacity retention over 200 cycles with CE of ~99.7%. A low cost wet chemical process was developed to coat porous Si/C material using pitch as the precursor. The single layer pouch cells of p-Si/C||NMC622 has demonstrated 95% capacity retention in 200 cycles and will be a good candidate for large scale application of silicon-based LIBs.

Patent application/Publication/Presentation

1. "Methods to stabilize porous silicon structure to enable highly stable silicon anode for Li-ion batteries," Ji-Guang Zhang, Ran Yi, and Sujong Chae, U.S. patent filled on October 2019.
2. "Silicon-Based Anodes for Li-Ion Batteries," Sujong Chae et al. submitted for publication in Encyclopedia of Sustainability Science and Technology.
3. "Stabilization of silicon Anode using Carbonate based Localized High Concentration Electrolytes," Haiping Jia, Xiaolin Li, Xia Cao, Ran Yi, Qiuyan Li, Peiyuan Gao, Wu Xu, and Ji-Guang (Jason) Zhang, presented in 236th ECS Meeting, Atlanta, GA, October 16, 2019.
4. High Performance silicon Anodes Enabled by Nonflammable Localized High Concentration Electrolytes, Haiping Jia, Xu Wu, Xiaolin Li, and Ji-Guang Zhang, presented in 236th ECS Meeting, Atlanta, GA, October 13, 2019.

Composite Silicon-Tin Anodes for Lithium-Ion Batteries (LBNL)

Wei Tong (LBNL)

Background

In FY19, we successfully developed a co-sputtering process using a multi-target sputtering instrument to produce Si_xSn_{1-x} composite thin films with control of composition. When compared to single phase silicon thin film electrodes, Si-Sn electrode consistently exhibits better cycling performance when of similar thickness. Using these binder and carbon free film as model electrodes, we conducted preliminary post-mortem analysis and demonstrated that Sn additive delays but does not completely suppress the cracking of thin film electrode, suggesting cracking is not the primary governing factor for capacity fade of Si-based intermetallic electrodes. In this quarter, we continued to carry out post-mortem analysis of the cycled silicon and Si-Sn electrodes to understand the different cycling behavior.

Results

As previously reported, silicon and $Si_{0.62}Sn_{0.38}$ thin films were directly deposited onto Cu foils by magnetron sputtering using a single target of silicon and Si-Sn, respectively. Si_xSn_{1-x} composite thin films were produced by co-sputtering a silicon target and Sn target simultaneously, where the film composition was tuned during the film preparation. All the as-deposited films were subsequently stored under vacuum to prevent air exposure. 2032-type coin cells were assembled using the as-produced films (1.6 cm^2) directly as the working electrodes, Li metal foils as the counter electrodes, and 1.2 M $LiPF_6$ in ethylene carbonate-ethyl methyl carbonate (3:7 by weight) as the electrolyte (Gen2). The cell was galvanostatically lithiated to 0.01 V or cycled between 1.5 and 0.01 V at C/20 based on experimental capacity. The lithiated or cycled electrodes were harvested by opening the coin cells, rinsing with dimethyl carbonate (DMC) and passive drying inside an Ar-filled glovebox. The electrode samples were quickly transferred to scanning electron microscopy (SEM) chamber for morphological and compositional studies.

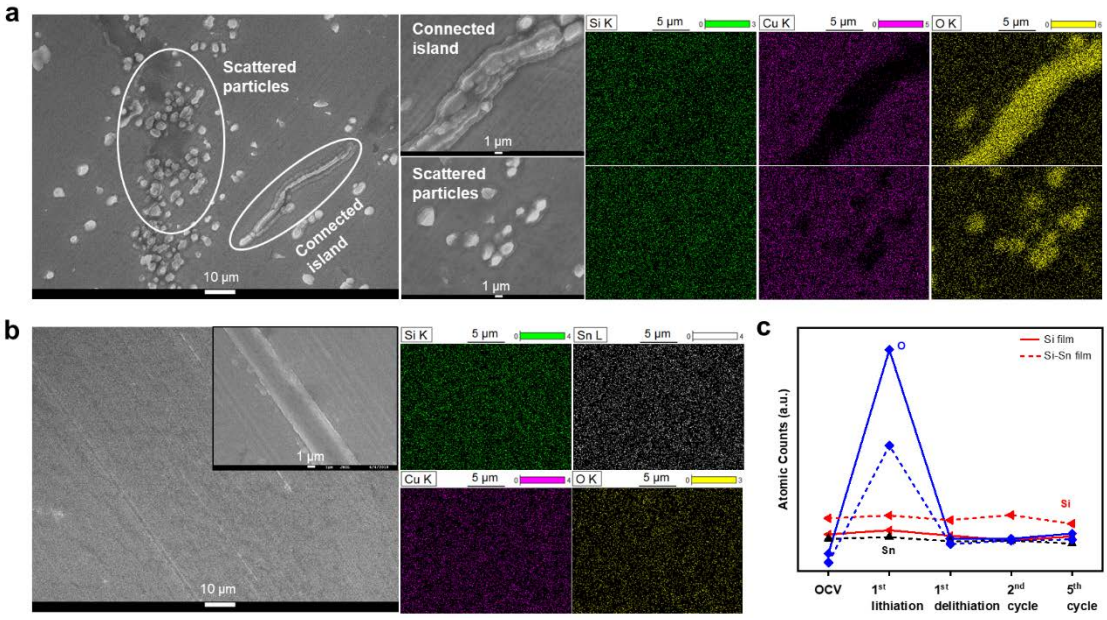

Figure 1. SEM images and EDS elemental mapping of (a) Si and (b) $Si_{0.62}Sn_{0.38}$ electrode films upon the first lithiation. (c) Elemental distribution of Si and $Si_{0.62}Sn_{0.38}$ electrode films at various states of charge upon electrochemical cycling.

Figure 1 shows the SEM images and energy-dispersive X-ray spectroscopy (EDS) elemental mapping after the first lithiation of silicon and $Si_{0.62}Sn_{0.38}$ films, respectively. As shown in **Figure 1a**, after the initial lithiation of silicon film, scattered particles at a scale of a few micrometers are found to distribute over the electrode surface, some of which are connected to exhibit strip-like feature. EDS mapping reveals the scattered and connected particles on the surface of the lithiated silicon film are oxide-rich (O-rich). In sharp contrast, the Si-Sn film after the first lithiation displays a uniform morphology and elemental distribution with the lack of such O-rich features (**Figure 1b**). We further examine the elemental distribution on the surface of silicon and Si-Sn films at different states of charge upon electrochemical cycling. For both electrode films, a dramatic increase in oxide content is observed at the first lithiated state, probably due to electrolyte solvent decomposition and solid electrolyte interphase (SEI) formation. Note that the oxide content on the lithiated silicon is almost double compared to that of the lithiated Si-Sn, consistent with the O-rich features revealed from the elemental mapping. Upon delithiation, the oxide content reduces to the level at pristine states for both electrode films, indicating the possible dissolution/decomposition of some SEI components during the delithiation process. The oxide content remains consistently low for silicon and Si-Sn at later delithiated states. These phenomena such as the variation of morphology and oxide content upon lithiation/delithiation of silicon and Si-Sn will be further investigated in a complete air-free environment to understand the possible relationship with electrochemical performance.

Conclusions

We continued to conduct an interfacial study on the cycled silicon vs. $Si_{0.62}Sn_{0.38}$ thin film electrodes. Beyond the observation of delayed electrode cracking upon cycling of Si-Sn electrode, SEM and EDS analysis reveal dramatically different morphology and elemental composition between silicon and Si-Sn upon initial lithiation. Lithiated silicon film surface exhibits O-rich particles/islands, which then disappear after delithiation; while the lithiated Si-Sn surface shows a uniform morphology and elemental distribution. Further post-mortem analysis in an air-free environment with a strong focus on oxide environment will be performed to understand these interfacial phenomena. Meanwhile, we will pursue the investigation of other metal additive to silicon to examine its impact on electrochemical response and interfacial properties.

Soluble SEI Species

Gao Liu (LBNL)

Background

The formation of solid electrolyte interphase (SEI) by electrolyte reaction or decomposition plays a crucial role enabling lithium-ion batteries (LIBs) as SEIs stabilizes the4 surface of the negative electrodes. In graphitic carbon systems with limited volume expansion on lithiation, the SEI layer is volumetrically stable and acts to extend cycle life significantly. Silicon is widely considered as a promising anode material for LIBs due to its high theoretical specific capacity. However, silicon alloy experiences dramatic volume expansion during the lithiation process, and undergoes reverse shrinking during delithiation process. The highly dynamic volume and surface area change promotes side reactions with the electrolyte, which often decrease the capacity and efficiency of LIBs. Organic and ceramic coating materials have proven effective for improvement of stability of silicon electrode surfaces. Electrolyte additives are often employed as sacrificial components for tuning the properties of silicon anode surface.

The objective of the present study is to develop a facile analytical protocol for separation and characterization of SEI and near SEI components for evaluation of additive's impact on silicon anode surface.

Results

We have established a gradient polarity solvent wash (gradient wash) technique for separation of SEI and near SEI components to facilitate characterization by Fourier transform infrared (FTIR) spectroscopy. Washing of electrodes before analysis is a common practice for battery research but is generally carried out with a single wash step and electrolyte solvents, which can often remove everything from the electrode surface, especially organic/polymeric species. The gradient wash technique utilizes a series of solvent washes with gradually increased polarities (i.e. 0%, 10%, 20%...100% ethyl acetate (EA)/ hexane (Hex)) to sequentially remove different SEI and near SEI components based on their chemical properties.

With this new concept of rationally controlled solvent wash technique, it was possible to expose the deeper components of the SEI and near SEI. As a model system, we utilized a TEGMA additive (Figure 1a, top) with its similar functionality to the PAA binder with a polyether side chain (a polar sidechain similar to the breakdown products of EC). It was found to polymerize effectively on Cu surface, but the polymer's signals on FTIR spectra overlapped with the adsorbed residue electrolyte species include solvent ethylene carbonate (EC) and the salt $LiPF_6$. A gradient wash was carried out to selectively remove the electrolyte species to confirm the presence of polymerized TEGMA on electrode surface. The gradient system was found to successfully separate the components and allow us to characterize the properties and identification of the degradation products.

Cu electrodes are electrochemically cycled with $LiPF_6$ ethylene carbonate/ethyl methyl carbonate (EC/EMC) electrolyte (Gen2) containing a TMA (a binder mimic with a non-polar sidechain) and TEGMA additive (Figure 1a, top) at 1, 10, 60 mV/min. The FTIR spectra of unwashed Cu electrodes are shown in Figure 1a. The two peaks around 1800 cm^{-1} are associated with EC and the peak at ~830 cm^{-1} is attributed to $LiPF_6$. It can be clearly seen that faster discharge rate (i.e. 10 and 60 mV/min) leads to significantly more EC/$LiPF_6$ adsorption, demonstrating that the discharge rate can have a key impact on near SEI layer. On the other hand, the additives have different behaviors based on their polarities. The non-polar TMA additive requires low discharge rate to undergo extensive polymerization. This is because that the non-polar nature of TMA repels the approach of polar bulk electrolyte and thus slows down the diffusion of TMA additive from bulk electrolyte phase to Cu surface. The polar TEGMA additive has no such problem and thus is found to smoothly polymerize under all discharge rates.

The gradient wash technique was preliminarily attempted on 500 nm silicon thin film electrode to demonstrate its feasibility on silicon anodes. The silicon electrodes were cycled at 10 mV/min with Gen2 electrolyte (no additive or with TMA/TEGMA). Without additive, the baseline Gen2 electrolyte produced lithium ethylene

di/mono-carbonate, along with adsorbed EC:$LiPF_6$. The gradient wash demonstrated that the adsorbed electrolyte species can be removed with 30% EA/Hex wash, which is consistent with the case of Cu electrode. After wash, the silicon electrode shows additional lithium silicon oxide product. Figure 1b and 1c shows the gradient wash results of silicon thin film electrodes cycled with TMA and TEGMA additives. The unwashed surface of silicon thin film electrode cycled with TMA additive presented poly-TMA (confirmed with synthetic sample), lithium ethylene di/mono-carbonate (1645, 1400, 1308 1070 cm^{-1}) and $LiPF_6$ (835 cm^{-1}) as shown in Figure 1b. These species were gradually washed off to leave a broad peak at 1433 cm^{-1}, which is attributed to a mixture of carboxylate salts and Li_2CO_3. No significant electrolyte adsorption was observed as the poly-TMA layer repulses bulk electrolyte. The TEGMA additive also formed poly-TEGMA (Figure 1c) on silicon electrode. The unwashed silicon surface presented EC:$LiPF_6$ (1802, 1771, 1406, 1188, 1084, 858 cm^{-1}) and lithium ethylene di/mono-carbonate (1632, 1316 cm^{-1}), which were gradually washed off to expose the poly-TEGMA film beneath (50% EA/Hex washed), as confirmed with synthetic poly-TEMGA. After washing procedures, $LiHCO_3$ (1601 cm^{-1}) and Li_2CO_3 (1502, 1454 cm^{-1}) could be identified unambiguously (Figure 1c, EA washed).

In conclusion, gradient polarity solvent wash of electrode surface was employed to characterize both model Cu electrodes and silicon electrodes. The decomposition products of EC-based electrolyte as well as the additive polymerization products are identified with FTIR spectroscopy in both cases. This methodology has proven to be a universal tool for battery electrode treatment. It serves as crucial complementary approach to reveal the deep SEI and near SEI components, and also helps spectroscopic analysis by demonstrating the internal correlations of different signals

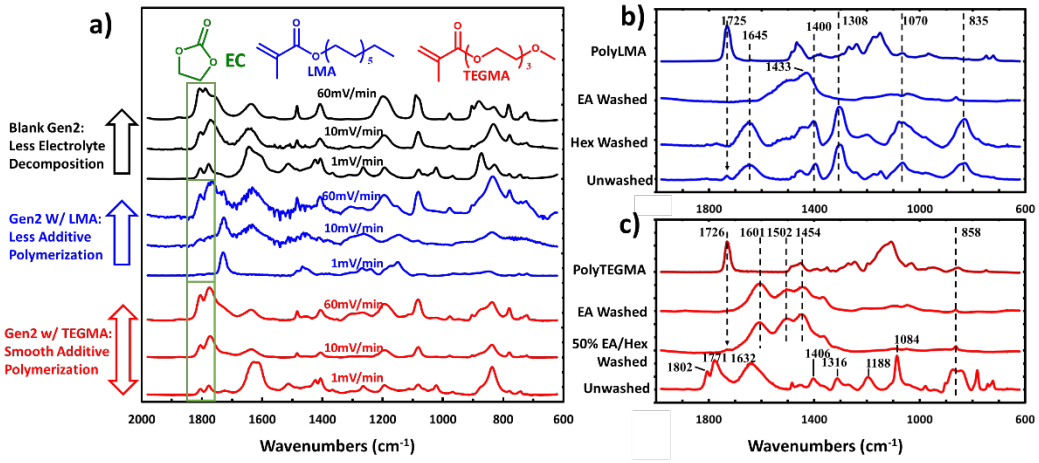

Figure 1 a) FTIR spectra of unwashed Cu electrode surfaces cycled at different discharge rates. b) FTIR spectra of Si thin film electrode cycled with TMA additive. c) FTIR spectra of Si thin film electrode cycled with TEGMA additive.

Conclusions

Gradient wash studies on these model electrode systems (no silicon) have been conducted. Molecules with polar groups were found to wash out even after surface polymerization, whereas models with non-polar sidechains were retained. When used in conjunction with a silicon thin film electrode, the unwashed surface of silicon thin film electrode was cycled with a TMA model compound and was found to form a poly-TMA, lithium ethylene di/mono-carbonate on the surface (by FTIR). These species were gradually washed off to leave a mixture of carboxylate salts and Li_2CO_3. Due to the non-polar sidechain, no significant electrolyte adsorption was observed as the poly-TMA layer as it repulses the polar components of the bulk electrolyte. The TEGMA molecule formed poly-TEGMA (Figure 1c) on silicon electrode. The unwashed silicon surface was found to be populated by electrolyte solvents and the breakdown products lithium ethylene di/mono-carbonate. After washing the poly-TEGMA film beneath (50% EA/Hex washed) was exposed. Further silicon electrode studies are planned.

Electrochemical Analysis of Si SEI (ANL)

Sisi Jiang, Zhengcheng Zhang, Zhangxing Shi, Lu Zhang, Gabriel Veith (ORNL), Christopher Johnson

Background

In association with the surface functionalization (led by J. Zhang) and model organic molecule synthesis (led by L. Zhang) DeepDive teams, this project seeks to understand the role of soluble species in the stabilization of the SEI on using a rotating ring disk electrode (RRDE) design with bi-potentiostat located in the Ar glovebox. A study of the trapping of lithium in the SEI and the electron transfer and stability of the SEI will be conducted. The following are the objectives moving forward.

- Measure by-products from electrochemical/chemical reactions that occur.
- Determine the location of the electron transfer event during (de)lithiation: for example, at the exterior of the SEI, interior of SEI, or the interface of SEI/Si buried surface.
- Studying any redox active products at the ring electrode coming of the material at the disk where the rotation speed will also allow us to probe the kinetics of the reactions.
- Study the nature of the silicon surface effect which can greatly affect the composition and thickness of the SEI layer.

Results

The evaluation of electrochemical reaction of TEMPO molecule with Si-N-type disk electrode and glassy carbon disk electrode were evaluated by means of cyclic voltammetry (CV) methods. The objective is to use this redox probe molecule to interrogate and evaluate the integrity and compactness of the SI SEI; the TEMPO must oxidize or reduce at the silicon electrode surface via electron tunneling through the SEI film. Figure 1 shows the CV response at the glassy carbon electrode that demonstrates ideal reversible electrochemical reaction behavior.

Based on these studies, TEMPO appears much more stable in the Gen2 electrolyte system over time as compared to ferrocene CV results (as reported in the 4th quarter of FY 2019 report). Figure 2 is the reaction of TEMPO at an idealized clean polished surface of a N-type doped silicon disk electrode; the electrochemical reversibility at the silicon electrode for this reaction is excellent.

The silicon N-type disk electrode was subjected to electrochemical discharge reaction (lithiation) in Gen2 electrolyte. Note that Figure 3 contains the results of this experiment. The SEI formation and the lithiation of this silicon electrode disk is occurring at the lower voltages. The formation of the SEI then totally blocks the electrochemical reaction of TEMPO molecule (20 mM) at the silicon surface. No current is observable, no diffusive behavior nor penetration of the TEMPO is possible. The electrochemical behavior is simply resistive.

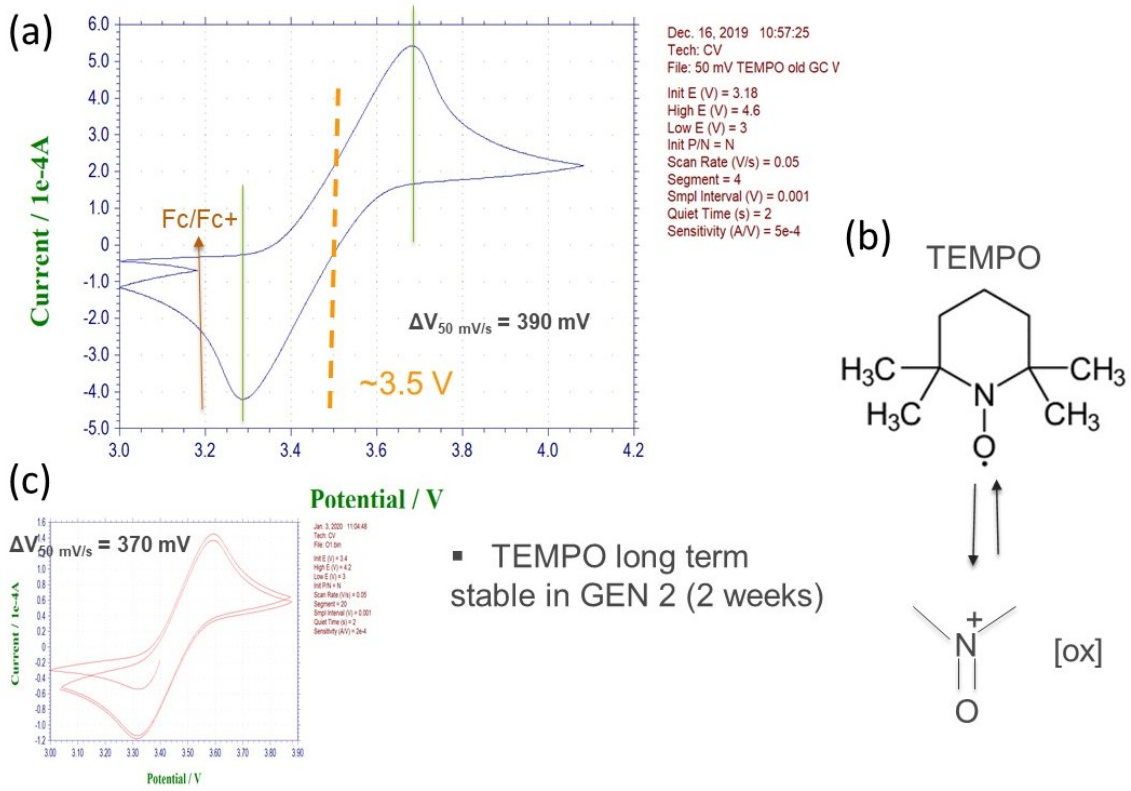

Fig.1. Glassy carbon disk electrode voltammetric (50 mV/s) results shown for the (a) electrochemical reaction of TEMPO (20 mM) in Gen2 electrolyte. (b) is the structure of the TEMPO molecule and its electrochemical reversible reaction. (c) shows the stability of the TEMPO molecule in Gen2 electrolyte over 2 week period. All voltages are versus a Li metal RE.

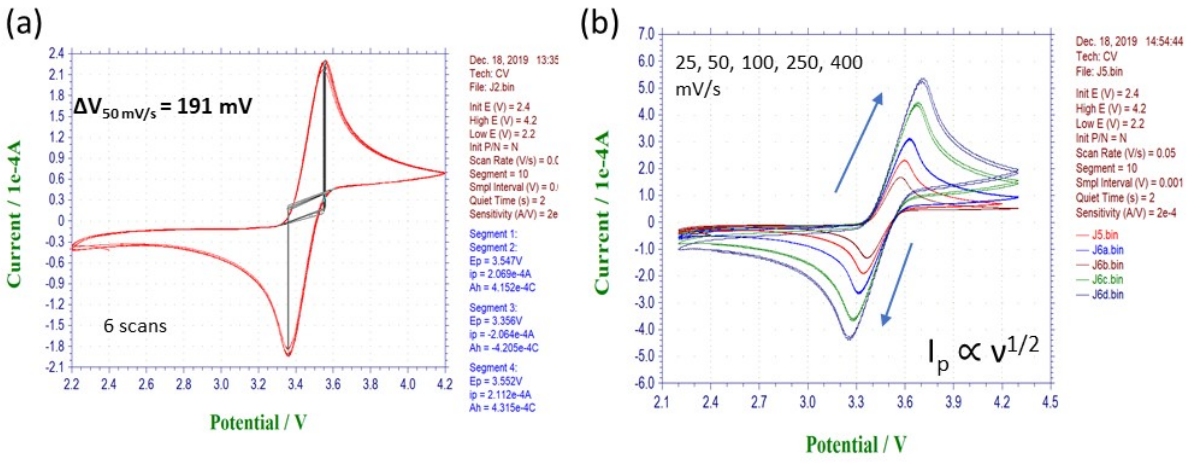

Fig.2. silicon N-type disk electrode voltammetric (50 mv/s) results shown for the (a) electrochemical reaction of TEMPO (20 mM) in Gen2 electrolyte. (b) is the sweep rate dependence that indicates ideal Randles-Sevcik molecular diffusion behavior of TEMPO at the un-modified 'clean' and SEI-free silicon electrode surface. The peak current is proportional to the sweep rate to the ½ power.

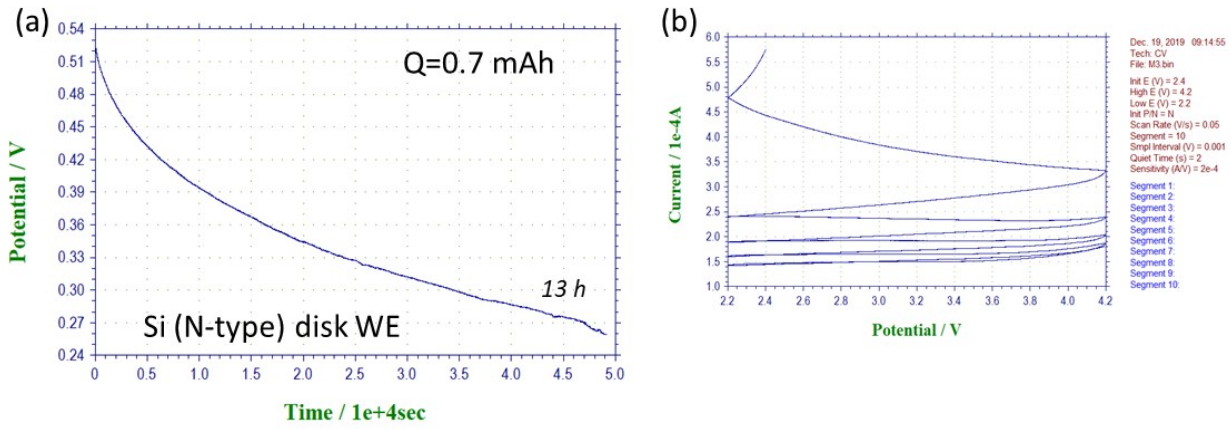

Fig.3. silicon N-type disk electrode (a) chronopotentiometric voltage versus time curve for the SEI formation and lithiation of the silicon electrode. (b) are the CV results (50 mV/s) of the cycling of TEMPO molecule (20 mM) in Gen2 at this electrode produced in (a)

Following the discharge, the Li_xSi electrode was charged to 0.6 V in order to de-lithiate the surface. As a result, the TEMPO molecule now shows electrochemical sluggish reversibility (Fig. 4) reactivity with the silicon electrode surface that indicates possible porosity of the SEI upon charge. This behavior might be associated with a poorly formed intrinsically 'oxidized' SEI with different morphological and/or electronic properties than the silicon SEI operating at lithiation potentials.

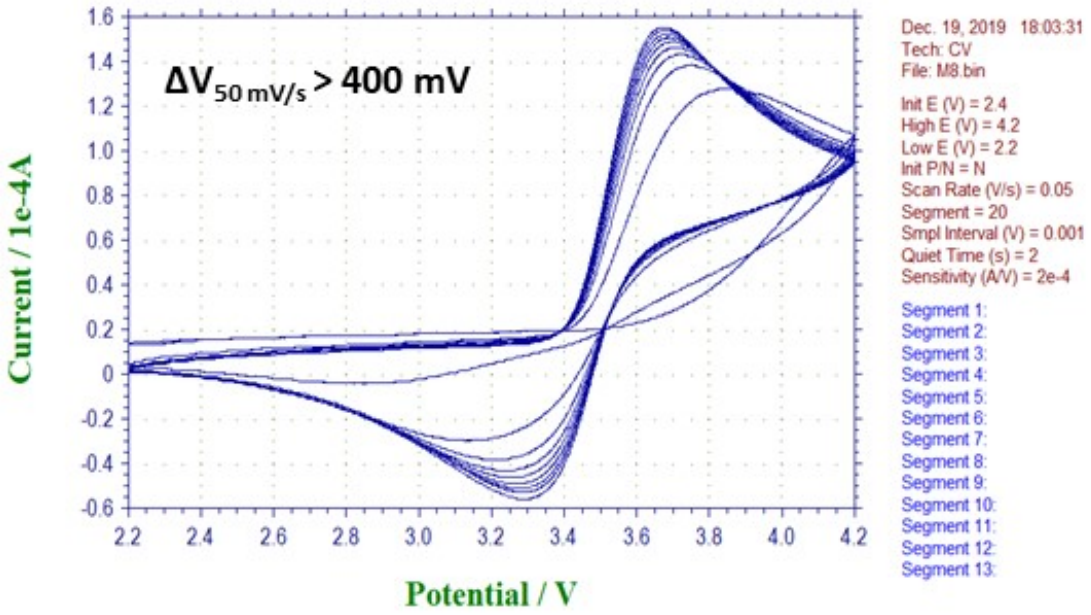

Fig.4. silicon N-type disk electrode CV results (50 mV/s) of the cycling of TEMPO molecule (20 mM) in Gen2 electrolyte post-de-lithiation from Fig. 3.

Conclusions

In this quarter we moved away from our ferrocene redox additive as its electrochemical behavior showed decomposition over time in Gen2 electrolyte. Various studies and consultation with Lu Zhang indicated that the TEMPO molecule was more stable and a better probe of the silicon SEI behavior *in operando* mode. The SEI made through constant current lithiation of the silicon N-type disk electrode is impenetrable to TEMPO molecule thus indicating ideal passivation behavior. Charge analysis of the TEMPO molecules electrochemical response implies that the silicon SEI is now porous and not passivating. Based on previous DeepDive work and analysis, silicon volumetric changes and SEI instability may be a cause. Future work will focus on (1) finding a lower voltage redox probe molecule, and (2) explore the efficacy of the silicon SEI through more experiments with TEMPO on silicon thin-films and silicon disk surface modification.

Electrode Studies

Impact of Processing Conditions on PAA-based Binder Systems (ORNL)

Beth L. Armstrong, Alexander M. Rogers, Katie Burdette, and Gabriel M. Veith (ORNL)

Background

Prior work on the impact of processing conditions of the uniformity of Si-Gr composite electrodes showed the use of PAA-based dispersants combined with PAA-based binders improved electrode homogeneity.[1,2] Reproducibility studies has identified significant silicon powder lot variability in addition to the elimination of graphite from the slurry composition were important to obtain reproducible electrodes. Recent work highlighted the need to further evaluate the reproducibility of PAA binder lots as a function of laboratory mixing techniques and aging conditions. The rheological properties of PAA and LiPAA aqueous binder solutions were measured as a function of mixing conditions. The shear rate/hysteresis behavior of the resulting solutions was studied to mimic CAMP casting protocols to evaluate the role of binder on the laminate stability and performance.

Results

In the pursuit to reproduce CAMP procedures as well as define the stability/usage window of binder stock systems used to fabricate silicon-based electrodes, various aqueous solutions of PAA and LiPAA binders were prepared a function of mixing conditions, and the viscosity was evaluated over a range of shear rates in the electrode casting regime. Visual observation identified differences in PAA and LiPAA solution viscosities based on the method of fabrication. Initially, three methods were evaluated; 1) stirring, 2) stirring with the addition of heat, and 3) heating. A viscosity shear rate sweep beginning at 5 and increasing to 3500 s^{-1}, an additional 5-minute hold at 3500 s^{-1} or 5-minute rest, and subsequent decreasing sweep back to 5 s^{-1} was conducted for each solution. The resulting flow behavior of the 450K molecular weight LiPAA solution, irrespective of mixing.

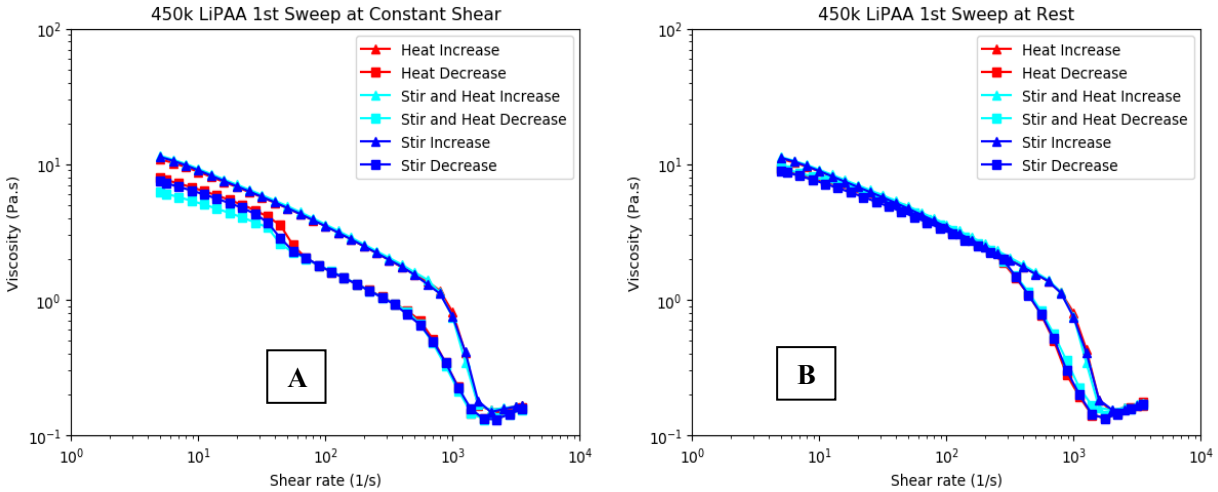

Figure 1A) Viscosity of 450K MW LiPAA as a function of shear rate with varying mixing methods and a constant shear hold at 3500 s-1 and B) Viscosity of 450K MW LiPAA as a function of shear rate with varying mixing methods with a shear rest.

properties have yet to be determined condition, exhibited hysteresis behavior indicating structural changes are occurring in the polymer solution as a function of processing conditions. The hysteresis also appears to be dependent upon shear history. This hysteresis will further impact the recovery of the electrode slurry after casting, which in turn will impact the outcome of potential casting defects in the final electrode structure. The impact of hysteresis on electrochemical properties has yet to be determined.

Conclusions

The effect of processing conditions involving shear during the handling of LiPAA binder solutions will impact the flow behavior, polymer structure, and ultimately the electrode castability and uniformity. The selection of mixing method will be dependent upon the needs of CAMP process and the resulting electrochemical behavior.

References

1. Armstrong, BL, Hays, K, Ruther, RE, and Veith, GM, "The Role of Dispersants on the Binder Selection for Si-Gr Composite Electrodes," EERE silicon Deep Dive Program, Q1 Report, FY 2019.
2. Ruther, RE, Armstrong, BL, Nanda, J, and Veith, GM, "Impact of Processing Conditions on Uniformity of Si-Gr Composite Electrodes," EERE Si Deep Dive Program, Q1 Report, FY 2019.

Processing Silicon Composite Electrode Components: Binders and Related Materials (ANL)

Zhangxing Shi, Lu Zhang (Argonne National Laboratory)

Background

Silicon (Si) based electrode materials, have relatively low cost and higher theoretical capacity (ca. 3600 mAh/g) than the conventional graphite materials (ca. 372 mAh/g). However, the large volumetric expansion (ca. 320%) of silicon during lithiation leads to unstable solid-electrolyte interphase (SEI), rapid loss of cohesion in the electrode matrix, particle pulverization, and capacity fading. Polymers compatible with presently used electrode processing methods, as well as materials with acceptable stability and elastomeric properties are under evaluation. These polymer binders have been utilized to mitigate these physical issues by providing strong adhesion/cohesion between active silicon materials, conductive carbon particles, and the current collector, which keeps them in electric contact despite the large volumetric changes of silicon particles during their electrochemical cycling. Among the reported binders, pre-lithiated PAA (PAA-Li) was selected as the standard binder for the Silicon Deep Dive program by CAMP researchers based on performance and laminate properties. Although PAA-Li binder has been widely used in laboratory development, the performance of silicon lithium-ion batteries using PAA-Li binder does not meet the requirement of practical use.

Previously we established a preliminary understanding regarding the pre-lithiation process for PAA binders and its potential impact on the cycling performance of the fabricated cells. The pre-lithiation process significantly increases the viscosity of PAA solutions, which potentially leads to improved slurry stability and subsequent robust electrodes. However, the same process also adversely affects chemical stability of silicon particles in the slurry, binding strength of PAA, and cycling performance of the silicon anodes due to the involvement of strong base (i.e. LiOH) and its ability to dissolve surface silica. To overcome this dilemma between slurry stability and cycling performance, ammonia (NH_3) was used to neutralize PAA solution instead of LiOH. This new alternative neutralization of PAA binder provides significant rheological improvements while maintaining the cycling performance of the fabricated electrodes.

Results

In our previous study, we showed that PAA solutions neutralized by NH_3 have significantly improved rheological properties than pristine PAA solution. Therefore, the resulting PAA-NH_3 slurry is dilute with respect to LiPAA systems with better dispersion of electrode materials and more resistant to drying-out caused by water evaporation. Compared to the state-of-the-art neutralization method (i.e., PAA solution neutralized by LiOH), PAA-NH_3 solutions have lower pH value which could reduce the unfavorable side reactions caused by high pH. In addition, NH_3 can be removed from the electrode by thermal decomposition of PAA-NH_3 during the drying

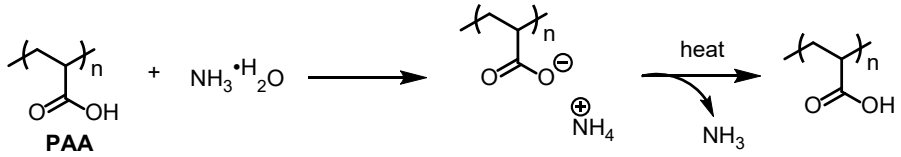

Scheme 1. The neutralization of PAA by NH3 and the thermal decomposition of PAA-NH3

process at high temperature (> 80 °C, **Scheme 1**). ATR-FTIR analysis of electrodes fabricated using PAA, PAA-NH_3, and PAA-Li binders were performed to confirm the proposed thermal decomposition mechanism. As shown in **Figure 1**, the carbonyl peak of PAA-NH_3 electrode overlaps with PAA electrode (1750 cm^{-1}), while the carbonyl peak of PAA-Li electrode showed at a 1630 cm^{-1} due to the shifted absorption between carboxylic acid and carboxylate. This result indicates the ammonium carboxylate groups converted to carboxylic acid groups after thermal decomposition as proposed. Therefore, the binding strength of PAA binder could be restored and provide improved cycling performance than PAA-Li binder. Another interesting phenomenon we found in

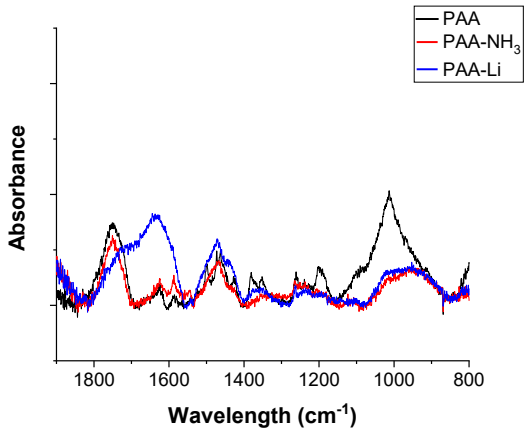

Figure 1. ATR-FTIR of silicon-graphite electrodes fabricated using PAA, PAA-Li, and PAA-NH_3

the IR analysis is the silica (SiO_2) content in each electrode. PAA electrode contains much more silica than PAA-Li and PAA-NH_3 electrodes. The differences might be caused by the raised pH of PAA-Li solution (pH = 6.0) and PAA-NH_3 solution (pH = 5.5) compared to PAA solution (pH = 2.1). The protective layer of the silicon partials could be partially removed since silica is soluble in basic solutions.

The representative cycling profiles of silicon-graphite composite electrodes fabricated using PAA, PAA-NH_3, and PAA-Li binders were summarized in **Figure 2**. The cells were subjected to three formation cycles between 0.01 V and 1.50 V at C/20 rate, followed by 100 aging cycles at C/3 rate. PAA-NH_3 cells have higher initial

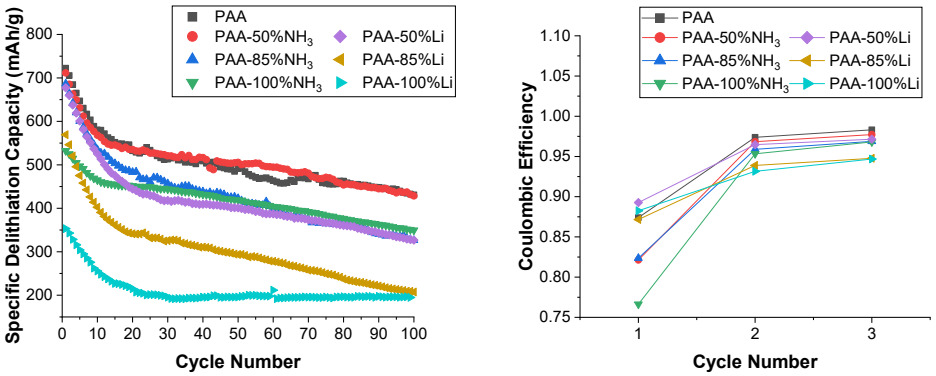

Figure 2. Specific delithiation capacity (left) and coulombic efficiency profiles (right) of Li half cells using electrodes containing 73 wt% graphite, 15 wt% Si, 10 wt% modified PAA binders, and 2 wt% C45 over 100 cycles at C/3 rate.

capacity, higher average capacity, and better capacity retention than those of PAA-Li cells. For example, PAA-85%NH_3 cells have initial capacity of 686 mAh/g (theoretical capacity ~860 mAh/g) and average capacity of 492 mAh/g while PAA-85%Li cells have initial capacity of 569 mAh/g and average capacity of 303 mAh/g. However, the initial coulombic efficiency of PAA-NH_3 cells is lower than that of PAA-Li cells. This is possibly due to the reduction of acidic protons of PAA during the discharge process since pristine PAA cells also have lower initial coulombic efficiency than PAA-Li cells. After the first formation cycle, the coulombic efficiency of PAA-NH_3 cells then became higher than that of PAA-Li cells, which makes the overall performance of PAA-NH_3 cells better than PAA-Li cells during formation cycles. Interestingly, PAA-100%NH_3 cells have lower initial capacity than PAA-85%NH_3 cells but less capacity fading during the first 40 aging cycles, then the cycling performance of these cells becomes pretty much identical. On the other hand, PAA-100%Li cells have the worst performance among the tested cells as expected due to the reasons mentioned previously. Overall, PAA-50% NH_3 solution seems to achieve a good balance with significantly improved rheological properties and comparable

performance to pristine PAA cells. We believe this new neutralization method of PAA binder is an efficient approach to resolve the poor processability of pristine PAA binder.

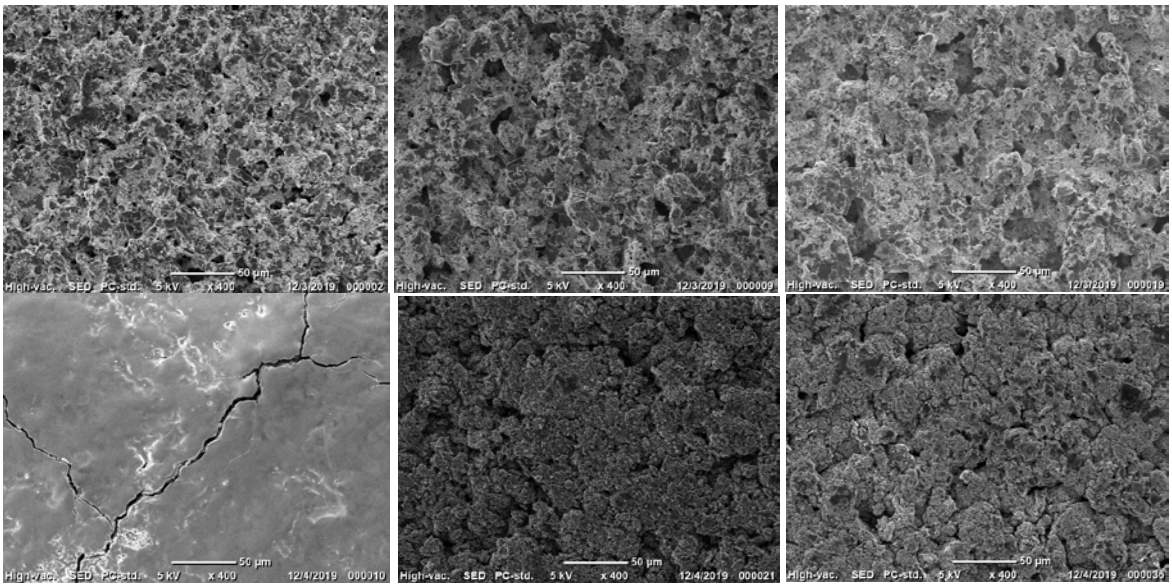

Figure 3. Surface SEM images of Si-graphite electrodes before (top) and after (bottom) aging cycles. The electrodes were fabricated using pristine PAA (left), PAA-NH_3 (mid), and PAA-Li (right) binders, respectively.

The surface of the fabricated electrodes before and after aging cycles was studied by scanning electron microscopy (SEM). Representative surface SEM images of pristine PAA electrodes, PAA-NH_3 electrodes, and PAA-Li electrodes are shown in **Figure 3**. All the electrodes look similar before cycling. After the 100 aging cycles, obvious cracks were found all over the surface of pristine PAA electrodes. The integrity of PAA-NH_3 electrodes and PAA-Li electrodes is better than that of pristine PAA electrodes since no cracks were observed for these electrodes. The morphology of pristine PAA electrodes is also different from the morphology of the

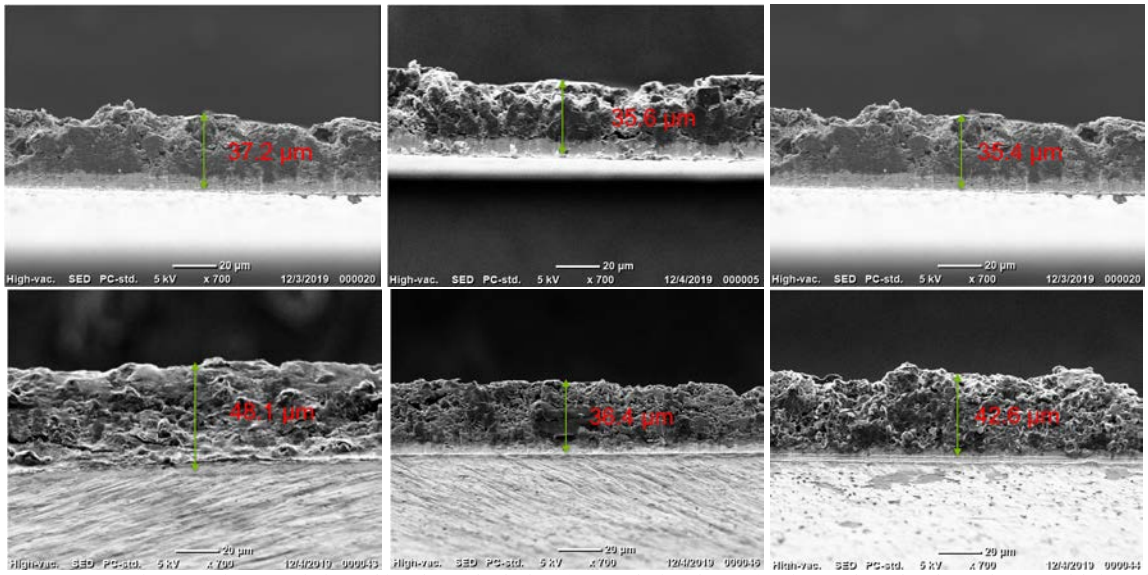

Figure 4. Cross-section SEM images of Si-graphite electrodes before (top) and after (bottom) aging cycles. The electrodes were fabricated using pristine PAA (left), PAA-NH_3 (mid), and PAA-Li (right) binders, respectively.

other electrodes. The surface of pristine PAA electrodes is flat and looks like there is a layer on top of the electrode materials. The surface of PAA-NH_3 electrodes and PAA-Li electrodes is still porous with observable particles after cycling. These differences might relate to the solvation behavior of modified PAA binders that we discussed in our previous study. The cross-section SEM of these electrodes before and after aging cycles were performed to study the volumetric changes of these electrodes. All the electrodes were charged to their fully delithiated state. As shown in **Figure 4**, pristine PAA electrodes have the largest volumetric expansion among these binders. PAA-Li electrodes have slightly less volumetric expansion than PAA electrodes, but the increase of the cross-section thickness is still significant. Overall, PAA-NH_3 electrodes have minimum volumetric expansion which indicates good binding performance to maintain the integrity of the electrode matrix.

Conclusions

An alternative neutralization method for PAA binder was developed using NH_3 instead of LiOH. The PAA-NH_3 binders showed promising viscosity improvements while maintaining the cycling performance of the silicon-graphite composite electrodes. The proposed thermal decomposition of PAA-NH_3 binders was confirmed by ATR-FTIR analysis. Surface and cross-section SEM of the electrodes fabricated using the modified PAA binders were performed to study the performance of these binders and their impacts on the integrity of electrodes.

References

1. Wu H.; Cui, Y. *Nano Today* **2012**, *7 (5)*, 414-429.
2. Hu B.; Shkrob I. A.; Zhang S.; Zhang L.; Zhang J.; Li Y.; Liao C.; Zhang Z.; Lu W.; Zhang L. *J. Power Sources* **2019**, *416*, 125-131.
3. Erogbogbo F.; Lin T.; Tucciarone P. M.; LaJoie K. M.; Lai L.; Patki G. D.; Prasad P. N.; Swihart M. T. *Nano Lett*. **2013**, *13(2)*, 451-456.

High Silicon Content Electrodes: CAMP Prototyping (ANL)

A.N. Jansen, S. Trask, A. Dunlop

Background

The CAMP Facility completed the first round of testing for the Zintl-phase forming electrolyte additives in single-layer pouch cells. Cells were fabricated in the fourth quarter of FY 2019. The electrodes used in this project were from the CAMP Facility's Electrode Library that consisted of high-silicon content anodes (LiPAA binder) paired with NMC532 or HE5050 cathodes – these electrodes are described in Figure 1. Two NMC532 cathodes were selected with different capacity loadings to test the effect of n:p ratio. Zintl-phase additives for the electrolytes were provided to the CAMP Facility by others in this program before the pouch cells were assembled. These electrolytes (including the baseline electrolyte) are described as follows:

- GenF : Gen2 + 10% FEC (baseline electrolyte)
- GenFM : GenF + 0.1M $Mg(TFSI)_2$
- GenFC : GenF + 0.1M $Ca(TFSI)_2$

The pouch cells (Figure 2) underwent cycling per the silicon deep dive protocol with a voltage window of 3.0 to 4.1 V for the NMC532, and 3.0 to 4.1 V for the HE5050 (after activation charge cycles to 4.5 V). Four pouch cells were made for each cell set.

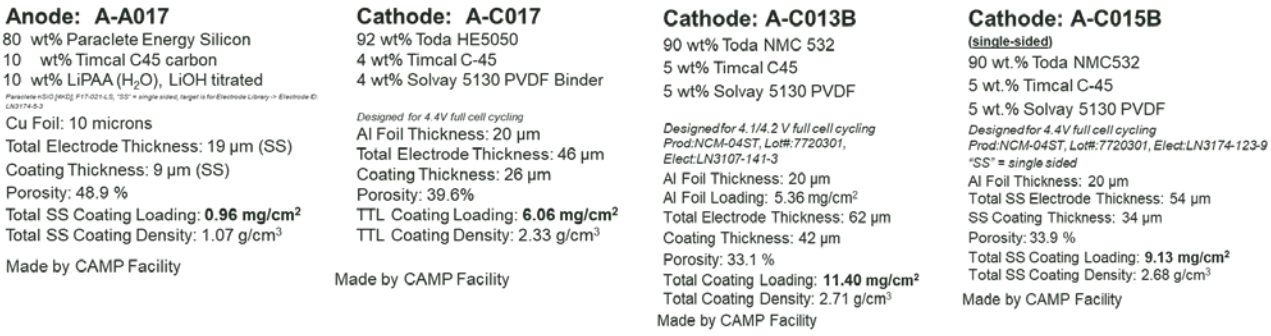

Figure 1. Electrodes used in single-layer pouch cells to test performance of "zintl phase" electrolytes.

Results

Figure 2. Single-layer pouch cells fabricated with 80 wt% Si electrodes versus NMC532 & HE5050 electrodes with "zintl phase" electrolytes (all pouch cells are not depicted in photo).

The pouch cells with the higher capacity-loading NMC532 cathodes (A-C013B) lost capacity at a faster than expected rate, regardless of the electrolyte. The pouch cells with the lower capacity-loading cathodes (HE5050 (A-C017) and NMC532 (A-C015B)) had better capacity retention that was relatively independent of the electrolyte used. One exception to this was the baseline electrolyte ("GenF") pouch cells that used the lower capacity-loading NMC532 electrodes (A-C015B). These results were not in agreement with the "zintl phase" coin cell studies that were done earlier by other groups. Representative pouch cells from each set were given to the Post-Test Facility for analysis. The pouch cells that used the higher capacity-loading NMC532 cathode (A-C013B) were cut open first, and the electrodes were photographed. One readily obvious observation was that the anode showed excessive signs of delamination (Figure 3) in the pouch cells with NMC532 at the higher capacity-loading (A-C013B cathode). The other cathode cell sets will be analyzed by the Post-Test Facility in the near future to check for signs of anode delamination.

Numerous conversations were had with the Si Deep Dive teams to determine if other researchers were observing delamination with this same electrode pair under similar test conditions. Majority of observations indicated that the anode remained well adhered to the copper foil during coin cell and reference electrode cells (large stainless-steel planar fixture) when the anode was only lithiated to the designed 100 mV (vs. Li/Li^+) cutoff. The CAMP Facility then did a series of tests to determine influence of: de-gassing and not de-gassing after formation cycles, ultrasonic welding of tabs versus mechanical-only contact, source of "GenF" electrolyte, and effect of applied pressure.

Figure 3. Harvested anode electrodes from single-layer pouch cells with baseline “GenF” electrolyte (left), “GenFM” electrolyte (center), and “GenFC” electrolyte (right) using the higher capacity-loading NMC532 cathode (A-C013B). Unexpected delamination seen on anodes, but not on cathodes. (Photos provided by Post-Test Facility).

Conclusions

Of all the conditions tried, only the effect of applied pressure had the most significant impact on cell performance. The initial pouch cells were cycled under ~4 psi (~30 kPa), whereas the wave spring in the coin cells is assumed to apply a greater pressure on the electrodes. Earlier work with electrodes with only 0 to 15 wt% silicon indicated that applied pressure (0.5, 2, 11, and 76 psi) had no significant effect on electrochemical performance (see Figure 4).

Silicon Milling: A Route to Functionalized Silicon

Mary K. Burdette (ORNL), Alexander M. Rogers (ORNL), David Hoelzer (ORNL), Beth L. Armstrong (ORNL), Gabriel M. Veith (ORNL)

Background

In our previous work we have determined that the surface chemistry of commercially available silicon sources is not sufficient for producing reproducible silicon anodes. Indeed, we have found significant batch to batch reproducibility issues with surface chemistry, particle sizes and surface areas, even crystallinity to amorphous ratios. To overcome these limitations, we have begun focusing on the production of Silicon Deep Dive Materials. Our approach focuses on using mechanochemical mixing/grinding of silicon boules to form silicon powders. Eventually we will directly functionalize the surface to obtain starting materials which will optimize electrode formulation and SEI formation

Results

Preliminary experiments have been performed to evaluate the role of milling time and energy on the resulting particles sizes, morphology and reproducibility. For the milling 200 grams of intrinsic silicon boules (~ 1-2 cm cubes) were added to a Zoz horizontal mill with 2 kg of 440c milling media. The milling media was reused for each experiment to evaluate aging and chemical contamination. The mill was operated at 700 and 900 RPM for various times to evaluate the effect of energy on the resulting particle sizes. Particle sizes were measured using light scattering and X-ray diffraction. Eleven batches of materials were prepared. From the particle size analysis we observed a bimodal distribution of particles. Roughly ¼ of the material were nanosized with average diameters less than 400 nm. The other ¾ of material had particle sizes on the order of microns. The resulting particle sizes are summarized graphically in Figure 1. Using the Sherrer Equation to analyze the particle size using X-ray diffraction we found the average primary particles were on the order of 35-50 nm in diameter, significantly smaller than the light scattering result. Interestingly, from the data presented in Figure 1 we see the size of the larger agglomerate *increasing* with time.

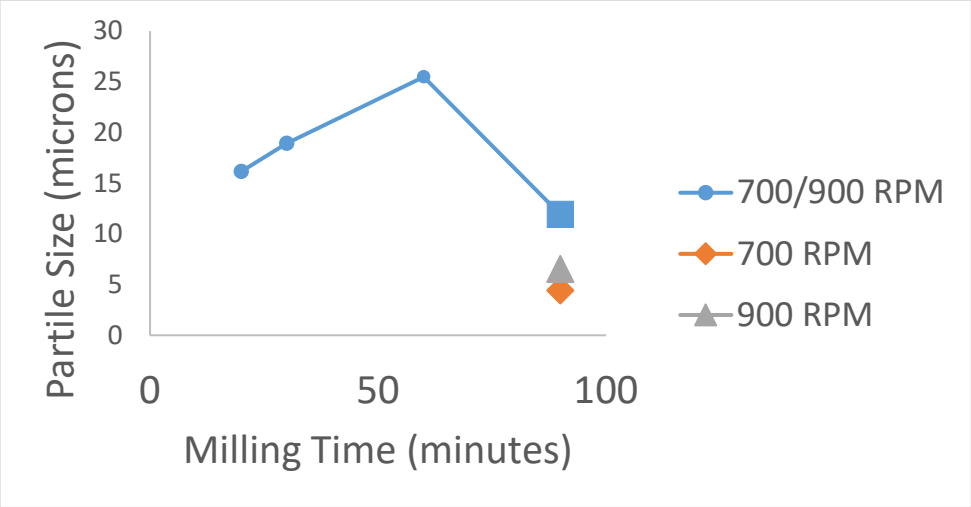

Figure 1. Particle size by light scattering as a function of milling time and speed.

Together this data indicates that the particles are breaking and refusing during the milling process. This means that the freshly exposed surfaces are extremely reactive and reform bonds with the freshly cleaved silicon. This refusing results in the larger particle sizes and points to the need to actively cool the reaction and/or provide a sacrificial reagent to react with the surface and prevent readhesion/bond formation.

To evaluate the purity of the milled silicon portions of the produced powders were dissolved in a mixture of sulfuric acid, hydrogen peroxide, and hydrofluoric acid. This process takes several days to complete at room temperature but is quite dangerous. Those reproducing this work should plan accordingly. Figure 2 shows the mg of Fe, Ni and Cr (components of the 440c milling media) per gram of silicon produced. Data were collected at two different metal absorption lines to check for instrument drift and reproducibility. Samples from left to right include the first milled silicon to the 9th batch of silicon along with standard G18 and F17 from Paraclete and two samples milled with sacrificial reagent. We clearly see high concentrations of Fe for the first set of milling runs, 0.98 mg Fe/g silicon, 0.36 mg Fe/g silicon, and 0.2 mg Fe/g silicon respectively. The concentration decreases quickly as the milling media is broken in. This points to the need to condition the milling media as a critical step to reduce contamination and produce a reproducible material.

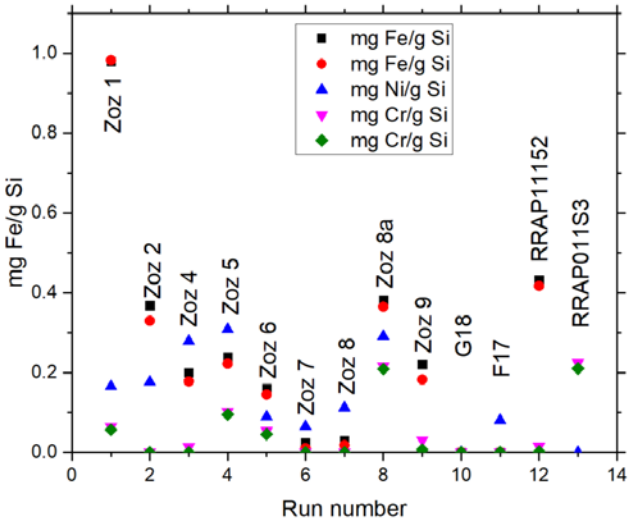

Figure 2. Concentration of iron (black squares and red circles), nickel (blue triangles), and chromium (pink upside down triangles and green diamonds) per gram of silicon as a function of milling parameters as found using inductively coupled plasma (ICP) of milled silicon powders.

Conclusions

Milling silicon boules into sub-10 µm powders has been successful. Low milling speeds, low energies and sacrificial reagents are needed to keep the silicon powder from re-agglomerating. After the sizing of the silicon is perfected, polymers will be introduced to the mill to create a uniform surface on the silicon powder. These polymers may act like an artificial SEI and a possible dispersant.

Fracture Behavior with Polymer Binder Capping Materials (NREL)

Jaclyn Coyle, Yanli Yin, Chelsea Cates Nathan Neale (NREL)

Background

Using silicon nanomaterials is a widely accepted strategy for mitigating the extreme volume expansion associated with the lithiation of silicon and the accompanying capacity fade. However, additionally the high surface area of silicon nanomaterials provides more opportunity for electrolyte decomposition, surface-binder interactions may interfere with lithium transport, and the natural silica passivation layer consumes more of the available silicon which leads to high irreversible capacity loss and low Coulombic efficiency. Silicon microparticles are available in large scale at a low cost and offer an alternative with lower surface area that have been shown to have high initial Coulombic efficiency [1, 2]. However, to make silicon microparticles viable, the drastic volume change and high stress of these larger particles must be mitigated. The goal of this project is to develop a more thorough understanding of the initial lithiation mechanics of the silicon crystalline microparticles through model crystalline electrodes.

The results of this work provide important analysis targeted at the initial crack formation of silicon and how polymer capping layers affect the lithiation depth and cracking formation of crystalline silicon. These findings may be applied to create a viable capping layer to reduce cracking in larger, more economical, silicon particles.

Results

In FY19, we found that the cracking mechanism of crystalline silicon is heavily dependent on the thickness of the silicon wafer, with thick 1 mm thick wafers showing behavior consistent with a LEFM mechanism.[1] In contrast, thinner wafers ≤675 μm thick exhibit much more complex cracking behavior that is more analogous to the cracking dynamics observed in real silicon nanoparticle electrodes[2] that is challenging to reproduce with model wafer systems as described in detail in our FY19 final report. Thus, we developed an alternative methodology to probe mechanical stress based on the Cantilever Beam Test (CBT) that, in conjunction with electrochemical performance data and microscopy data of silicon nanoparticle electrodes, can be used to quantify the relationship between the mechanical properties of the surface capping layer and the cracking propagation of silicon electrodes.

In Q1FY20, we worked diligently toward the Q1 Milestone: Evaluate the relationship between PAA-based binder chemical composition and silicon surface chemistry (SiO_x, SiH_x) on the ability of the binder to mitigate crack formation on silicon wafer electrodes. We have been careful in validating the CBT methodology to ensure reproducible and meaningful results (described in detail below), and thus did not complete the Q1 Milestone. The Program Manager (Brian Cunningham) granted an extension on 17-Dec-2019 to meet this Milestone by Q2FY20.

To validate the CBT method using PAA-based polymers relevant for the FY20 Milestones, we devised an approach based on partial esterification of PAA to make esterified PAA (E-PAA) as shown in Figure 1. The pentyl ester groups have minimal ability to hydrogen-bond to hydroxyl groups on native oxide SiO_x surfaces, and thus we hypothesized that with increasing ester content, the binding energy between the SiO_x-coated silicon wafer surface would be decreased.

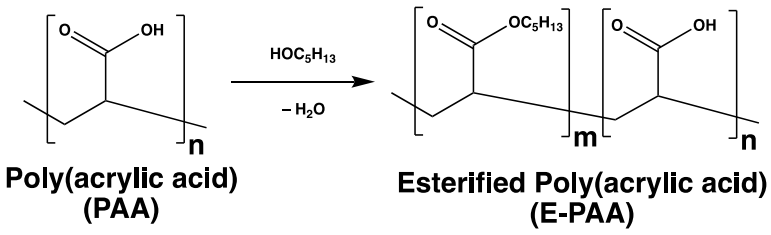

Figure 1. Esterification of polyacrylic acid (PAA) using a condensation reaction between PAA and n-penatnol (HOC_5H_{13}) to generate Esterified PAA (E-PAA). E-PAA with 90% COOH acid groups (m = 10%, n = 90%) and 80% COOH acid groups (m = 20%, n = 80%) were prepared.

The experimental apparatus for the CBT method is described in our FY19 final report. In brief, CBT is an advanced version of a conventional peel test. Though a conventional peel test used to measure adhesion force of a material to a substrate, it does not account for *subcritical de-bonding*: when delamination occurs at a finite rate at driving forces below its critical strain energy release rate, G_c. This phenomenon may occur in polymer-silicon systems due to the viscoelastic behavior of the polymer and/or stress-enabled chemical reactions with environmental species, such as electrolyte, humidity, etc.[3] The CBT methodology, which accounts for this subcritical bonding, thus provides a much more accurate measure of the force required to de-bond a polymer from a surface. Figure 2 (Left) shows a series of five repeated measurements where the titanium beam is slowly pulled upwards and the PAA film begins to de-bond from the silicon wafer surface. At these points the load values exhibit local maxima (yield points). In addition, we wrote a data analysis program to expedite the processing of many CBT datasets concurrently and to generate statistical information for subsequent error analysis. Figure 2 (Center) shows the data from Figure 2 (Left) replotted with dual y axes versus time to illustrate how the data analysis algorithm determines yield points and regions of tensile and compressive strain. Using this algorithm, we can derive linear fits over the initial tensile strain zones in the yield stress curves are used to calculate the compliance (μ/N), which is used to determine the cantilever de-bond length used for the subsequent de-bond energy calculations.

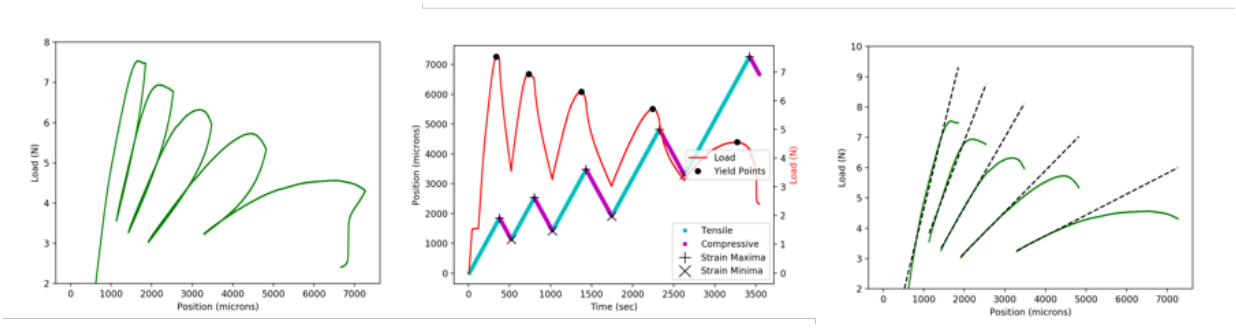

Figure 2. Left: Example cantilever beam test (CBT) data for the 20% ester side-chain E-PAA sample. Center: Example algorithm output for CBT data analysis. Right: Data from Figure 1 plotted with linear fits over the initial tensile strain zones as highlighted in the Center panel.

Control experiments were conducted to ensure that the CBT method was reproducible and provided meaningful results. Figure 3 shows calibration data using four different titanium cantilever beams, each of which was independently affixed to the polymer/silicon wafer surface via epoxy. In this way, we tested the reproducibility of the epoxy adhesion method to both the polymer and the titanium beam. These data show minimal error between samples giving us confidence in the experimental method.

Finally, we applied all this newly developed data collection and analysis methodology to our model system, PAA and E-PAA on SiOx-terminated silicon wafers (Figure 4). Each data point in Figure 4 is calculated from approximately 10 to 12 measurements across two separate experiments. As expected, the data show a systematic decrease in de-bond energy as the molar percent of hydrogen-bonding acid groups decreases (equivalently, non-H-bonding ester side-chains increases). The large error bars are due to the inherent errors

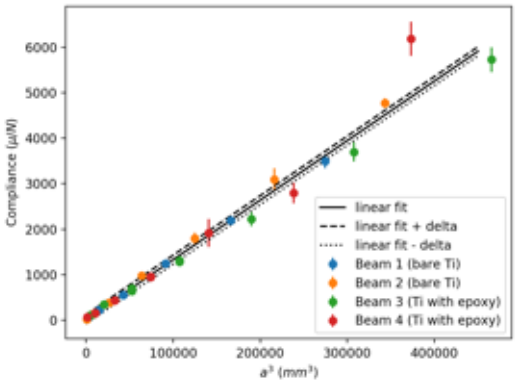

Figure 3. Calibration data which are used to determine the cantilever beam de-bond length (a) for a given compliance value, which is determined using the linear fits shown in Figure 2 (Right panel). Four different titanium beams were tested to determine the inherent errors in the calculation.

that are introduced in the curve fitting and beam de-bond length calculations but are mostly due to significant variations in PAA film thickness. Future experiments will aim to reduce these errors by depositing PAA films using a controlled spin-coating procedure as opposed to drop-casting that was used to generate these data.

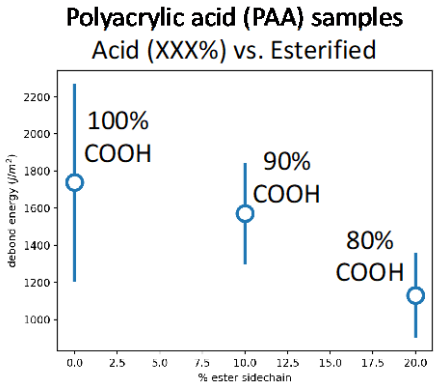

Figure 4. Mean de-bond energy values measured for PAA (100%) and E-PAA samples with 90% and 80% acid (COOH) groups.

Conclusions

In Q1FY20, we focused on full validation of the cantilever beam test (CBT) approach and demonstrated that our experimental methodology successfully quantifies the expected binding force trends for PAA and esterified PAA on SiO_x-terminated silicon wafers. In Q2FY20, we will optimize our polymer thickness by using spin coating rather than drop casting, which should minimize errors in the mean de-bond energy values. We plan to complete the study of PAA vs. Esterified PAA samples and compare these to modified PAA samples provided by Lu Zhang at ANL.

Stress calculations and models (with Andrew Colclasure (NREL)) are planned to model the data collected including (1) feed the force parameters we measure between polymer binder and silicon and (2) map 3D electrode morphology (pore structure, component heterogeneity) via HRTEM imaging that will greatly assist in refining the model used for his calculations as well as the degree of cracking in cycled microparticles.

We additionally plan to compare the mean de-bond energies between these model systems and capacity fade rate (along with post-mortem HRTEM to evaluate cracking) in silicon particle-based batteries using identical surface chemistries and polymers as binder. After initial work on SiH_x- and SiO_x-terminated silicon is completed, this approach will be applied to new surface chemistries and binders currently being developed under the Deep Dive and the SEISta programs.

References

1. Meyers, M.A. and K.K. Chawla, *Mechanical Behavior of Materials*. 1999, Upper Saddle River, New Jersey: Prentice-Hall, Inc.

2. Sarkar, A., P. Shrotriya, and A. Chandra, *Fracture Modeling of Lithium-Silicon Battery Based on Variable Elastic Moduli.* Journal of The Electrochemical Society, 2017. **164**(11): p. E3606-E3612.

3. Bosco, N., J. Tracy, and R. Dauskardt, *Environmental Influence on Module Delamination Rate.* IEEE Journal of Photovoltaics, 2019. **9**(2): p. 469-475.

Surface Modifications

In-Situ Ternary Zintl Coatings: Cell Builds

Steve Trask, James A. Gilbert, Alison Dunlop, Baris Key, Fulya Dogan, Jack Vaughey (ANL)

Background

As part of the DeepDive silicon effort, promising advances made in the lab are evaluated and tested, and if the advance is sustained, additional characterization and effort is applied. Recent work has identified a new class of electrolyte additives that, in coin cells, extended cycle life and enhanced coulombic efficiency. Diagnostic studies identified surface formation of a series of a redox stable $Li_{14}MgSi_4$ phases that are far less reactive towards cell components that the purely lithiated phase. These coatings have been electrochemically evaluated with regard to electrolyte composition, specific alkaline earth cation, and concentration. In this quarter we scaled up the electrolyte additives, and with CAMP and Post Test, evaluated the electrochemical properties in pouch cells.

Results

Extensive effort has been made to study the Zintl phase formation and how it affects the thermodynamic stability the silicon anodes. Previously, we demonstrated the effect of substituting using an in-situ mechanism different multivalent metal cations (Mg, Zn, Al, Ca) into a silicon-based electrode. Various techniques, including traditional diffraction techniques that are sensitive to the substituted heavy atoms were used to identify the inorganic surface phases present. For Li-containing materials and amorphous silicon (notably after cycling). high-resolution solid-state NMR was used to probe the local Li and silicon environments at different state of charge for silicon anodes cycled with Gen2+10%FEC (Gen2/FEC) and Gen2+10%FEC+ 0.1M $Mg(TFSI)_2$ (Gne2/FEC/Mg) electrolytes. More detail on this aspect of our effort is included in our SEISta FY20Q1 report.

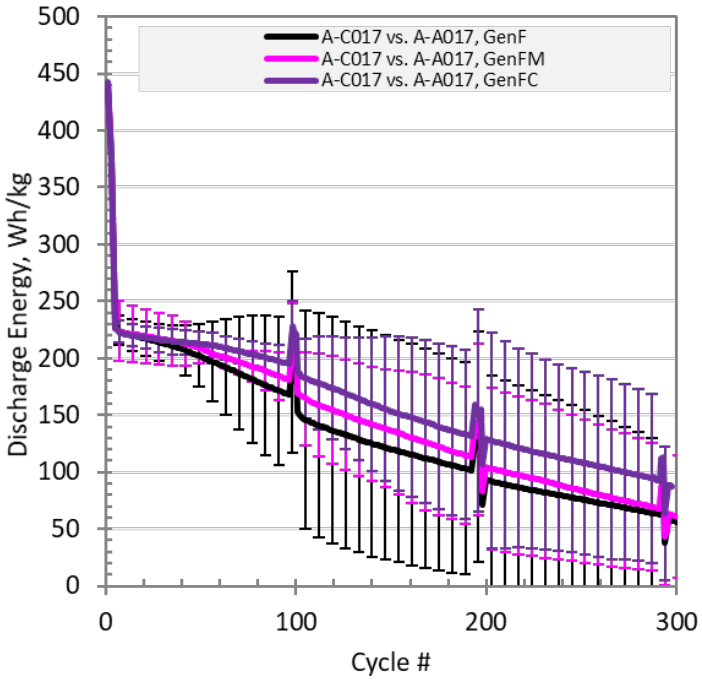

Figure 1. Discharge energy (Wh/kg) of the tested cells (CAMP) using the three different electrolytes.

To help reach the FY19Q4 milestones, the electrolyte system was scaled up, purified, and used in a series of CAMP pouch cells. Initial studies by Dogan and Han indicated that the electrolyte samples were stable but appeared to slightly darken in color over a two weeks period, indicative of side reactions. The exact cause has not been identified, but variables such as light or water sensitivity, complex cation formation on solution, and possible $[TFSI]^-$ anion decomposition is being assessed however none have been definitively determined to be the cause. Similar results from Gen2 electrolytes are found to results from a combination of light and water sensitivity. Thus, the electrolyte used for the study was purified and delivered to CAMP as needed to minimize this variable.

In these pouch cells, multiple full cells (cathode – NMC532) were constructed and evaluated. The data, shown in Figures 1 and 2, highlights the effect on additive on Coulombic efficiency of these cells with three different electrolytes, Gen2/FEC, Gen2/FEC/Mg, and Gen2/FEC/Ca. In these extensively studies, the cells were cycled in the voltage window from 3.0 - 4.1V.

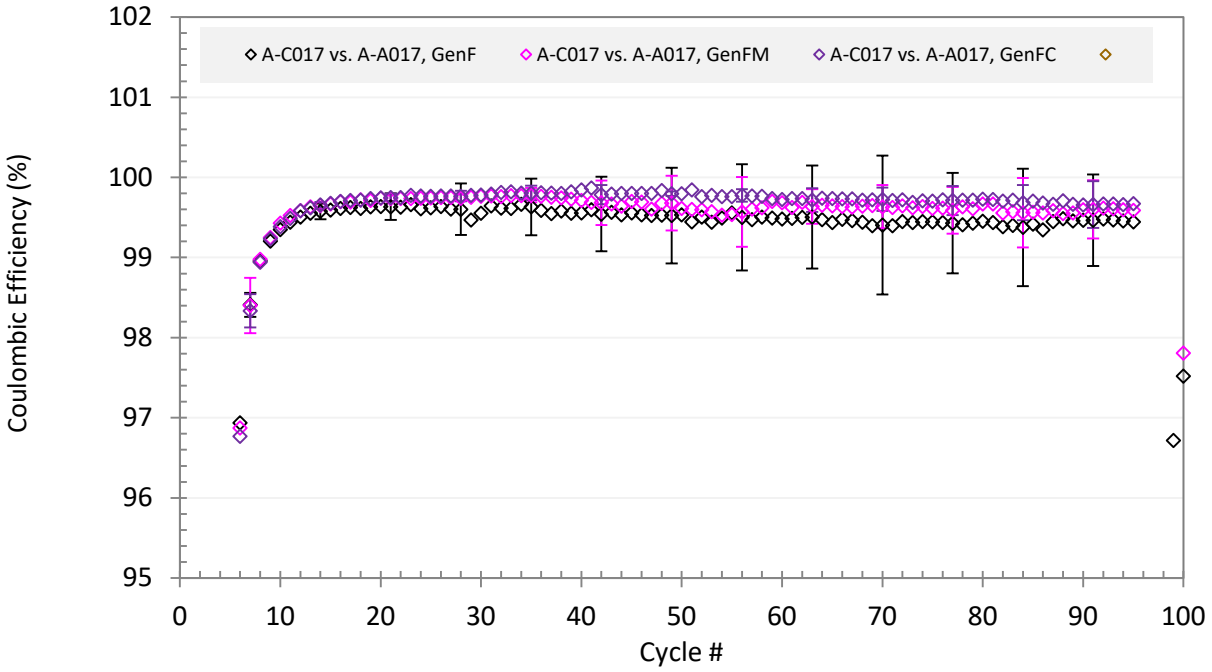

Figure 2. Coulombic efficiency studies of a series of pouch cells that use the electrolyte additives.

Overall, the additives have a consistent positive effect on the electrochemical performance. The data indicate that, compared to baseline, the Mg and Ca additives have a lower capacity fade and better CE. Combined these are key contributors to the performance. Spectroscopic studies performed at NREL (Stetson, Al-Jassim) confirm earlier EQCM reports that the SEI layer formed in the presence of additives is thinner than the one formed in Gen2/FEC alone. The surface reactions are thought to eliminate the redox activity of the surface against the electrolyte, and a thinner SEI would be an expected outcome.

While the CE efficiency appears to be stable with the Ca additive providing the best performance, the capacity fade is noted (over 300 cycles). Cells were handed to the Post-Test facility and studied. Data on this analysis is presented in Z.Z. Yang and Ira Blooms contribution. In short, evidence suggests delamination was more profound in the pouch cells than in coin cells. CAMP and PT are analyzing these results to identify a path to more stable electrochemical performance at the electrode level.

Conclusions

In this work, the role of MV additives in pouch cells and a diagnostic analysis of the cycles cells is reports. In all cases the additives result in a consistent 0.1-0.2% increase in CE and better retention of cycling capacity Combined with data from NREL, PT, and CAMP, the main advantage appears to be that the elimination of surface redox activity by Mg (or ca) substitution appears to eliminate side reactions with the electrolyte at high states of charge. Data consistent with thinner SEI has been reported at various Face2Face meetings and compositional changes are being evaluated.

Evaluation of Zintl-Phase Forming Mixed Salt Electrolytes (ANL)

Zhen Zhen Yang, Ira Bloom, Binghong Han, Steve Trask, Fulya Dogan, Baris Key

Background

Within the Deep Dive program, a multi-lab approach has been undertaken to better understand the role of forming in-situ ternary Zintl phases on a silicon electrode. Studies led by Key, have shown that addition of a small amount of $Mg(TFSI)_2$ to a standard Gen2 electrolyte extends cell life and raises Coulombic efficiency over extended cycling. In support of the FY19 Q4 milestone, the Post-Test facility has examined the effect of cycling on these cells in association with CAMP and examined the role Mg appears to have played in this cycling improvement.

Results

In conjunction with CAMP, we have evaluated the role of cycling on a series of standard cells created to evaluate the role of Mg (or Ca) salts in the standard Gen2+FEC Deep Dive Silicon electrolyte. Upon cell opening, it was apparent that several of the cells had lost contact with the current collectors (delamination) and that cell breakdown had occurred in some, but not all the cells. SEM studies of these electrodes are shown in Figure 1. Later discussions with CAMP had indicated that this was an issue that they were becoming aware of with respect to this specific electrode when used in pouch cells, but not coin cells. Further diagnostic evaluation by ANL and

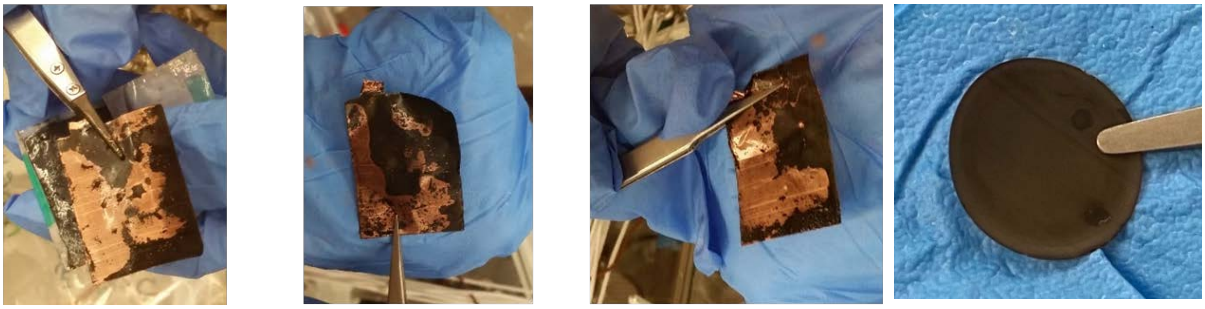

Figure 1. Selected SEM studies of three cycled pouch cell electrodes, and one cycled in a coin cell.

ORNL researchers was underway. For these cycled electrode studies, evaluation indicated that the electrode had undergone expansion by approximately 130% when compared to the pristine electrode. For the pouch cells,

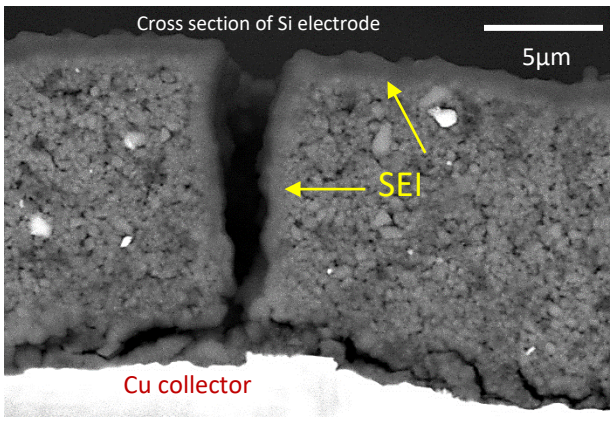

Figure 2. Particle cracking with SEI Film formation.

cracking of the laminated active material was observed, which when extend to the base of the electrode resulted in delamination from the copper current collector. In association with this observation, the gaps formed were

seen to be filled by SEI materials as the cycling has passivated the newly exposed surfaces. This is seen in Figure 2.

In addition to these observations, there has been significant discussion regarding how quickly the Mg added to the system in the electrolyte homogenized into the bulk of the silicon particle. Earlier TEM studies by Han and Dogan had shown that initial cycling indicated the surface was significantly enhanced in Mg content (as $Li_{14}MgSi_4$) relative to the bulk. Using similar techniques, on extended cycling (> 400 cycles) the bulk and

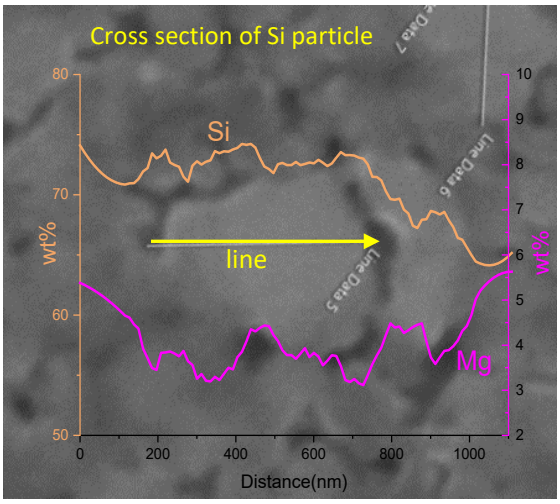

Figure 3. Cross sectional analysis of a cycled silicon particle highlights that after 100 cycles the Mg-ion concentration is concentrated at the surface.

surface were closer in Mg concentration. With this result, it has been postulated that on longer term testing, the sample would become more homogeneous with regard to Mg-ion distribution. In these Post-Test Facility studies, SEM/EDX cross sectional analysis has been done and shown that, after 100 cycles, there is evidence that the Mg is still much more concentrated at the surface than the bulk. This is shown in Figure 3 and is consistent with the previous reports.

As reported by Sa et al., in their EQCM studies of these systems, the SEI layer on these cycled electrodes appears different than in systems with added Mg (or Ca). We performed XPS analysis on these cycled electrodes using Gen2+FEC, Gen2+FEC+$Ca(TFSI)_2$, and Gen2+FEC+$Mg(TFSI)_2$. Data form these analyses are shown in Figure 4, and indicate that there are differences in carbon, fluoride, and phosphorus content based on the additives. Compared to the Gen2+FEC baseline, the calcium containing electrolytes contained CaF_2 in the SEI with less carbonates and more fluorophosphates. The Mg additive systems also contained MgF_2, less carbonates, and less phosphates than the baseline. Inorganic Mg species were mainly present as a magnesium silicate, magnesium

oxide, magnesium fluoride, and magnesium hydroxide.

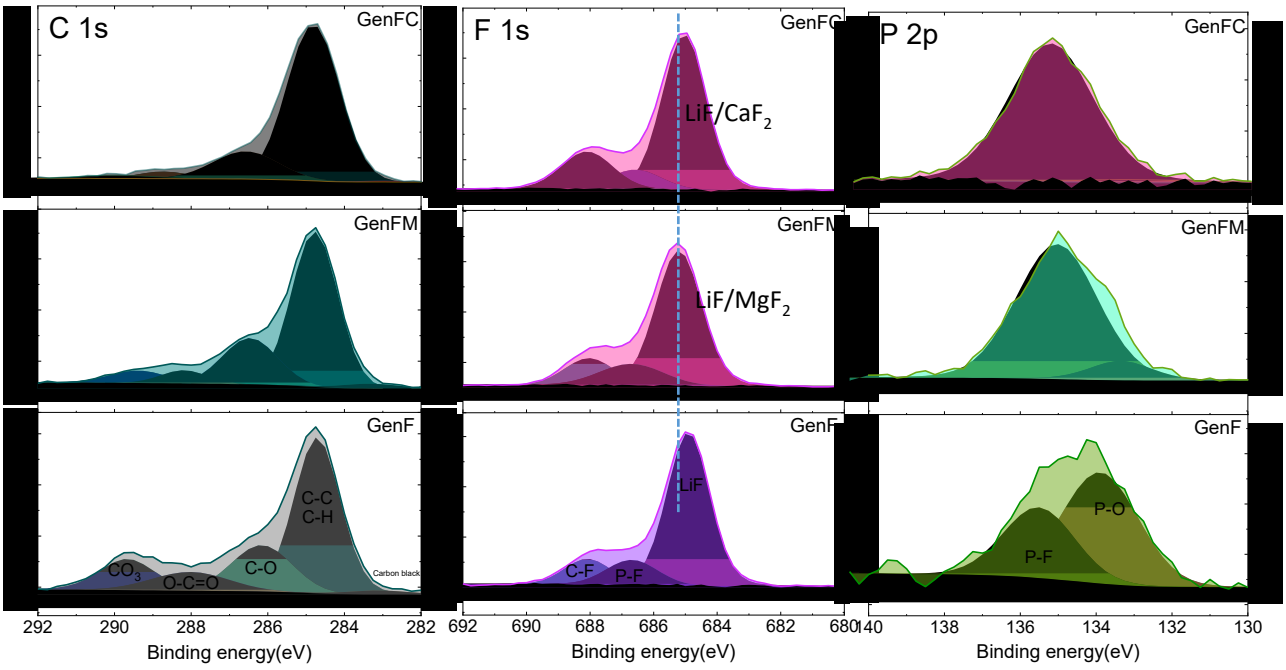

Figure 4. XPS study of cycled silicon cells with a calcium or magnesium electrolyte additive.

Conclusions

Silicon full cells have been cycled against a NMC532 cathode and evaluated for the role of magnesium additives and the disposition of the additive cations. A combination of SEM, EDX, and XPS studies have indicated that the multivalent cation is incorporated into the surface of the silicon electrode to form the phase a material like $Li_{14}MgSi_4$. Studies indicate that the addition changes the SEI composition, forming more fluorides and less carbonates and phosphate species. The enhanced cycling observed may be due to these factors and track the diffusion of the Mg into the bulk of the electrode particles and the different SEI components formed on extended cycling.

3

Silicon Surface Functionalization (ANL)

John Zhang, Sisi Jiang (ANL)

Background

We have continued our efforts to exert chemical control and design on the electrode – electrolyte interface. Previous studies have shown that this interface is very reactive with electrolyte components and our earlier work has demonstrated that enhanced cycling is achieved when this critical interface is tempered by an organic buffer layer. In this quarter, we continued our work reengineering the surface of the silicon particle with a cyclic carbonate group to introduce a reductively decomposable SEI precursor that could form a resilient SEI that could enhance the cycling performance of the silicon anode. Specifically, EC-surface functionalized SiNPs were synthesized via a Pt-catalyzed hydrosilylation reaction between H-terminated SiNPs and an allyl-carbonate precursor. Introduction of surface carbonate on the silicon surface altered the chemical composition and properties of SEI, leading to performance improvement demonstrated in both half- and full-cell.

Results

In this quarter, we reengineered the silicon particle surface with a cyclic carbonate group to introduce a reductively decomposable SEI precursor that could form a resilient SEI layer that could enhance the cycling performance of the silicon anode. The detailed synthesis is outlined in Scheme 1 and the surface analysis on the particle level and the electrochemical performance was performed. All these data indicate the cyclic carbonate functionalization is an efficient way to further improve the electrochemical performance.

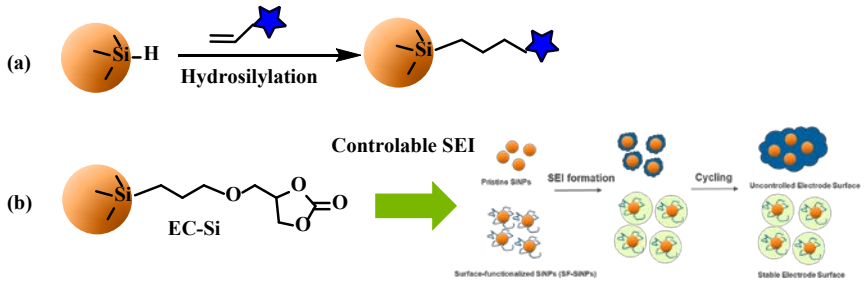

Scheme 1. (a) Synthetic route for cyclic carbonate-functionalized silicon nanoparticles EC-silicon by a hydrosilylation reaction and (b) the proposed protection mechanism.

Figures 1 shows TEM images and XPS analysis data of the SiNPs before and after surface functionalization. Attachment of cyclic carbonate group onto the surface of silicon was confirmed new C_{1s} XPS peaks for carbonyl (288 eV) and C-O (286 eV), which are not present for the unfunctionalized pristine one. TEM image of EC-SiNPs clearly shows an amorphous organic coating on particle surface while the crystallinity of the particles in the bulk are still preserved.

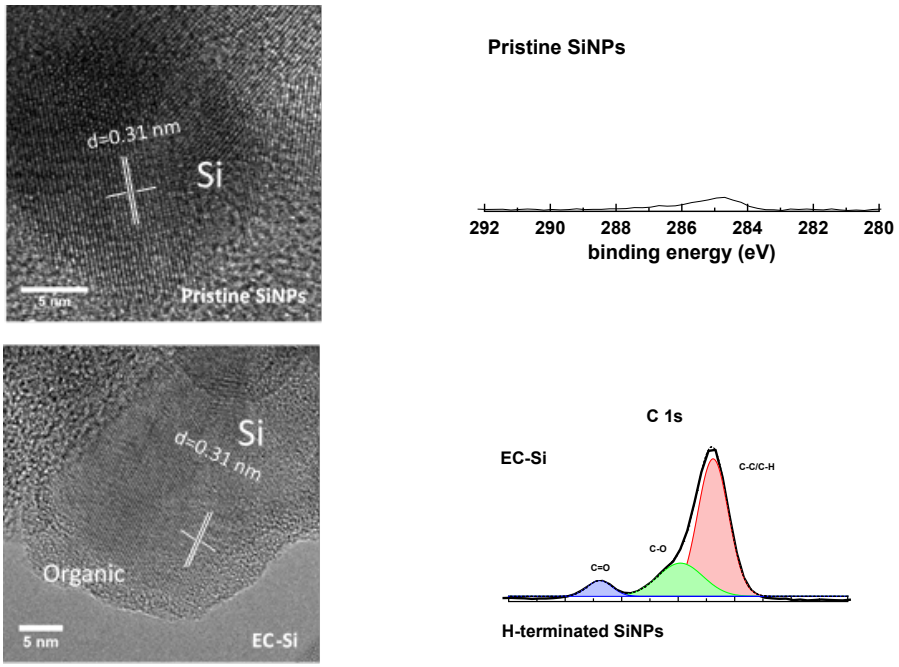

Figure 1. TEM micrographs of the pristine and EC-silicon nanoparticles (right), and C_{1s} XPS spectra of pristine and EC-silicon nanoparticles.

Figure 2 shows the electrochemical performance of the synthesized EC-silicon anode in half and full cells. The new anode exhibited improved initial capacity and Coulombic efficiency (CE) compared with pristine anode. Under extensive cycling, the EC-silicon anode demonstrated a capacity of an average 1925 mAh/g with a capacity retention of 87.1 % for 100 cycle (Figure 2a). In addition, CE of EC-silicon electrode gradually increased and was stabilized at > 99% after 50 cycles.

Not only in half cell, the performance improvement of EC-SiNPs is also demonstrated in full cell where silicon anode is coupled with a $LiNi_{0.6}Mn_{0.2}Co_{0.2}O_2$ (NMC622) cathode. The cells underwent three formation cycles at C/20 with a cutoff voltage of 3.0-4.2 V followed by C/3 cycling. The cycling performance is summarized in **Figure 2b**. The pristine anode/NMC622 cell suffered from a gradual capacity while the EC-Si/NMC622 cell showed much higher capacity retention (70%) in 100 cycles.

Post-test analysis was performed on the cyled silicon anodes. Figure 3 shows SEM/EDX analysis results. EC functionalization effectively stabilizes the anode interface as revealed by SEM images where less surface growth (determined by cross -section SEM analysis of electrodes before and after cycling) were observed for the cycled EC-silicon anode. In addition, EDX results indicate EC functionalization also affects the surface compositions. The fluorine content on the surface of cycled pristine silicon anode is 2 times that of the cycled EC-silicon anode, indicating more side reactions took place on the surface of pristine anode during repeated cycling.

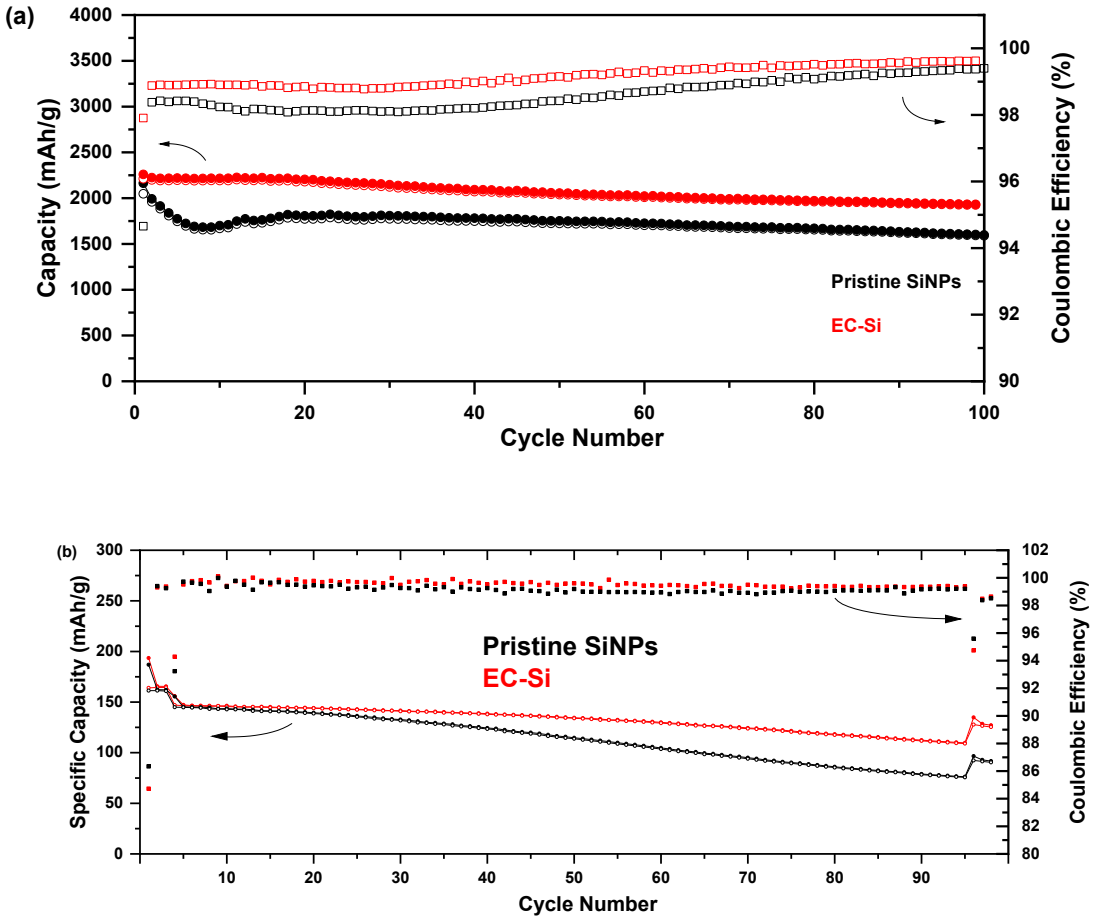

Figure 2. Cycling performance and Coulombic efficiency of (a) Si/Li half-cell and (b) NMC622/Si full-cell.

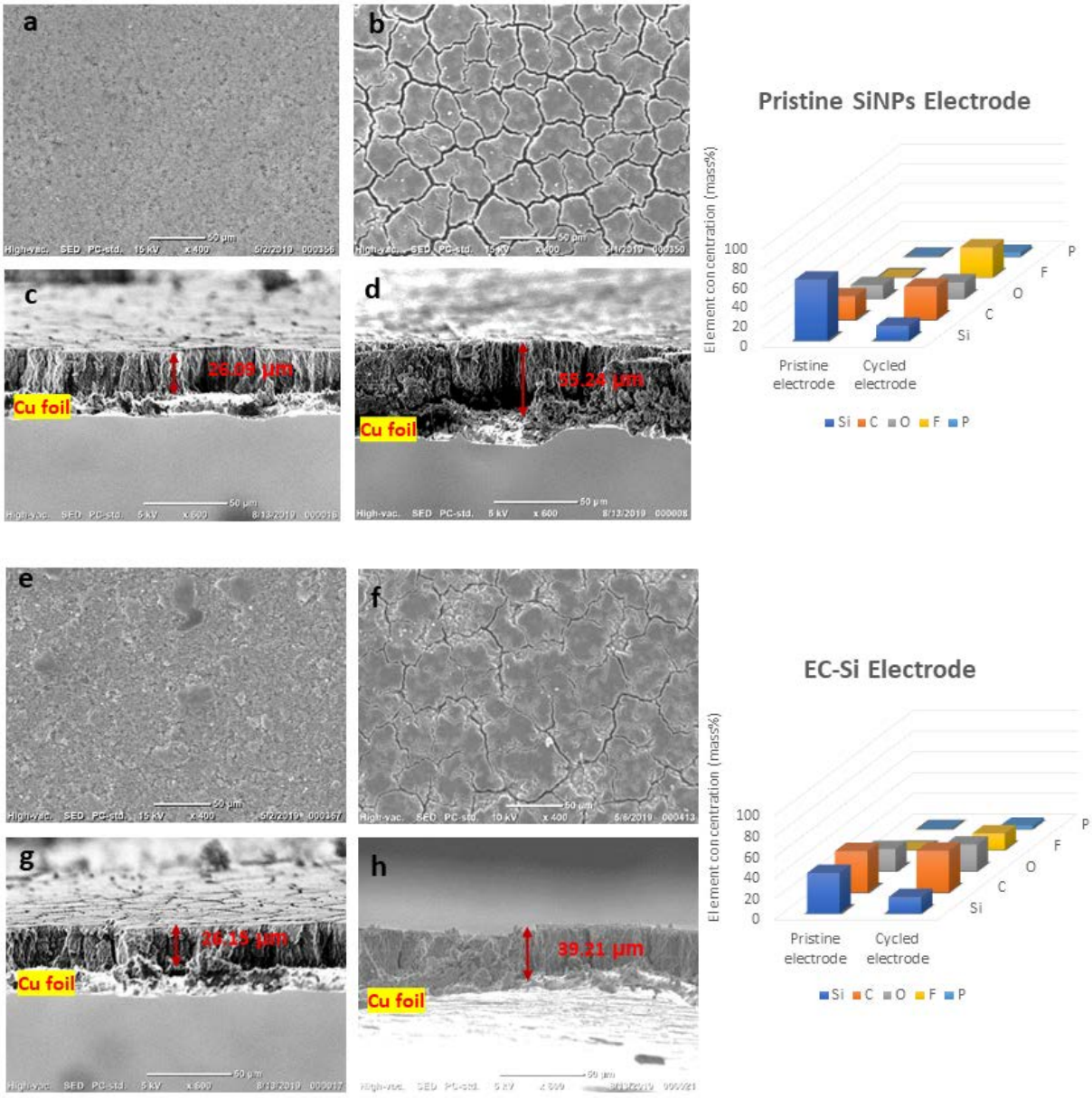

Figure 3. SEM/EDX data for (a-b) pristine electrode before and after cycling; (c-d) cross-section SEM micrographs of the pristine anode before and after cycling; (e-f) SEM micrographs of EC-silicon anode before and after cycling, and (g-h) cross-section SEM micrographs of EC-silicon anode before and after cycling.

In summary, EC-surface functionalized SiNPs were synthesized via a Pt-catalyzed hydrosilylation reaction between H-terminated SiNPs and the allyl-carbonate precursor. Introduction of surface carbonate on the silicon surface altered the chemical composition and properties of SEI, leading to performance improvement demonstrated in both half- and full-cell.

Mechanistic Studies of Surface Zintl Phase Formation (ANL)

Wenquan Lu, Yan Qin, Yanjie Cui

Background

The improved electrochemical performance of a silicon electrode has been seen when the ternary Zintl phase $Li_{14}MgSi_4$ is formed on the surface of the active particles. In reports by Key, et al., the ternary phase was made by adding a $Mg(TFSI)_2$ salt was added into the electrolyte forming $Li_xMg_ySi_z$ on the silicon during charge and discharge cycles. While the ternary phase has been noted to have very good redox stability and be a good lithium ion conductor, limited reports on the binary phases have been reported. These phases, notably Mg_2Si or $Mg_{2-x}Li_xSi$, may form kinetically on insertion and gradually lithiate as an alternative formation mechanism. In our studies, Mg will be vapor coated on the surface of silicon powder to form a film or coating of Mg_2Si on silicon. Mg_2Si coated silicon particle will be characterized and their electrochemical performance will be investigated.

Results

Various reports have note that Mg_2Si can be used as an active anode material for lithium ion battery, although the reported mechanisms have highlighted the disproportionation of the compound to form elemental magnesium as the counter reaction, in essence a form of Mg battery. Initial samples of the compound were obtained commercially (Sigma-Aldrich) and made into electrodes using the ratios 83% Mg_2Si, 15% LiPAA binder, and 0.7% CNT. The electrode was fabricated into 2032 coin-type cell using a Li metal anode. The electrolyte consisted of 1.2 M LiPF6 in EC/EMC (3/7), plus 10% FEC additive. The electrochemical differential capacity plot of Mg_2Si was shown in Figure 1 (left). Multiple peaks were observed during charge and discharge processes between 10 mV and 1.5V, which are correlated to the phase transitions as depicted phase diagram (Figure 1 right)[1].

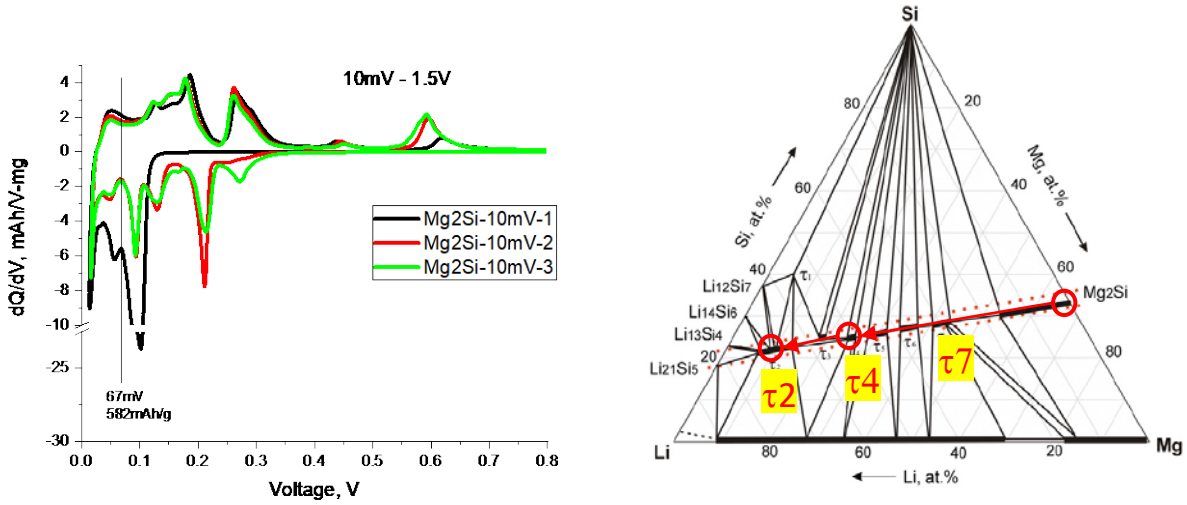

Figure 1 Differential capacity plot of Mg_2Si electrode (left) and Li-Mg-Si phase diagram (right)

[1] High hydrogen content super-lightweight intermetallics from the Li-Mg-Si system, Volodymyr Pavlyuk, Grygoriy Dmytriv, Ihor Chumak, Oliver Gutfleisch, Inge Lindemann, Helmut Ehrenberg, Inter. Nat. J. Hydrogen Energy **38**, *2013*, 5724-5737

Cycling studies were extended to establish the role of cut-off voltage effect on the capacity retention of Mg_2Si electrode, shown in Figure 2. Three curves are presented from top to bottom with three different cut-off voltages: 10mV – 1.5V, 20mV – 0.4V, and 50mV – 0.4V. Clearly, the wider the voltage window, the more capacity was delivered. However, the capacity retention fading rate also increases with wider voltage window. The Mg_2Si electrode demonstrated very good cycle performance when the lower cut-off voltage is above 50mV. Further studies will include examining the electrode matrix of the cycled electrode at the Post Test facility to examine the ability of Mg to diffuse back into the active electrode structure on delithiation.

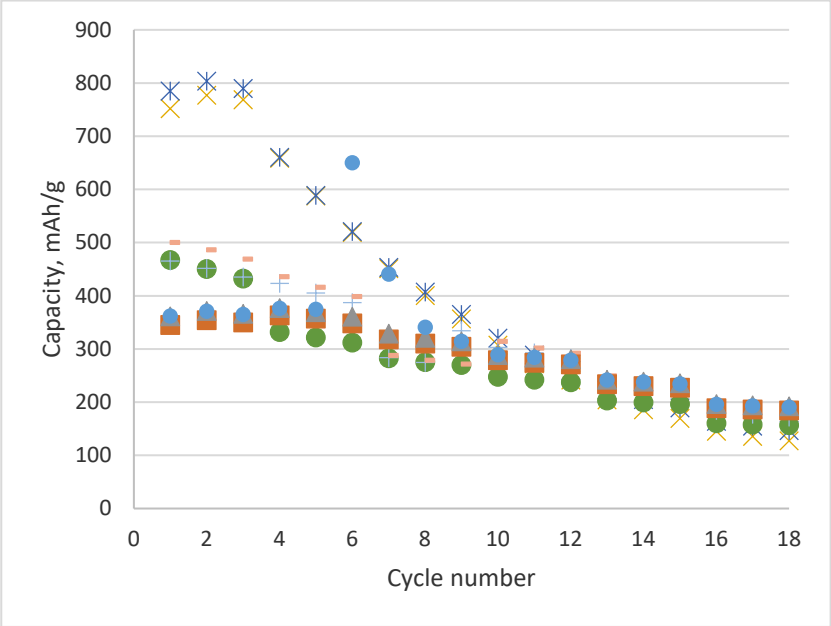

Figure 2 Charge and discharge capacity of Mg_2Si electrode with various cut-off voltages top curve: 10mV – 1.5V; middle: 20mV -0.4V; bottom: 50mV – 0.4V

Vapor Synthesis: A stoichiometric amount of Mg metal was put into a large crucible, then a small crucible filled with Si particles was put inside of larger crucible. The whole set-up was covered and sintered under Ar gas. The schematic diagram of this set-up is shown in Figure 3. A total of four samples were synthesized with 4 different conditions: 1) 400°C dried Si powder/700°C/1 hr; 2) 400°C dried Si powder/700°C/20 hr; 3) 400°C dried Si powder/900°C/5 hr; and 4) pristine Si powder/900°C/5 hr.

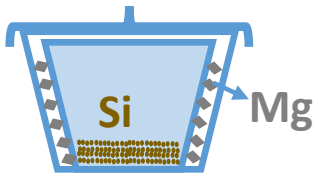

Figure 3 Schematic diagram of Mg coating set-up

Four samples were made into electrodes with same electrode composition and tested in 2032 coin-type cell configuration as Mg_2Si. The cut-off voltages are between 10mV and 1.5V. The electrode capacity and coulombic efficiency during first three formation cycles are shown in Figure 4. First, the capacity of Mg_2Si coated Si electrode decreased with increasing the sintering temperature. We believe that the Mg_2Si coating contribute less

capacity compared to Si. The higher sintering temperature caused more Mg_2Si coating, leading to overall less electrode capacity. On the other hand, the 1st coulombic efficiency increases with increasing with higher sintering temperature.

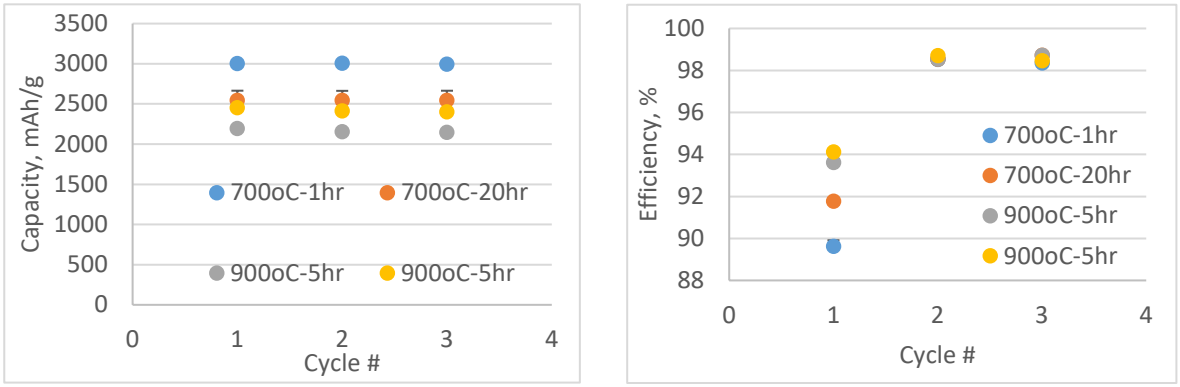

Figure 4 Specific capacity (left) and coulombic efficiency (right) of Mg2Si coated silicon electrode during three formation cycles

Conclusions

Mg_2Si coating on silicon particles were conducted using four reaction conditions. All four powders were made into electrode and electrochemically tested. The preliminary results indicate that the more Mg coated was obtained when higher temperature or longer reaction time were applied. We also found that the better coulombic efficiency was achieved with Mg coating.

In addition to Mg coating, we also electrochemical investigated the Mg_2Si since it is believed to be the coating product of Mg coated silicon particle. It is confirmed that the Mg_2Si is an electrochemical active material as reported. The better capacity retention was observed when narrower cut-off voltage window was used.

Mechanistic Studies of Zintl Electrolyte Additives

Niya Sa (UMB), Saida Cora (UMB), J. Vaughey (ANL)

Background

Our major focus in this quarter has been to continue our investigations on the mechanism of the multivalent ion additive insertion, i.e. Mg^{2+}, into a Si thin film anode. Initial effort focused on systematic control experiments to identify the role of Mg^{2+} and Li^{+} intercalation into silicon. At the F2F meetings, several mechanisms have been proposed and are under investigation, including

- $Si + 2Mg \rightarrow Mg_2Si$;
  $Mg_2Si + xLi \rightarrow Mg_{1-x}Li_{2x}Si$ (WLu Group)

- $Mg + xLi \rightarrow Li_2Mg$;
  $Li_2Mg + 4\text{-}xLi + Si \rightarrow Li_{4-2x}Mg_xSi$ (Zakuyatev Group)

- $4Li + Si \rightarrow Li_4Si$;
  $Li_4Si + xMg \rightarrow Li_{4-2x}Mg_xSi$ (Han Group)

As the mechanism of Mg^{+2} insertion is critical to its longevity is solution and as an ion the solid state, understanding its mode of insertion, solution coordination, and dispensation on cycling is key to extending its positive Coulombic efficiency effects and cycle life extension.

In addition, a continuation of our study on the role of a Mg concentration effect as the additive to the Gen2+10%FEC electrolyte is reported, where Mg concentrations are varied from 50 mM, 200 mM, 500 mM into the Gen2+10FEC electrolyte.

Results

A series of four systematic control experiments have been performed to assess the various models of Mg insertion in to a silicon LIB anode. Our half-cell experiments performed can be summarized as:

Electrolyte A) 0.2 M $Mg(TFSI)_2$ in EC:EMC (3:7), where there is no active lithium salt; silicon thin film anode (referenced to Li metal);

Electrolyte B) 1.0 M $LiPF_6$ containing Gen2 electrolyte on Si thin film anode, with no FEC and no Mg salts (referenced to Li metal);

Electrolyte C) Gen2 + 10%FEC electrolyte; Si thin film anode, the base electrolyte used to add Mg salt (referenced to Li metal);

Electrolyte D) Gen2+0.2 M $Mg(TFSI)_2$ electrolyte; silicon thin film anode, No added FEC (referenced to Li metal).

These experiments have provided mechanistic insights into the surface coating formation mechanism. Notably the two initial important findings from the control experiments (see **Figure 1**) include for systems studied using electrolyte A (0.2 M of $Mg(TFSI)_2$ into the EC:EMC 3:7), there was no electrochemical activity observed on the silicon anode. These results suggest that under typical conditions used, the Mg does not intercalate into Si alone and lithium salt is needed for ion intercalation. This reaction step is utilized by Mechanism-1 and might be evidence it is not a significant contributor to the energy storage mechanism. Using electrolyte D (Gen2 with $Mg(TFSI)_2$, but no FEC), ion intercalation is seen on Si with results comparable to the Gen2 alone with a silicon anode. Under these conditions, the added Mg salts do not change the electrochemical properties observed although they may be included, however the expected CE enhancement was not clearly observed.

While it has been demonstrated that adding Mg salts to the Gen2+FEC electrolyte has a positive effect on cell performance, the amount of Mg salt added and its effect on the solution salt structure has not been examined. As the bulkiness of the salt can affect its solution dynamics and interfacial diffusion properties, understanding the role of concentration is important for the electrolyte modeling and development team. Three electrolytes were synthesized in order to study the role of Mg^{+2} concentration on SEI formation. The three electrolytes studied had a set 10wt% FEC concentrations but varied Mg salt concentrations, and were

Electrolyte E) 0.05 M $Mg(TFSI)_2$ in Gen2+10%FEC electrolyte;
Electrolyte F) 0.20 M $Mg(TFSI)_2$ in Gen2+10%FEC electrolyte;
Electrolyte G) 0.50 M $Mg(TFSI)_2$ in Gen2+10%FEC electrolyte.

Electrolytes effect were systematically investigated at various lithiation depths. Based on the three electrolytes being investigated (**Figure 1**), electrolyte E (PURPLE), electrolyte F (BLACK), and electrolyte G (BLUE), it is evident that that adding Mg^{+2} salts to the electrolyte initially hinders the complicated lithiation of silicon and consequently constrains the complicated phase formation of silicon. This is consistent with observations that Mg^{+2} inclusion may alter some solution equilibriums and favor complex cation formation as a species to transport the Mg^{+2} salts to the electrode surface, leading to new interfacial phase formations (~ $Li_{14}MgSi_4$). EQCM measurements of SEI formation are consistent with observations that observed side reactions of the silicon surface are prominently hindered by the Mg component in electrolyte at low lithiation depth. Experimentally, at lithiation depth of 40 mV, 10 mV and 5 mV, significant hinderance of the SEI side reactions is observed, while no significant difference was observed once the lithiation depth was set at 115 mV or above. These results are

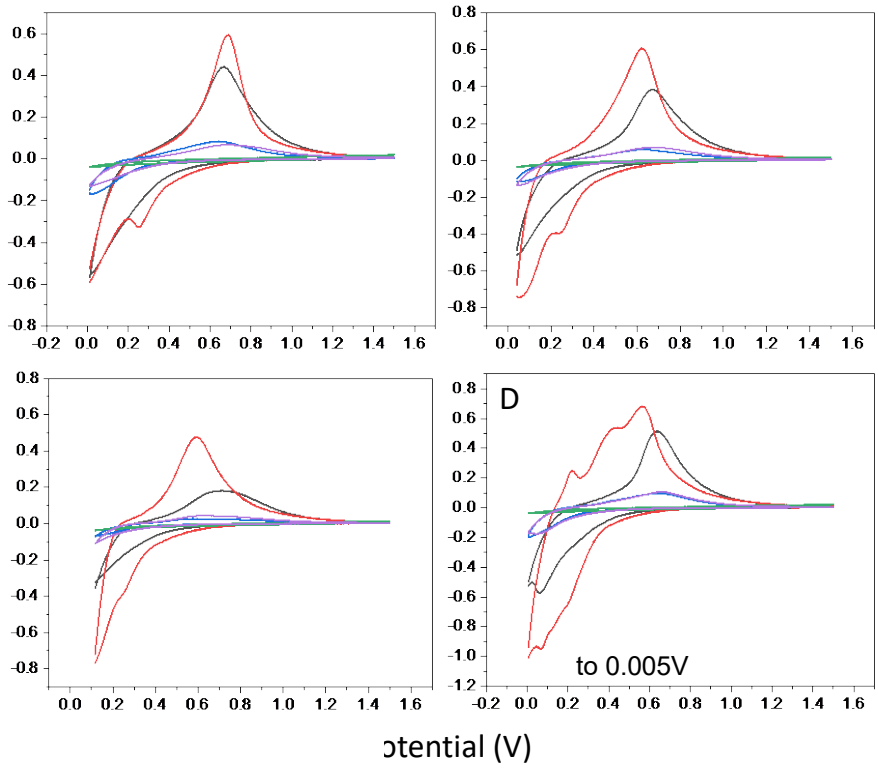

Figure 1. Electrochemical cycles at different lithiation depth for silicon thin film anode in various electrolytes. Electrolytes used here include two control electrolytes, the Gen2+10%FEC (RED) and 0.2 $Mg(TFSI)_2$ in EC:EMC 3:7 without lithium salt (GREEN). Three testing electrolytes are: 0.05 M $Mg(TFSI)_2$ in Gen2+10%FEC (PURPLE), 0.20 M $Mg(TFSI)_2$ in Gen2+10%FEC (BLACK), and 0.50 M $Mg(TFSI)_2$ in Gen2+10%FEC (BLUE); **(A)** electrochemical cycles at lithiation depth at 10 mV; **(B)** electrochemical cycles at lithiation depth at 40 mV; **(C)** electrochemical cycles at lithiation depth at 115 mV; **(D)** electrochemical cycles at lithiation depth at 5 mV;

an indication that Mg inclusion into the surface of the lithiated silicon occurs at a composition near $Li_{15}Si_4$, consistent with Mechanism-3.

In a concentration dependence study to ascertain the relationship between Mg salt concentration and SEI properties, data (shown in **Figure 2**) suggests that the initial SEI formation in Gen2+ FEC has a Mg concentration

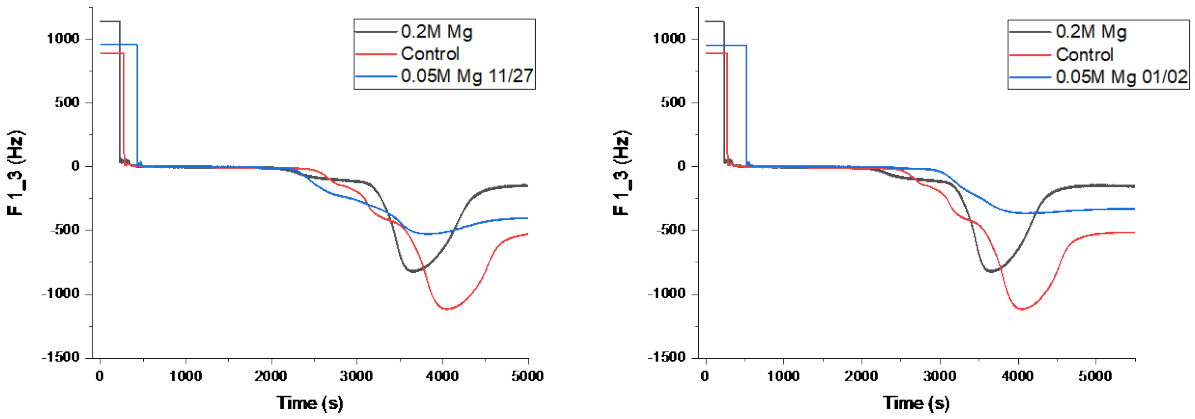

Figure 2. Frequency shift (3rd overtone) for the *early SEI formation* on silicon thin film anode in the Gen2+10%FEC (RED), 0.2 M Mg(TFSI)2 in Gen2+10%FEC (BLACK), and in 50 mM Mg(TFSI)2 in Gen2+10%FEC (BLUE). The left panel and the right panel used the same electrolytes formula but performed on different runs on different silicon anode, the purpose is to show the reproducibility and consistance for this type of experiment.

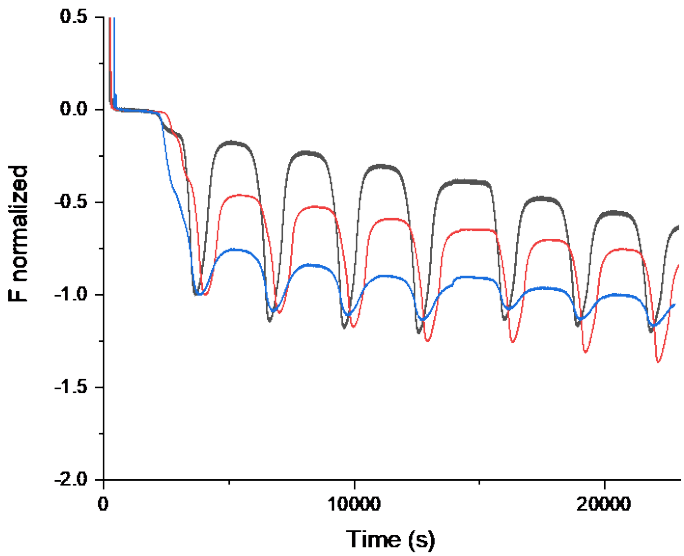

Figure 3. Frequency shift (3rd overtone) for the early *SEI formation (before 4000 second) and lithiation (6 electrochemical cycles)* on silicon thin film anode in the Gen2+10%FEC (RED), 0.2 M Mg(TFSI)2 in Gen2+10%FEC (BLACK), and in 50 mM Mg(TFSI)2 in Gen2+10%FEC (BLUE). Continous electrochemical cycles are ran at intercalation voltage from 1.5 V to 10 mV (first 3 electrochemical cycles) and from 1.5 V to 40 mV (the last 3 electrochemical cycles).

dependence. For instance, by lowering the amount of $Mg(TFSI)_2$ in Gen2+10%FEC electrolyte from 200 mM to 50 mM, there is a clear decrease of frequency for the SEI formation step, indicating densification of the Sei, when compared to baseline.

Figure 3 presents results for a high Mg concentration versus a low Mg concentration mixed electrolyte in Gen2+10%FEC electrolyte, designated electrolytes E-G. A systematic evaluation for continuously monitoring the frequency drift for initial SEI formation, followed by lithiation of the silicon thin film was performed. An interesting finding is that SEI appears to be more dynamic with low Mg concentration. For instance, from the change of the frequency baseline shift, the SEI layer appears to be more stable as it undergoes lithiation. This finding could possibly suggest a better long-term cycling performance for a lowered Mg additive in the electrolyte content. Further investigation for the Mg content is currently carrying.

Conclusions

A combination of electrochemical and EQCM measurements has provided new insights into the relationship between Mg salt addition, electrochemical response, and SEI formation. Initial studies have provided evidence that Mg salt addition to the electrolyte is altering some of the stable solution species and helps mediates the transport of Mg^{+2} to the surface, possibly as part of a larger multi-cation species. Additionally, the Mg^{+2} appears to be most active in extending cycle life vis formation of a mixed Zintl species when FEC is present, possibly related to FEC coordination in the complex cation thought to exist in solution or in an FEC-derived film formation. Electrochemical evidence for the various proposed mechanisms has found support for the Mg^{+2} ion exchange mechanism with a fully lithiated silicon anode material. Evidence for direct magnesiation of silicon was not seen, as was evidence of a lithium-magnesium intermetallic phase.